

KIT SCIENTIFIC REPORTS 7702

# **Annual Report 2014 of the Institute for Nuclear and Energy Technologies**

Thomas Schulenberg



Thomas Schulenberg

**Annual Report 2014 of the Institute  
for Nuclear and Energy Technologies**

**Karlsruhe Institute of Technology**  
**KIT SCIENTIFIC REPORTS 7702**

# Annual Report 2014 of the Institute for Nuclear and Energy Technologies

by  
Thomas Schulenberg

## Report-Nr. KIT-SR 7702

### Impressum



Karlsruher Institut für Technologie (KIT)  
KIT Scientific Publishing  
Straße am Forum 2  
D-76131 Karlsruhe

KIT Scientific Publishing is a registered trademark of Karlsruhe  
Institute of Technology. Reprint using the book cover is not allowed.

[www.ksp.kit.edu](http://www.ksp.kit.edu)



*This document – excluding the cover, pictures and graphs – is licensed  
under the Creative Commons Attribution-Share Alike 3.0 DE License  
(CC BY-SA 3.0 DE): <http://creativecommons.org/licenses/by-sa/3.0/de/>*



*The cover page is licensed under the Creative Commons  
Attribution-No Derivatives 3.0 DE License (CC BY-ND 3.0 DE):  
<http://creativecommons.org/licenses/by-nd/3.0/de/>*

Print on Demand 2015

ISSN 1869-9669

ISBN 978-3-7315-0407-8

DOI: 10.5445/KSP/1000047907

## Content

<b>Institute for Nuclear and Energy Technologies .....</b>	<b>1</b>
Structure and Activities of the Institute for Nuclear and Energy Technologies .....	1
Mission .....	1
Organizational structure .....	1
Personnel resources .....	2
Some Research Highlights of 2014.....	3
References .....	6
<b>Group: Magnetohydrodynamics .....</b>	<b>7</b>
Magnetohydrodynamics for Nuclear Fusion Reactors .....	7
Liquid metal blanket design development: Magnetohydrodynamic flow in rectangular ducts with discontinuous electrical insulation .....	7
Validity of quasi 2D models for magneto-convection .....	9
Experimental study of instabilities in magnetohydrodynamic boundary layers.....	11
References .....	12
<b>Group: Transmutation .....</b>	<b>15</b>
Simulations of PHÉNIX Control Rod Withdrawal Tests with SIMMER-IV .....	15
Abstract .....	15
PHÉNIX Reactor Core Geometry Model and Meshing System.....	15
Results of Simulations and Discussion .....	16
Simulation of Power Shape Deformation in Experiment.....	16
Conclusions.....	18
References .....	18
<b>Group: Accident Analysis .....</b>	<b>21</b>
Analysis of Design Basis and Severe Accidents .....	21
Introduction.....	21
LIVE experiments .....	21
DISCO experiments .....	23
MOCKA experiments.....	24
COSMOS experiments.....	25
WENKA experiments.....	26
Application of the MELCOR code .....	27
References .....	29
<b>Group: KARlsruhe Liquid metal LABORatory.....</b>	<b>31</b>
Liquid Metal Technologies for Energy Conversion.....	31
Introduction.....	31
Core thermal-hydraulic experiments with LBE .....	31
Methane cracking .....	33

Concentrated Solar Power (CSP) .....	34
Conclusions .....	35
References .....	36
<b>Group: Accident Management Systems .....</b>	<b>39</b>
International Conference on Information Systems for Crisis Response and Management .....	39
Abstract .....	39
Introduction .....	39
Knowledge database .....	40
Crowd sourcing .....	41
Virtual meeting room .....	41
Web component .....	42
Conclusions and outlook .....	42
References .....	42
<b>Group: Hydrogen .....</b>	<b>45</b>
Some Highlights of the Hydrogen Group in 2014 .....	45
LOCA Containment Analysis of APR1400 .....	45
GASFLOW Simulations for Containment Venting Systems .....	46
Parallelization of GASFLOW .....	47
Setting up the Cyber Laboratory .....	48
References .....	49
<b>Group: AREVA Nuclear Professional School .....</b>	<b>51</b>
Pressure Drop in Fuel Assemblies .....	51
Introduction .....	51
Pressure drop correlations .....	52
Numerical study .....	52
Conclusions .....	55
References .....	56
<b>Group: Energy and Process Engineering .....</b>	<b>59</b>
Experimental Validation of a Numerical Model – Application of an Open Source Code towards Geothermal Conditions .....	59
Introduction .....	59
Methodology .....	59
Elementary Tools .....	60
Equations .....	61
Experimental setup .....	62
Preliminary Results .....	63
Discussion and Outlook .....	64
References .....	64

## Structure and Activities of the Institute for Nuclear and Energy Technologies

Thomas Schulenberg

### Mission

The Institute for Nuclear and Energy Technologies (Institut für Kern- und Energietechnik, IKET) is situated with its offices and research laboratories on the North Campus of KIT. It is focused on nuclear, fusion and renewable energy technologies for electric power production and on hydrogen technologies as an alternative energy carrier. Its research topics include analyses and tests of thermal-hydraulic phenomena, combustion phenomena and neutron physics which are typical for normal operation or for accidental conditions in nuclear power plants, for future nuclear fusions reactors, for geothermal or solar power plants, but also for mobile systems. Most subjects are application oriented, supported by some basic research projects, if needed.

### Organizational structure

IKET is structured into nine working groups as indicated in Fig. 1. Working groups on accident analyses, on accidents management systems and on transmutation as well as the AREVA Nuclear Professional School have been concentrating in 2013 primarily on nuclear applications, whereas the Karlsruhe Liquid metal Laboratory (KALLA) and the Hydrogen group were addressing nuclear as well as other energy technologies, as will be outlined below. The working group on magneto-hydrodynamics is primarily working on nuclear fusion applications, whereas the working group on energy and process engineering is rather concentrating on geothermal energies. Thus, the institute covers a wide field of different energy technologies, and the share of its personnel resources on the different research topics

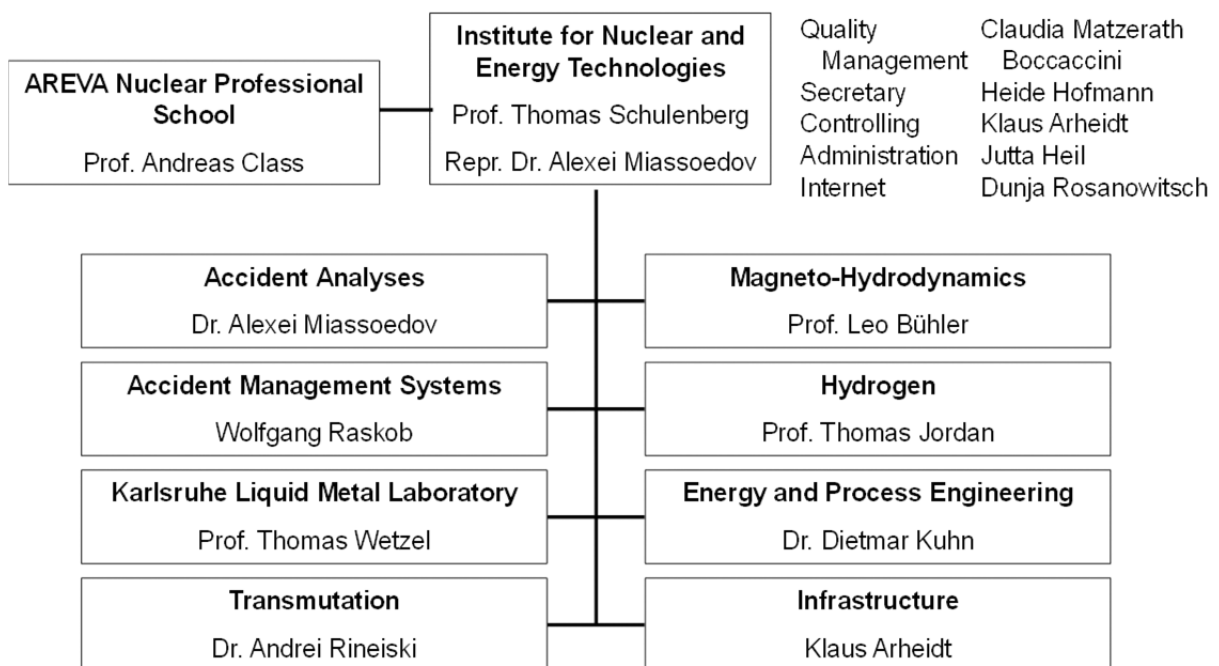


Fig. 1: Organizational structure of the Institute for Nuclear and Energy Technologies (IKET)

is determined each year by the worldwide market request for energy research.

Having a larger share of nuclear and fusion research, IKET has built up a quality management system according to the international standard ISO 9001. Internal audits are performed every year to train the use of its quality guidelines and to improve the quality level further on.

### Personnel resources

By the end of 2014, IKET had employed more than 120 (full time equivalent, FTE) scientists, engineers, technicians and other personnel. Around half of the employees were funded in 2014 by the Helmholtz Gemeinschaft (HGF), the others by third party funds of the European Commission, by industry, by German ministries or by other research funds. Doctoral students as well as students of the Baden-Wuerttemberg Cooperative State University (DHBW) were filling around 20% of these positions at IKET. The active role of the institute in education and training is also expressed by 35 to 40 additional students per year, who perform their bachelor or master theses or who spend an internship in the research laboratories of IKET

The structure of research programs to be funded by HGF in their 3<sup>rd</sup> funding period 2015 to 2020, was discussed and evaluated in 2014. A new program on energy storage and cross-linked infrastructures (SCI) has been initiated, to which IKET is planning to contribute part of its hydrogen group with topics on safety issues of hydrogen as an energy carrier.

Therefore, while around 75% of the personnel resources of IKET were allocated in 2013 to projects on nuclear safety (NUSAFE), this share was reduced to 67%, allowing 8% of the personnel to work in this new program SCI instead. The planned allocation of personnel resources for 2015 is shown in Fig. 1. Besides NUSAFE and SCI, IKET is planning to contribute to HGF research on renewable energies (RE) with work on concentrated solar power and on geothermal energies, as well as to HGF research on nuclear fusion technologies (FUSION).

In 2014, the institute had an annual budget of around 12 M€, of which around 7 M€ were provided by HGF and around 5 M€ by third parties.

The number of publications, as usual in research organizations, expresses the productivity of the institute. Almost 200 publications, around 3 per scientist and year, were given in 2014 to international journals, to conference proceedings and to KIT Scientific Publishing.

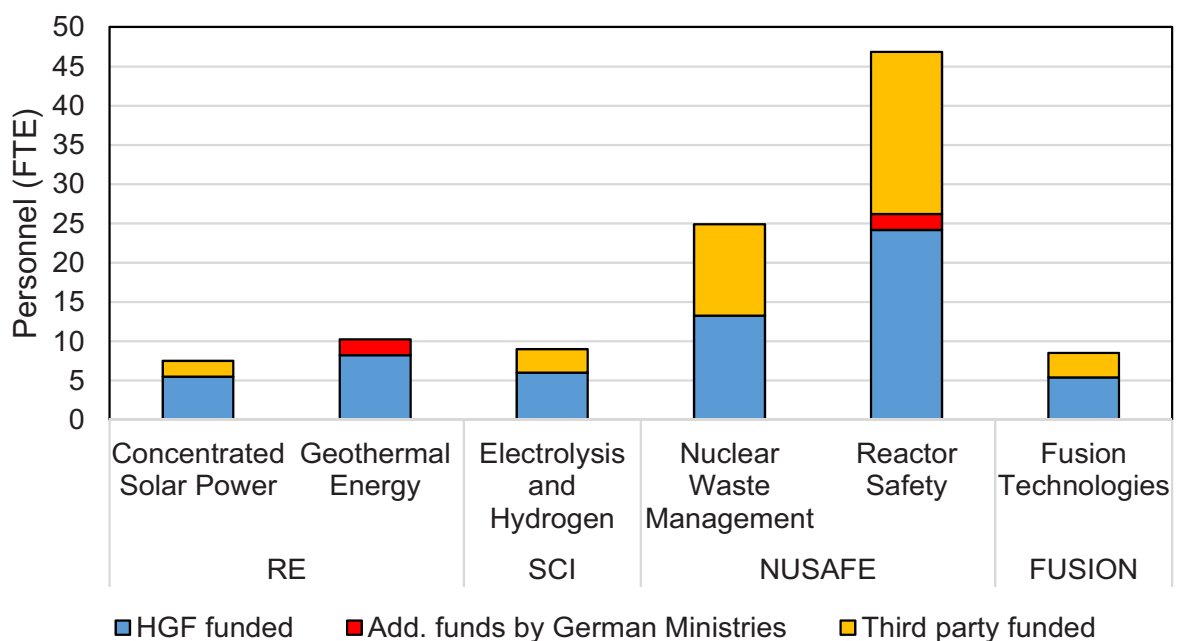


Fig. 2: Planned allocation of personnel resources on HGF research programs in their 3<sup>rd</sup> funding period.

The KIT mission on education and training along with scientific research is impressively demonstrated by up to 1000 semester hours, which employees of IKET were giving in recent years not only on the university campus of KIT, but also at the Baden-Wuerttemberg Cooperative State University (DHBW), at the Hector School of KIT, in the AREVA Nuclear Professional School of KIT, and in Universities of Applied Sciences (FH). A statistic of teaching activities is shown in Fig. 3.

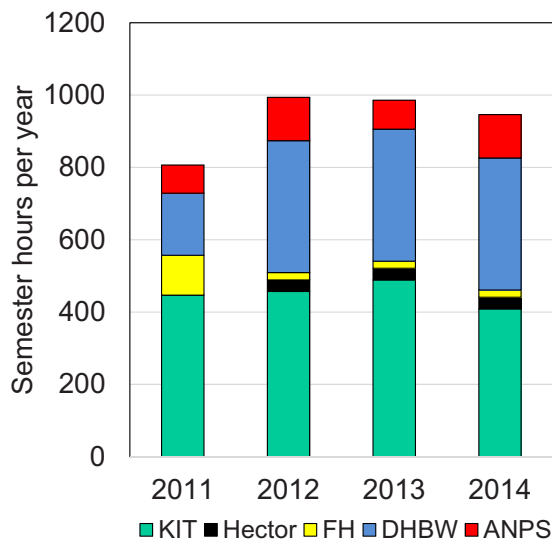


Fig. 3: Teaching activities of employees of IKET, given at different universities.

The AREVA Nuclear Professional School is an IKET working group for education and training of young scientist in nuclear engineering, sponsored by AREVA GmbH since 2009. Supported by lecturers of other organizations, this school has been offering compact courses in 2014 on nuclear technologies and methods. Moreover, this group is supervising doctoral students who are financially supported by AREVA, RWE, the European Commission or by other organizations.

### Some Research Highlights of 2014

Participation in European research programs is used at IKET also to motivate and train young scientists in the AREVA Nuclear Professional School. Innovative nuclear research programs, in particular, appeared to be most suited to attract young nuclear engineers. An example is the European project THINS (Thermal-Hydraulics of

Innovative Nuclear Systems), to which the AREVA Nuclear Professional School contributed with analyses of flow and heat transfer in fuel assemblies. Moreover, the School contributed to the European project SCWR-FQT in collaboration with Chinese research organizations. In this context, two doctoral theses have been completed in 2014 at the AREVA Nuclear Professional School, focusing on the analysis of safety systems and on risk assessment for a supercritical water test loop with a small scale fuel assembly, to be installed in a research reactor in the Czech Republic. As an example, Fig. 4 shows the retention of pressure tube fragments by the surrounding thermal insulation and the surrounding water, predicted for a postulated pressure tube failure inside the research reactor.

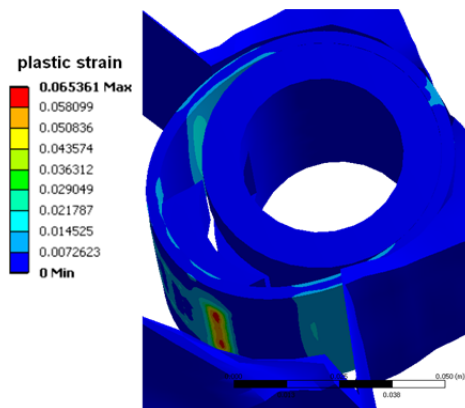


Fig. 4: Prediction of the retention of a pressure tube fragment after a postulated brittle failure in the planned fuel qualification test facility SCWR-FQT [1].

Retention of core melt inside the reactor pressure vessel during a severe accident of a nuclear power plant is an economic concept of some latest boiling water reactors or pressurized water reactors. Limits of such in-vessel core melt retention is studied experimentally by the Accident Analyses Group of IKET with their LIVE facility. Tests with granite and salt, simulating solid oxide and liquid metal phases of the core melt, have been performed in 2014. A typical result is shown in Fig. 5. While the core melt forms an insulating crust in the bottom part of the cooled reactor wall, a thin crust found near the top layer of the molten corium, indicating the location of maximum thermal loading of the reactor pressure vessel in case of such an accident.

The Accident Management Systems Group participated in an international benchmark on soft-

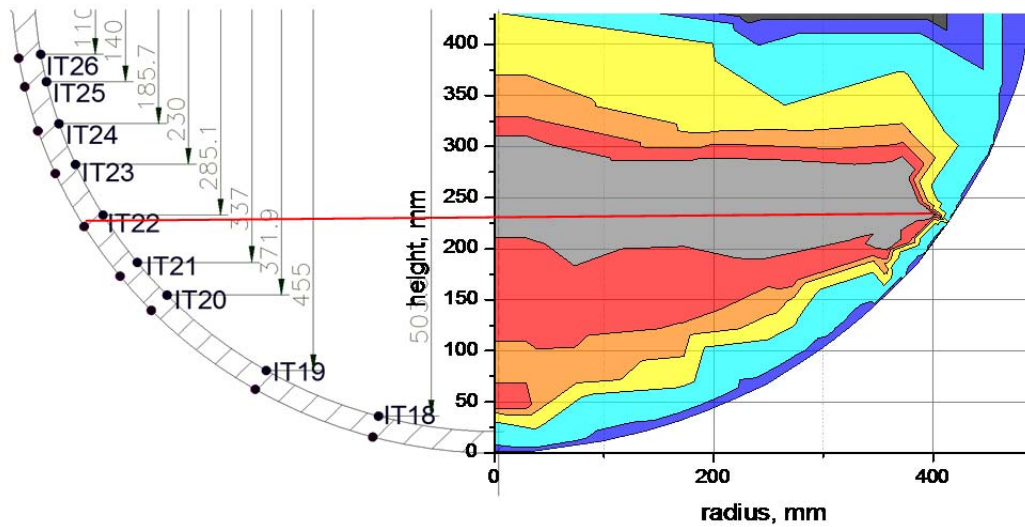


Fig. 5: Temperature measurements of simulated core melt inside a cooled reactor pressure vessel during a severe accident [2].

were tools used to estimate consequences of accidents at nuclear facilities such as power reactors, research reactors and fuel reprocessing facilities, organised by the OECD/NEA. Twenty organizations, representing twelve countries and two international organizations, participated in this benchmarking project. The benchmarking was intended to help identifying the strengths and weaknesses of the tools used for source term modelling and dose assessments and to recognize the knowledge gaps, as well as to

propose improvements to modelling capabilities. Within the exercise, the interface between source term models developed by GRS and the RODOS system was also successfully tested. Fig. 6 shows results for the site Peach Bottom based on an atmospheric dispersion run performed by the RODOS system.

The main activities of the Transmutation group are on safety studies of reactors, which can be used for transmutation of nuclear waste. The

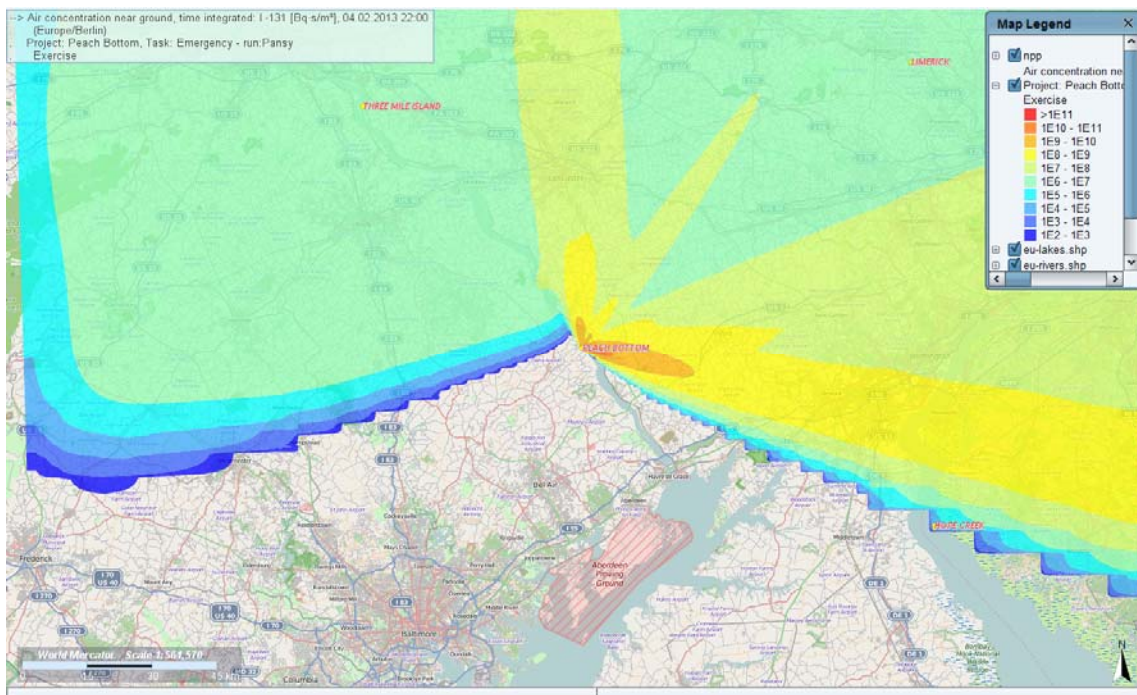


Fig. 6: Time integrated air concentration of the isotope I-131 following a release of about three days [3].

employed models and codes are validated by participation in challenging international research projects. An example is a benchmark analysis of a control rod withdrawal test of the PHÉNIX reactor, a sodium cooled fast reactor, which was operated in France until 2009. The Transmutation Group used the SIMMER code in its new, three-dimensional version IV to predict the transient response of the neutron flux, of mass flows, of temperatures and of pressures during the tests. Fig. 7 shows the distribution of the fuel assembly power after withdrawal of a single control rod in the right half of the core. The coupled analyses include the effect of flow, temperature and isotopic composition of fuel and control rods on reactivity.

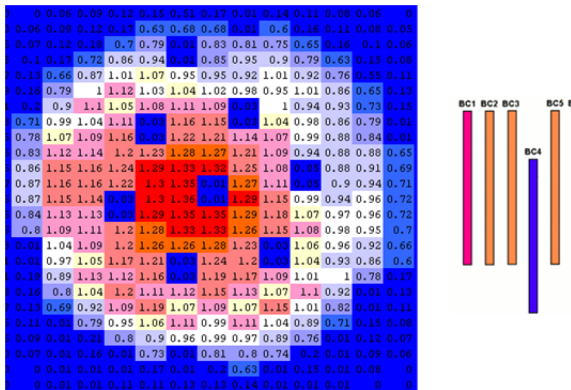


Fig. 7: Power distribution of fuel assemblies predicted for the control rod withdrawal test in the PHÉNIX reactor [4].

The Karlsruhe Liquid Metal Laboratory KALLA at IKET hosted an international workshop on Heavy Liquid Metal (HLM) Technology from 7<sup>th</sup> to 10<sup>th</sup> October, 2014. The workshop included 5 keynote lectures and 41 technical presentations, covering topics of core thermal-hydraulic and core components; steam generator and cooling safety; coolant chemistry control and HLM corrosion; fuel and fuel safety; among others. With 85 registered participants, the workshop succeeded in its goal of promoting the technical information exchange within the scientific community working on HLM systems. The workshop is part of the training and dissemination activities of the EU FP7-Projects SEARCH and MAXSIMA. Conference proceedings were published based on the individual abstracts and presentations ([www.iket.kit.edu/590.php](http://www.iket.kit.edu/590.php)).



Fig. 8: Participants of the International Workshop on Heavy Liquid Metal Technology, hosted by IKET in 2014.

The Hydrogen Group has been involved in several severe accident analyses motivated by the Fukushima accident. For three different PWR containments of two European existing reactors and one Korean design, Fig. 9, the effectiveness of hydrogen mitigation technologies have been assessed. In particular, the configuration of passive autocatalytic recombiners and the water spray systems have been analyzed in detail. Similarly, the containment ventilation strategies for some selected installations have been re-assessed. The work has been supported by industry.

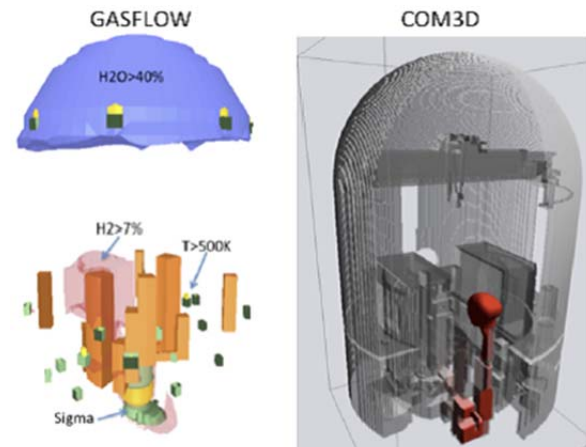


Fig. 9: Snapshot of the late phase LOCA analysis in APR1400; left: steam and hydrogen distribution simulated with GASFLOW highlighting the critical Sigma-cloud in the cavity (recombiners in green, without water spray activation); right: subsequent COM3D combustion simulation showing hydrogen flame propagation into the reactor containment 0.93 sec after ignition (800K isotherm in red) [5].

Another focus in 2014 was the parallelization of the GASFLOW code. The replacement of internal solver procedures by calls to the open source PETSc library and a major revision of the whole

code including physical models yielded a new version, which is actually considered as a new software product: GASFLOW-MPI. Compatibility with previous GASFLOW serial versions is provided, such that identical input, same functionality will produce identical results with a considerable linear speed-up. Computations requiring response times of several weeks on expensive vector machines like NEC SX9 in the past, may now run on affordable small computer systems within one day. Validation is almost completed and the first version will be released in April 2015.

An experimental setup has been designed by the Magneto-Hydrodynamics Group, simulating a flow with high velocities, using flow channel inserts for electrical insulation to reduce magneto-hydrodynamic pressure losses in a dual coolant blanket of a fusion reactor. Numerical predictions confirm the expected effect. Fig. 10 shows the traversing velocity measurement system of the test section. This test shall contribute to the EUROfusion work program and shall be performed in the MEKKA laboratory of IKET.

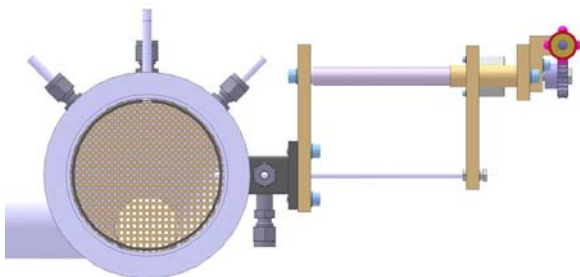


Fig. 10: Flow and pressure measurement systems for a magneto-hydrodynamic experiment with high flow velocities [6].

While the new mobile geothermal power conversion system MONIKA is being constructed, the Energy and Process Engineering Group at IKET was focusing in 2014 on scale and gas release effects of brine from the geothermal power plant Unterhaching, Bavaria. With its extremely high concentration of salts and dissolved gases, such water from deep underground can easily plug tubes by scale, when the pressure is suddenly reduced to the conditions of the power plant. A local test laboratory, shown in Fig.11, has been installed in this power plant to measure such effects in-situ. The facility is operated by the Energy and Process Engineering Group in several measurement campaigns.



Fig. 11: Measurement of scale and released gases at the geothermal power plant Unterhaching [7].

The following sections shall provide some deeper insight into selected research topics of these eight scientific working groups.

## References

- (1) Zeiger, T., Auswirkungen eines postulierten Druckrohrversagens während des SCWR Fuel Qualification Test, Dissertation, KIT, 2014.
- (2) Gaus-Liu, X., not published
- (3) Raskob, W., „Benchmarking of fast-running software tools used to model releases during nuclear accidents“, Nuclear Energy Agency, Committee on the Safety of Nuclear Installations, NEA/CSNI/R (2014), not published.
- (4) Kriventsev, V.; Gabrielli, F.; Rineiski, A.; “Coupled thermal-hydraulic and neutronic simulation of Phenix control rod withdrawal tests with SIMMER-IV“. 10th International Topical Meeting on Nuclear Thermal-Hydraulics, Operation and Safety (NUTHOS 2014), Okinawa, J, December 14-18, 2014, Proceedings on USB-Stick Paper NUTHOS10-1123.
- (5) Royl, P., “Use of the KIT HYCODES System with a Conservative Source for the Simulation of Hydrogen Distribution and Combustion with/without Spray in a Large Break LOCA in the Korean APR1400“, 46<sup>th</sup> Annual Meeting on Nuclear Technology, Berlin, May 5 – 7, 2015.
- (6) Köhly, Ch., not published.
- (7) Kuhn, D., not published.

## Magnetohydrodynamics for Nuclear Fusion Reactors

Leo Bühler, Thomas Arlt, Hans-Jörg Brinkmann, Victor Chowdhury, Sebastian Ehrhard, Christina Köhly, Chiara Mistrangelo

### Liquid metal blanket design development: Magnetohydrodynamic flow in rectangular ducts with discontinuous electrical insulation

The main magnetohydrodynamic (MHD) issues in liquid metal blankets consist in the occurrence of increased pressure drop and modified flow distribution compared to hydrodynamic conditions. Electromagnetic Lorentz forces result from interactions of induced electric currents with the magnetic field. They tend to slow down the bulk flow and they are balanced by large pressure heads. The resulting additional MHD pressure losses are proportional to the total electric currents induced in the fluid. They can be minimized by suitable insulation at channel walls. The use of insulating flow channel inserts (FCI) inside long channels to electrically and thermally decouple the flowing lead lithium from the load-bearing steel wall is a key technical feature in dual coolant blankets [1]. Liquid metal flows in ducts with FCIs have been studied in the past focusing on 2D fully developed conditions [2] and few studies have been dedicated to 3D MHD effects in ducts with insulating internal liners [3] [4] [5]. Two types of electric currents can contribute to the total pressure drop in the blanket system. In channels where the flow is nearly fully developed the MHD pressure drop is mainly related to cross-sectional currents that close through boundary layers or in electrically conducting walls. However, in a blanket most of the pressure losses associated with electromagnetic forces are caused by 3D currents for instance due to changes in duct cross-section or electrical properties of the wall and to the presence of non-uniform magnetic fields. An example is represented by 3D MHD phenomena that occur in case of a gap between flow channel inserts, as discussed in the following. Discontinuous insulation can be present in long ducts where a num-

ber of FCIs is required to cover the entire length of the channels. Numerical simulations have been performed to study the influence on pressure drop and velocity distribution of the interruption of the insulating liner in a rectangular duct by using the European dual coolant lead lithium blanket concept as reference for the geometry of the duct [6].

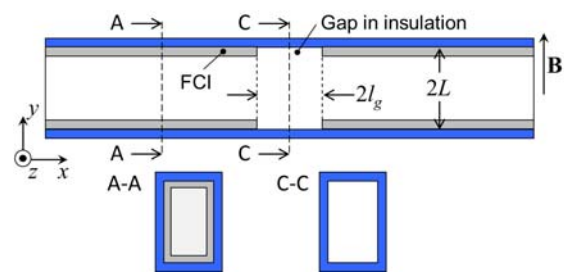


Figure 1: Rectangular duct with two flow channel inserts separated by a gap of length  $2l_g$ .

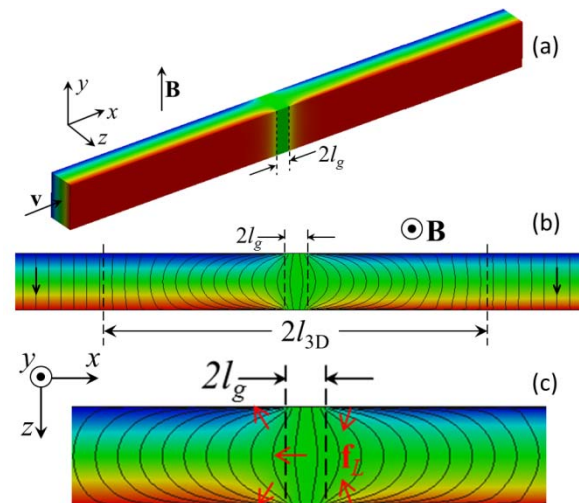


Figure 2: Flow at  $Ha=1000$ ,  $N=71$ . Contours of electric potential (a) on the surface of the duct and (b) on the symmetry plane  $y=0$  together with current streamlines; (c) enlarged view of the zone where 3D currents are present.  $f_L$  are Lorentz forces.

We consider MHD flows in a long rectangular duct of  $yz$  cross-section  $2L \times 1.25L$ , where the ty-

pical length  $L = 0.1675\text{m}$  is the half size of the channel along magnetic field lines. Two semi-infinite FCIs cover the internal surface of the channel. In the present example the liners are ideally electrically insulating and the insulation is discontinuous i.e. the inserts are separated by a gap,  $l_g = 0.25L$ , as shown in Figure 1. A uniform magnetic field is imposed in  $y$ -direction. Far enough upstream and downstream of the gap the flow is fully developed, while around the opening intense 3D MHD phenomena occur. The characteristics of the flow near the gap depend on the length of the gap and on the electric conductivity of the external duct wall. In a first conservative example the external channel is assumed to be perfectly conducting. Results are presented in non-dimensional form and coordinates are normalized by the typical size  $L$  of the duct. Velocity, pressure, electric current density and magnetic field are normalized by  $u_0$ ,  $\sigma u_0 B_0^2 L$ ,  $\sigma u_0 B_0$ , and  $B_0$ , respectively.  $\sigma$  is the electric conductivity of the fluid,  $B_0$  the magnitude of the magnetic field and  $u_0$ , the average velocity in the duct cross-section. The dimensionless parameters describing the flow are the Hartmann number  $Ha$  and the interaction parameter  $N$

$$Ha = B_0 L \sqrt{\sigma / (\rho \nu)}, \quad N = \sigma L B_0^2 / (\rho u_0)$$

Results are discussed for a Hartmann number  $Ha = 1000$ . The computational mesh consists of  $170(y) \times 100(z)$  points in the duct cross-section. Higher spatial resolution in viscous boundary layers and near the insulation gap has been achieved by non-equidistant spacing. The fully developed velocity profile in the inlet and outlet ducts at some distance from the gap has been compared with an analytical solution [7] and the relative error for pressure gradient is smaller than 1%. In Figure 2 the electric potential is shown on the surface of the duct (a) and on the symmetry plane  $y=0$  (b,c) together with electric current streamlines. Upstream and downstream at some distance from the FCI interruption the flow is fully developed and hence  $\partial_x \phi = 0$ . In the core the electric potential is constant along magnetic field lines, and in transverse direction  $\partial_z \phi \approx 1$ . In the region of the channel for  $-l_g < x < l_g$ , as a result of the jump in the wall electric conductivity, the transverse potential gradient reduces to zero and an axial potential gradient  $\partial_x \phi$  arises for

$-l_{3D} < x < l_{3D}$ . The latter drives axial currents whose magnitude increases by approaching the side walls parallel to the magnetic field. The axial extent of the region where  $j_x \neq 0$  is called  $l_{3D}$ , since it corresponds to the zone where strong 3D MHD effects occur. The current streamlines displayed on the plane  $y=0$  in Figure 2(b) show, that for the considered flow parameters the influence of the gap in the insulation extends much farther upstream and downstream compared to the actual size of the opening.

From the engineering point of view we are interested in quantifying the additional pressure losses caused by induced 3D currents and by resulting electromagnetic forces. In Figure 3 the pressure is plotted along two lines, one in the middle of the duct ( $y=z=0$ ) and one close to the side wall ( $y=0, z=0.57$ ). When approaching the region where the insulation is missing the pressure reduces significantly due to the occurrence of axial Lorentz forces that brake the flow. Near parallel walls the pressure is larger for  $x < 0$  and smaller for  $x > 0$  than in the center of the duct owing to transverse electromagnetic forces that push the liquid metal towards the walls and towards the channel center, respectively (see Figure 2(c)). In Figure 3 the nondimensional MHD pressure drop related to 3D electromagnetic phenomena is indicated as  $\Delta p_{3D}$ .

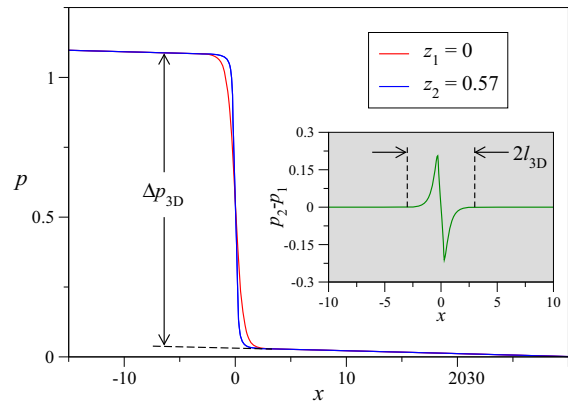


Figure 3: Axial distribution of pressure on the symmetry plane  $y=0$  at two transversal positions for  $Ha=1000$ ,  $N=71$ . In the subplot the pressure difference  $p_2(z_2=0.57) - p_1(z_1=0)$  is plotted along  $x$ .

In Figure 4 electric potential contours, which serve as approximate streamlines, are shown on the surface of the channel and velocity distributions are displayed at various axial locations. The

3D MHD interactions cause significant modifications of the velocity distribution. A parametric study has been performed to investigate the influence of the mean flow rate on the axial size of the region where 3D MHD phenomena occur. For small interaction parameters  $N$  a long development length  $l_d$  is required to reach downstream fully developed conditions for the velocity, while the effects on electric currents and pressure are confined to a much shorter axial extent  $l_{3D}$ . When inertia effects are negligible,  $l_d$  and  $l_{3D}$  become comparable.

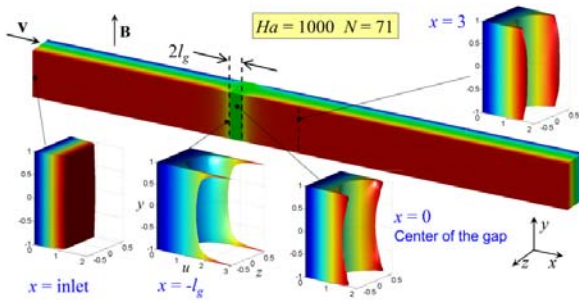


Figure 4: Electric potential on duct surface and velocity distributions at various axial locations. Owing to the jump in wall electric conductivity and ensuing 3D MHD effects the velocity increases in the side layers and reduces in the core. A jet-like velocity distribution appears.

### Validity of quasi 2D models for magneto-convection

For applications in nuclear fusion reactors where magnetic fields are very strong, liquid metal flows in the cores of ducts can often be regarded as inertialess and practically inviscid, while viscous effects are localized in thin boundary layers. The intense electromagnetic Lorentz forces, resulting from the interaction of induced electric currents and imposed magnetic field, tend to remove flow variations along magnetic field lines and they force the fluid to circulate mainly in planes perpendicular to the field. The established quasi-two dimensional (Q2D) MHD flow can be predicted by means of an approximate model by reducing the basic governing equations to a 2D problem by analytical integration along magnetic field lines. Such models have been applied in the past by numerous authors to investigate duct flow problems and magneto-convection. However, limitations of those Q2D approaches have never been systematically studied. The purpose of the

present work is showing that Q2D models may yield good results for a large number of applications but also to highlight the limitations of those approximations. As an example we consider buoyant MHD flows in a horizontal liquid metal layer of height  $H$ , length  $lH$  and width  $2aH$  (see Figure 5). Such geometries are typical in horizontal Bridgman crystal growth or for liquid metal blankets of fusion reactors. We apply the Q2D model equations and compare results with 3D numerical simulations based on full governing equations.

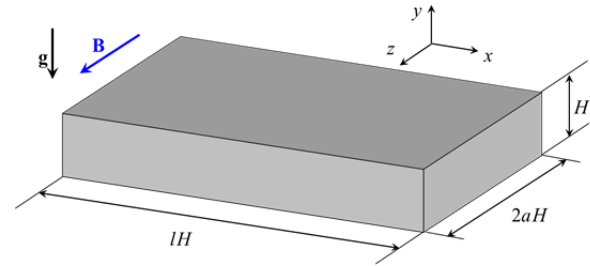


Figure 5: Sketch of geometry and coordinates. The flat cavity, filled with liquid metal, is differentially heated at  $x/H = \pm 1/2l$ , such that a mean axial temperature gradient  $G\hat{x}$  establishes. Top and bottom walls at  $y/H = \pm 1/2$  have temperature profiles that vary linearly between the values of the differentially heated walls. The other walls are adiabatic. The convective motion is damped by a horizontal magnetic field in  $z$ -direction.

Buoyant flows of incompressible, viscous, electrically conducting fluids in a uniform horizontal magnetic field are described by nondimensional equations for a balance of energy, momentum and mass, by Ohm's law and by an electric potential equation to ensure charge conservation. The governing equations and the derivation of the Q2D model is described in [8] and omitted here.

Dimensionless parameters are the Prandtl number, the Grashof number and the Hartmann number:

$$Pr = \frac{\nu}{\kappa}, \quad Gr = \frac{g\beta H^3 \Delta T}{\nu^2}, \quad Ha = B_0 H \sqrt{\frac{\sigma}{\rho \nu}}.$$

Kinematic viscosity  $\nu$ , thermal diffusivity  $\kappa$  and electric conductivity  $\sigma$  are assumed to be constant,  $\rho$  is the density at the reference temperature and  $\beta$  is the coefficient of volumetric thermal expansion.  $B_0$  is a typical magnitude of the magnetic field,  $u_0 = \nu/H$  a characteristic velocity and  $\Delta T$  is derived from the mean horizontal tempera-

ture gradient  $G\hat{x}$  as  $\Delta T = GH$ . At all walls we have no-slip  $\mathbf{u} = 0$ .

**Insulating walls:** Let us first consider flows in cavities with walls that are electrically insulating as considered for instance in [9]. Results from numerical simulations using Q2D model and full 3D equations are compared (the latter ones with up to  $8.6 \cdot 10^6$  grid points, all layers well resolved, grid-independent results achieved). Contours of velocity magnitude for  $a = 1$ ,  $Pr = 0.015$ ,  $Gr = 10^7$ ,  $Ha = 1000$  are shown in Figure 6. It can be observed that a single stationary global recirculation establishes. Near the hot and cold end of the geometry the fluid moves upward and downward respectively, while in the central part the flow is preferentially horizontal and aligned parallel to the mean temperature gradient. A qualitative comparison displayed in the figure shows already good agreement between Q2D and 3D simulations.

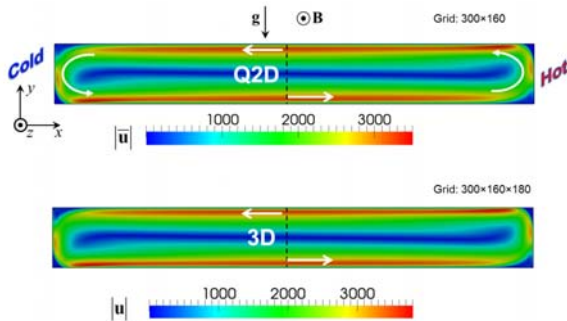


Figure 6: Colored contours of velocity magnitude in the vertical symmetry plane  $z = 0$  obtained by Q2D and 3D simulations for  $a = 1$ ,  $Gr = 10^7$ ,  $Pr = 0.015$ ,  $Ha = 1000$ ,  $c = 0$ .

This is further confirmed by comparing velocity and temperature along a vertical line in the middle of the cavity as shown in Figure 7. For parameters used in the simulations the Q2D model is able to predict well the velocity distribution in the core and reasonably well the decay towards the field aligned walls at  $y = \pm 1/2$ . Nevertheless, one can observe still minor differences between the Q2D model and 3D simulations. More precisely the Q2D model slightly underestimates the velocity when approaching top and bottom walls. The prediction of the vertical temperature distribution is also good.

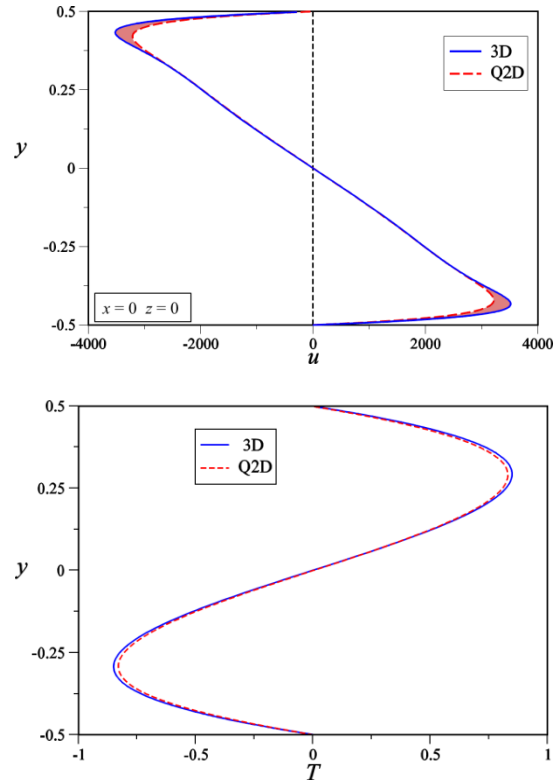


Figure 7: Comparison of axial velocity and temperature along  $y$  at  $(x,z)=(0,0)$  obtained by Q2D and 3D simulations for  $a = 1$ ,  $Gr = 10^7$ ,  $Pr = 0.015$ ,  $Ha = 1000$ , and electrically insulating walls .

**Conducting walls:** As a second case we consider magneto-convection in a perfectly electrically conducting cavity. In this case we observe a strong disagreement between Q2D and 3D simulations. The high-velocity jets along the horizontal walls, which are predicted by 3D simulations, cannot be reproduced by the Q2D model. A significant disagreement is present in layers along horizontal walls, while in the core the two solutions still agree quite well. Nevertheless, since the layers carry the major mass flux a 3D simulation is mandatory and Q2D results are practically useless as shown in [8].

Finally we may conclude that for electrically insulating walls Q2D models give reasonable estimates for velocity and heat transfer for both stationary and time-dependent flows. For electrically conducting walls, however, Q2D results become useless so that 3D simulations are mandatory.

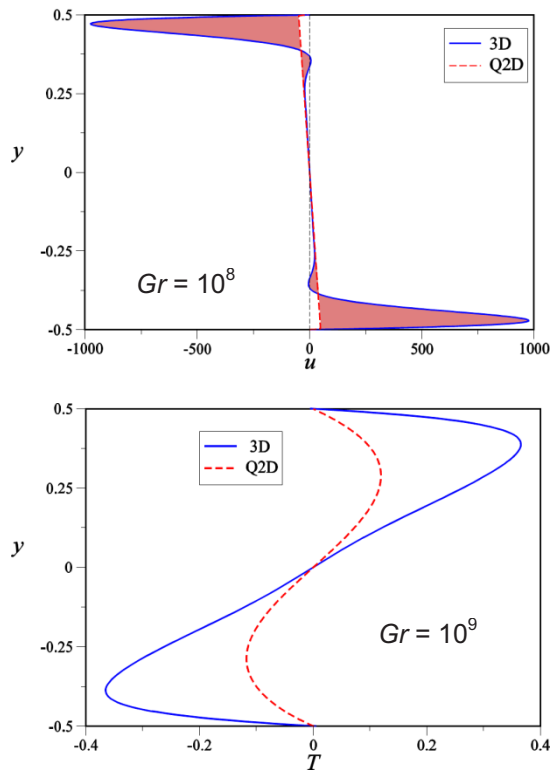


Figure 8: Comparison of axial velocity and temperature along  $y$  at  $(x,z) = (0,0)$  obtained by Q2D and 3D simulations for  $a = 1$ ,  $Pr = 0.015$ ,  $Ha = 1000$ , and perfectly conducting walls.

### Experimental study of instabilities in magnetohydrodynamic boundary layers

The study of liquid metal flows in strong magnetic fields plays an essential role in the development of nuclear fusion reactors where breeding of tritium and heat extraction can be accomplished by circulating in the blanket a lithium-containing alloy. Experiments to investigate instabilities in fundamental MHD flows are required both to obtain data for validation of computational codes and to reach a deep understanding of basic MHD phenomena needed for the physical interpretation of complex, coupled problems. Experiments have been performed in the MEKKA laboratory to analyze liquid metal flows in rectangular channels under the influence of intense magnetic fields.

The aim is to investigate firstly the flow stability depending on flow rates and strength of the magnetic field and secondly to determine effects of unstable side layers on velocity and electric potential distributions. In the test section used for the experimental campaigns walls parallel to the

magnetic field are electrically insulating and those perpendicular are covered by thin foils of copper to achieve a well-defined electric wall conductance. These electric boundary conditions correspond to the classical Hunt-type MHD flow [10] and they give rise to jet-like velocity patterns which are potentially unstable [11]. Instabilities can lead to the formation of complex vortical structures, which may enhance the momentum transport from side layers to the core region with consequences for heat transfer and convective transport of dissolved species like corrosion products or tritium.

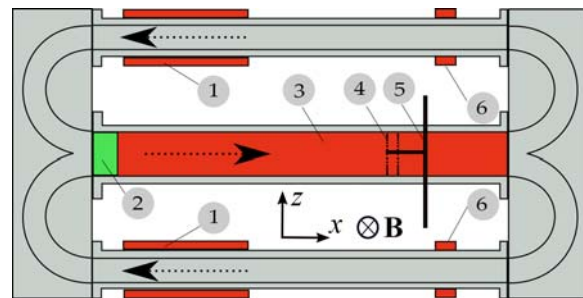


Figure 9: GalnSn loop with (1) electromagnetic pumps, (2) flow straightener, (3) test section with conducting Hartmann walls, (4) potential probes on duct wall, (5) traversable probe and (6) flow meters.

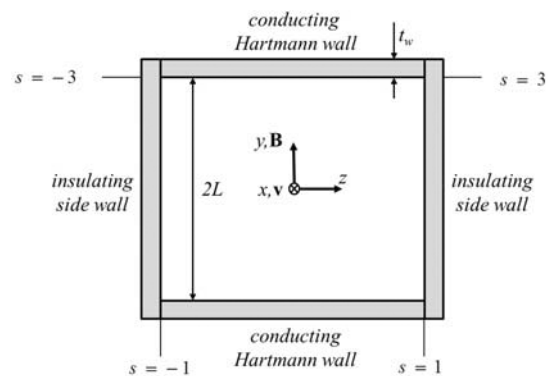


Figure 10: Duct geometry and coordinates.

The investigated MHD flows are characterized by two nondimensional groups, the Hartmann number ( $Ha$ ) describing the magnetic field strength and the Reynolds number ( $Re$ ) describing the average axial velocity. The design of the employed liquid metal loop and details of the test section are shown in Figure 9 and Figure 10. Two lateral ducts serve as electromagnetic conduction pumps that feed the test section in the middle. A traversable 4-pole probe is used to measure of the transverse potential gradient

which approximates the axial velocity. The eutectic alloy *GalSn* is used as model fluid. Its melting point is at 10.5°C, so that the experiments can be performed at room temperature. The entire loop is exposed to a uniform magnetic field.

Results of time-averaged potential distribution are depicted in Figure 11 as a function of the circumferential coordinate  $s$  (see Figure 10). For laminar flow at the smallest Reynolds number shown in the figure the potential distribution is in very good agreement with the analytical results. When the Reynolds number is increased to  $Re=15637$  we observe small deviations in the potential distribution. The magnitude of potential on the sidewalls is slightly reduced, which is an indication that the mass flux through the side layers is also smaller. Measurements of time-averaged axial velocity profiles within the flow at  $y=0$  are shown in Figure 12. Also here there is a very good agreement between experimental and analytical results in the core region. For  $Re=15637$  the maximum velocity of the jets reduces significantly and the side layers thicken, as expected from measurements of wall potential.

These observations are clear hints for unstable side layers at large Reynolds numbers which are characterized by an increased momentum transport from the sides towards the core region [12]. Such instabilities are relevant for applications in liquid metal blankets. For more details see [13]. A detailed stability analysis by theoretical and numerical approaches and by experiments is ongoing.

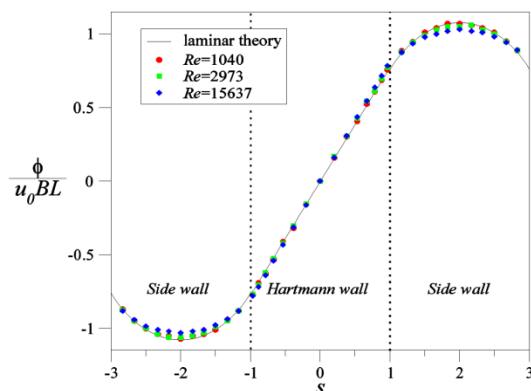


Figure 11: Time-averaged potential profiles on sidewalls and Hartmann wall for  $Ha \approx 1000$ .

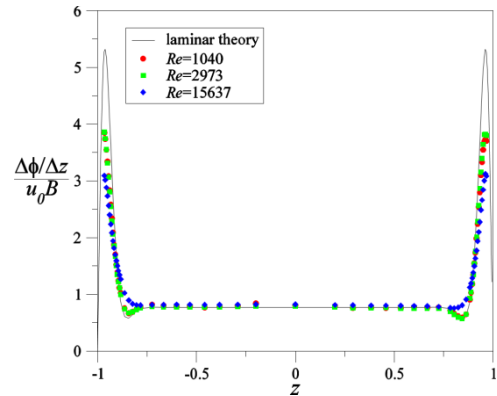


Figure 12: Profiles of time-averaged potential gradient (indicates velocity) at  $y = 0$  for  $Ha \approx 1000$ .

## References

- (1) Tillack, M. S. and Malang, S., "High Performance PbLi Blanket," in *Proceedings of the 17th IEEE/NPSS Symposium Fusion Engineering, San Diego, California October 6-10*, vol. 2, Institute of Electrical and Electronics Engineers, Inc., 1997, pp. 1000-1004.
- (2) Smolentsev, S., Morley, N. B. and Abdou, M., "Magnetohydrodynamic and Thermal Issues of the SiCf/SiC Flow Channel Insert," *Fusion Science and Technology*, vol. 50, no. 1, pp. 107-119, 2006.
- (3) Bühler, L., "The influence of small cracks in insulating coatings on the flow structure and pressure drop in MHD channel flow," *Fusion Engineering and Design*, vol. 27, pp. 650-658, 1995.
- (4) Bühler, L. and Mistrangelo, C., "Liquid metal MHD flows near non-insulated gaps between flow channel inserts in DCLL blankets," *IEEE Transactions on Plasma Science*, vol. 42, no. 3, pp. 510-515, 2014.
- (5) Sutevski, D., Smolentsev, S. and Abdou, M., "3D numerical study of pressure equalization in MHD flow in a rectangular duct with insulating flow channel insert," *Fusion Engineering and Design*, vol. 89, no. 7-8, pp. 1370-1374, 2014.
- (6) Norajitra, P., Bühler, L., Fischer, U., Malang, S., Reimann, G. and Schnauder, H., "The EU advanced dual coolant blanket concept," *Fusion Engineering and Design*, Vols. 61-62, pp. 449-453, 2002.

- (7) Shercliff, J. A., "Steady motion of conducting fluids in pipes under transverse magnetic fields," *Proc.Camb.Phil.Soc.*, vol. 49, pp. 136-144, 1953.
- (8) Bühler, L., Mistrangelo, C. and Molokov, S., "Validity of quasi-2D models for magneto-convection," *Magnetohydrodynamics*, vol. in print, 2015.
- (9) Gelfgat, A. Y. and Molokov, S., "Quasi-two-dimensional convection in a three-dimensional laterally heated box in a strong magnetic field normal to main circulation," *Physics of Fluids*, vol. 23, no. 3, pp. 034101-1-13, 2011.
- (10) Hunt, J. C. R., "Magnetohydrodynamic flow in rectangular ducts," *Journal of Fluid Mechanics*, vol. 21, pp. 577-590, 1965.
- (11) Priede, J., Aleksandrova, S. and Molokov, S., "Linear stability of Hunt's flow," *Journal of Fluid Mechanics*, vol. 649, pp. 115-134, 2010.
- (12) Bühler, L. and Horanyi, S., "Measurements of time-dependent liquid metal magnetohydrodynamic flows in a flat rectangular duct," *Fusion Engineering and Design*, vol. 84, pp. 518-521, 2009.
- (13) Bühler, L., Chowdhury, V., Mistrangelo, C. und Brinkmann, H.-J., „Experimental study of instabilities in magnetohydrodynamic boundary layers," *Fusion Engineering and Design*, p. accepted, 2015.
- Read more:
- (14) Aiello, G.; Mistrangelo, C.; Bühler, L.; Mas de les Valls, E.; Aubert, J.; Li-Puma, A.; Rapisarda, D.; Del Nevo, A.; "MHD issues related to the use of lithium lead eutectic as breeder material for blankets of fusion power plants". Fundamental and Applied MHD: Thermo acoustic and Space Technologies; 9th PAMIR International Conference, Riga, LV, June 16-20. 2014, Proceedings Vol.1 pp.373-378, also on CD-ROM.
- (15) Arlt, T.; Priede, J.; Bühler, L.; "Linear stability analysis of MHD-duct-flows for high Hartmann numbers". 15th MHD Days, Potsdam, December 2-3, 2014.
- (16) Arlt, T.; Chowdhury, V.; Bühler, L.; "Magnetically induced instabilities (Project A3)". LIMTECH PhD Summer School, Dresden, July 22-23, 2014.
- (17) Arlt, T.; Bühler, L.; "Numerical investigations of magnetically induced instabilities in duct flows". LIMTECH PhD Summer School, Dresden, July 22-23, 2014.
- (18) Bühler, L.; Mistrangelo, C.; "Flüssigmetallströmungen in starken Magnetfeldern. Numerische Simulation und Experimente". Arbeitskreis Strömungsmechanik und Strömungssimulation, Georgsmarienhütte, 20. Februar 2014.
- (19) Bühler, L.; "Introduction to Magneto Hydro Dynamics (MHD)". International Seminar 'Computational Fluid Dynamics in Metallurgy', Mönchengladbach, December 1-3, 2014.
- (20) Bühler, L.; Mistrangelo, C.; "Liquid metal magnetohydrodynamic flows for fusion applications: Blankets and high heat flux components". Lorentz Workshop 'Where no material dares to go', Leiden, NL, January 6-10, 2014.
- (21) Bühler, L.; Mistrangelo, C.; "Liquid metal MHD flows near noninsulated gaps between flow channel inserts in DCLL blankets". *IEEE Transactions on Plasma Science*, 42 (2014) 510-515.
- (22) Bühler, L.; Mistrangelo, C.; Najuch, T.; "Magnetohydrodynamic flows in model porous structures". 28th Symposium on Fusion Technology (SOFT 2014), San Sebastian, E, September 29 - October 3, 2014.
- (23) Bühler, L.; Mistrangelo, C.; Molokov, S.; "Validity of quasi-2D models for magneto-convection". Fundamental and Applied MHD: Thermo acoustic and Space Technologies; 9th PAMIR International Conference, Riga, LV, June 16-20. 2014.
- (24) Chowdhury, V.; Bühler, L.; "Experimental investigation of MHD liquid metal duct flow". LIMTECH PhD Summer School, Dresden, July 22-23, 2014.
- (25) Chowdhury, V.; Bühler, L.; Mistrangelo, C.; Brinkmann, H.J.; "Experimental study of instabilities in magnetohydrodynamic boundary layers". 28th Symposium on Fusion Technology (SOFT 2014), San Sebastian, E, September 29 - October 3, 2014.
- (26) Chowdhury, V.; Bühler, L.; Mistrangelo, C.; "Influence of surface oxidation on electric potential measurements in MHD liquid metal flows". *Fusion Engineering and Design* 89 (2014) 1299-1303.

(27) Ehrhard, S.; Buehler, L.; "Influence of magnetic field deformation by ferromagnetic wall materials on MHD flows in pipes and ducts of fusion blankets". *Fusion Engineering and Design* 89 (2014) 1451-1454.

(28) Köhly, C.; Tillack, M.S.; Wang, X.R.; Najmabadi, F.; Malang, S.; ARIES Team; "Comparison of possible flow distribution systems for PbLi self-cooled blankets with respect to MHD, fabrication, and maintenance". *IEEE Transactions on Plasma Science* 42 (2014) 516-523.

(29) Mistrangelo, C.; Bühler, L.; Aiello, G.; "Buoyant-MHD flows in HCLL blankets caused by spatially varying thermal loads". *IEEE Transactions on Plasma Science* 42 (2014) 1407-1412.

(30) Mistrangelo, C.; Bühler, L.; "Liquid metal magnetohydrodynamic flows in manifolds of dual coolant lead lithium blankets". *Fusion Engineering and Design* 89 (2014) 1319-1323.

(31) Mistrangelo, C.; Bühler, L.; "Magneto convective instabilities driven by internal uniform volumetric heating". Fundamental and Applied MHD: Thermo acoustic and Space Technologies; 9th PAMIR International Conference, Riga, LV, June 16-20. 2014, Proceedings Vol.1 pp.6-11, also on CD-ROM.

(32) Mistrangelo, C.; Bühler, L.; "Magnetoconvection in HCLL blankets". KIT Scientific Reports, KIT-SR 7672 (Juli 2014).

(33) Mistrangelo, C.; Bühler, L.; "MHD flow in a prototypical manifold of DCLL blankets". KIT Scientific Reports, KIT-SR 7673 (Juli 2014).

(34) Mistrangelo, C.; Bühler, L.; Mistrangelo, C.; Molokov, S.; "Validity of quasi-2D models for magneto-convection". Fundamental and Applied MHD: Thermo acoustic and Space Technologies; 9th PAMIR International Conference, Riga, LV, June 16-20. 2014, Proceedings Vol.1 pp.70-74, also on CD-ROM.

(35) Reimann, J.; Brun, E.; Ferrero, C.; Vicente, J.; "Pebble bed structures in the vicinity of concave and convex walls". 28th Symposium on Fusion Technology (SOFT 2014), San Sebastian, E, September 29 - October 3, 2014.

(36) Reimann, J.; Fretz, B.; Papeschi, S.; "Thermo-mechanical screening tests to qualify beryllium pebble beds with non-spherical pebbles". 28th Symposium on Fusion Technology (SOFT 2014), San Sebastian, E, September 29 - October 3, 2014, Book of Abstracts p. 561.

# Simulations of PHÉNIX Control Rod Withdrawal Tests with SIMMER-IV

Vladimir Kriventsev, Fabrizio Gabrielli, Marco Marchetti, Mattia Massone, Andrei Rineiski

## Abstract

“End-of-life” tests performed in the French PHÉNIX reactor before its final shutdown in 2009, in particular the Control Rod (CR) withdrawal experiments provide an opportunity for validation of computer codes. SIMMER-IV, a modern 3D reactor safety code, developed by JAEA, CEA, KIT and other partners has been employed at KIT/IKET for simulating the mentioned experiments. This benchmark activity was organized by IAEA. Other benchmark partners applied static neutronics codes, not coupled to thermal-hydraulics models. The study confirms that the SIMMER code can accurately predict major fast reactor neutronics and thermal hydraulic parameters, provided that a special treatment is employed for CR modeling.

## PHÉNIX Reactor Core Geometry Model and Meshing System

A 2D reactor model for SIMMER often includes the core pumps, heat exchangers and other in-vessel elements, but a full 3D modelling for the entire reactor vessel is time-consuming and unnecessary for the CR Withdrawal benchmark. Therefore the SIMMER-IV geometry model includes only the reactor core domain. The material distribution is represented by employing the mesh shown in Figure 1. Since SIMMER-IV utilizes the Cartesian XYZ geometry option, every hexagonal subassembly is modelled by two rectangular meshes in plane with the same areas as shown in the upper part of Figure 1. The trans-

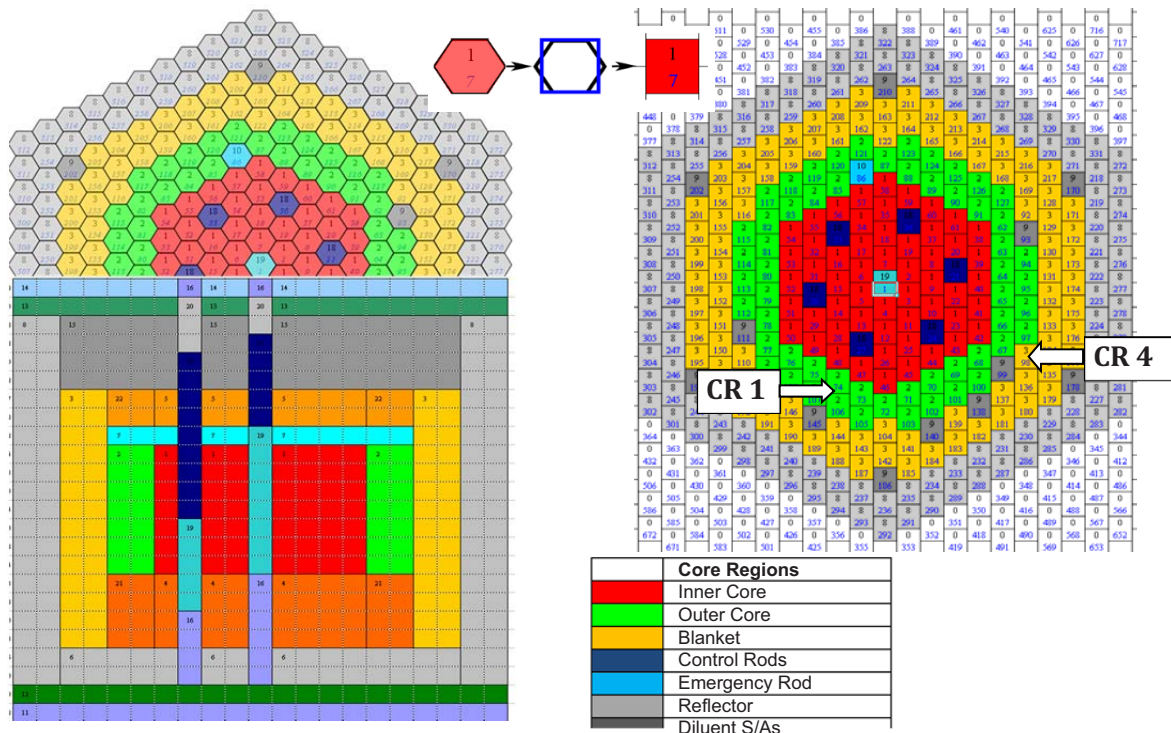


Fig. 1 SIMMER-IV X-Y-Z Mesh: Each Hexagonal S/A is Transformed in Two Rectangular Cells.

formation assures that the flow area and coolant flow rate in the rectangular mesh are conserved the same as in the original hexagonal subassembly. The thermal-hydraulics boundary conditions are the nominal inlet temperature, 380°C, and the inlet and outlet pressures. The inlet pressure is set up according to the input data set, while the outlet pressure is determined from the maximal coolant flow rate in reactor subassemblies (S/As). In SIMMER, the coolant flow rate is calculated on the basis of the boundary conditions, internal friction and hydraulic resistance of the S/As. Thus, proper orifice coefficients have to be assigned at S/A inlets to match the flow rate distribution given in the input data set.

## Results of Simulations and Discussion

### Control Rod Bank Reactivity Worth and Absorber Heterogeneity Modelling

After establishing the SIMMER model and evaluating the nominal steady-state conditions, the reactivity level for different CR positions was simulated. This was done by all benchmark participants and the results of the post-test calculations are shown in Figure 2. The SIMMER-IV result obtained with standard SIMMER computation options (-8701 pcm) overestimates the total CR bank reactivity worth as compared to the results of other benchmark participants. To improve our understanding and the SIMMER computation model, an additional study has been performed.

It has been found that the origin of the mentioned discrepancy mainly arises from the treatment of the neutron cross-sections (XSs), namely the heterogeneity effects are not taken into account in the XS processing. The adjustment of the Boron enrichment by  $^{10}\text{B}$  in the  $\text{B}_4\text{C}$  absorber of CR is one of the methods developed in the past to improve the accuracy in predicting control rod reactivity effects. Having this in mind, neutronics investigations of the PHÉNIX reactor have been performed at KIT also with the ERANOS code. ERANOS can employ a similar to SIMMER geometry model of CR and a more detailed one: to evaluate the factor to be applied to the  $^{10}\text{B}$  enrichment in SIMMER simulations.

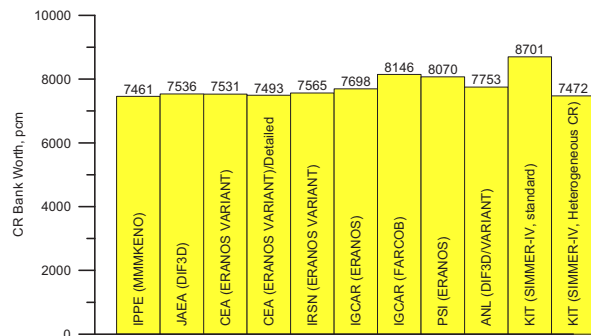


Fig. 2 Total Control Rod Bank Reactivity Worth

The updated SIMMER result for the CR bank reactivity worth is shown in the last column in Figure 2. One can see that taking into account of the absorber heterogeneity effect allows to get a SIMMER estimation that is very close to the ERANOS ones while the homogeneous CR model overestimates the total bank worth in the PHÉNIX reactor by about 1250 pcm that is in line with the heterogeneity effect value (~1500 pcm) obtained earlier also by other benchmark participants.

### Simulation of Power Shape Deformation in Experiment

The power shape deformation test phase was dedicated to study distorted radial power maps at a full power state. Opposite control rods CR #1 and CR #4 were progressively and slowly offset in relation to each other. The total power was kept constant by a uniform adjustment of all other control rods acting as a bank. Four configurations shown in Figure 3 have been simulated to create distorted radial power distributions.

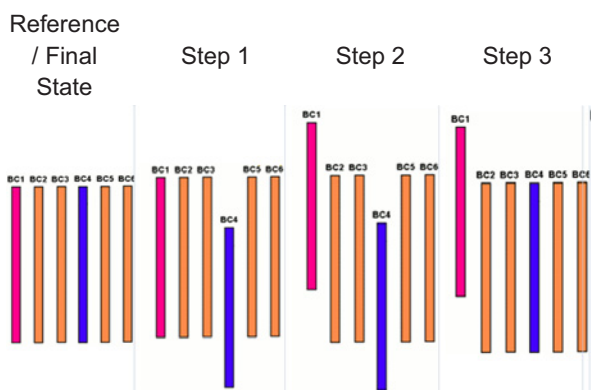


Fig. 3 Control Rod Withdrawal/Insertion in Experiment

The deviations of the maximal neutron flux (at the core mid-plane) from the reference state is shown in Figure 4. For the non-disturbed reference state, the maximum flux value  $\sim 3.90 \times 10^{15}$  (n/cm<sup>2</sup>·s) is reached in the second row fuel S/A (21/19 and 20/19). Among experimental steps, the maximal flux  $\sim 4.06 \times 10^{15}$  (n/cm<sup>2</sup>·s) is observed for Step 2 in the same S/A (20/19). The maximal deviation in the neutron flux (about -25%) is observed for Step 1 and Step 2. The detailed comparison of maximal neutron flux values given in Table 1 shows a good agreement between all codes used in the benchmark.

Table 1. Comparison on maximal neutron flux,  $\times 10^{15}$  n/cm<sup>2</sup>/s

	Refer-ence	Step-1	Step-2	Step-3	Final State
CEA (ERANOS)	3.94	4.02	4.07	3.99	3.94
IGCAR (ERANOS)	3.98	4.05	4.10	4.01	3.98
IGCAR (FARCOB)	4.02	4.10	4.14	4.06	4.02
IPPE (MMMKENO)	4.02	4.09	4.13	4.05	-
IRSN (ERANOS)	3.98	4.05	4.10	4.02	4.00
JAEA (DIF3D)	4.02	4.10	4.15	4.06	4.02
<b>KIT (SIMMER-IV)</b>	<b>3.90</b>	<b>4.00</b>	<b>4.06</b>	<b>3.96</b>	<b>3.90</b>
PSI (ERANOS)	3.95	4.07	4.11	3.99	-

The S/A power distributions for the reference case and three sequential CR withdrawal tests are shown in Figure 5 where S/As are numbered counter-clock-wise, starting from the core center according to the input data sheet. The maximal power reaches 3.91 MW (S/A 20/19) on Step 2. Obviously, the maximal power deviations about +/- 40% are observed for the inserted/withdrawn control rods CR #1 and CR #4. Among the fuel S/As, the maximal positive deviation is about 16% on Step 2 at the outermost ring of the inner core near the withdrawn control rod position (S/A 19/17). The maximal negative deviation -14% is observed in the inner core S/A (22/22) near the inserted control rod.

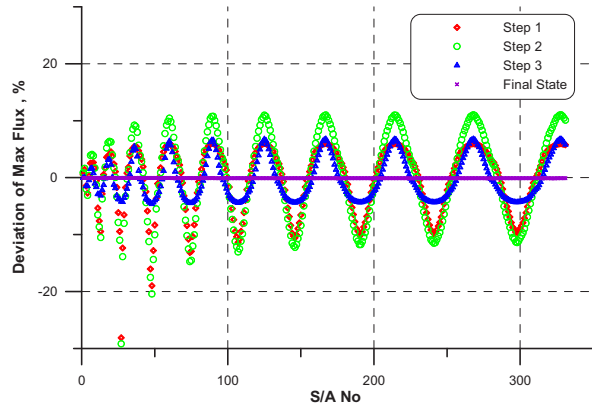


Fig. 4 Deviation of Maximal Neutron Flux for CR Withdrawal Test Steps

All codes used in the CR Withdrawal Test benchmark are capable to calculate the reactivity level and distributions of the neutron flux and power within the core. SIMMER-IV, as a coupled thermal-hydraulics and neutronics code, can - in addition to these parameters - predict coolant flow and temperature distributions. Figure 5 shows the distribution of the sodium outlet temperature for the all experiment steps.

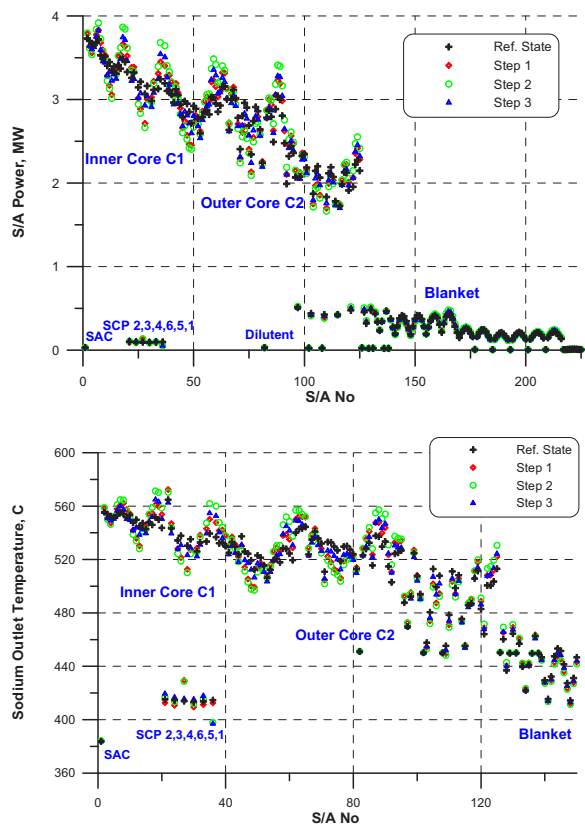


Fig. 5 Calculated Power per S/A [MW] and Outlet Coolant Temperature Distribution During Test Steps

The maximal temperature  $\sim 572^{\circ}\text{C}$  is reached in several S/As for Step 1 and Step 2. The highest relative change in the outlet temperature values is observed in inserted/withdrawn control rods channels SCP 4 and SCP 1 (SCP means "Système de Commande Principale").

## Conclusions

The "End-of-Life" tests performed in the PHÉNIX reactor in 2009 have been used for validation of SIMMER-IV, a modern 3D safety code. The code has been used for the simulations of Control Rod Withdrawal experiments and the results have been compared to those obtained with several other codes, not coupled to thermal-hydraulics models, in the framework of a IAEA benchmark. The simulation results show that the standard SIMMER model is capable to predict the reactor reactivity, power, and neutron flux distributions reasonably accurate. However, the efficiency of the control rods is overestimated. The reason is that the standard SIMMER cross-section generation procedure neglects heterogeneity (fine geometry) effects in the absorber rod sub-regions. To take the heterogeneity effects into account, a simple but accurate model has been introduced and verified.

The power distribution deformations in the four experimental test steps have been successfully reproduced with SIMMER-IV. The analyses confirm that the code is capable to predict the most important fast reactor neutronics parameters, provided that a special treatment is employed for CR modelling. The SIMMER-IV ability to simulate complex 3D reactor configurations has been demonstrated. The study contributes to SIMMER validation and verification activities. It has been published in IAEA-TECDOC-1742 and presented at international conferences.

## References

(1) Andriolo, L.; Rineiski, A.; Chen, X.N.; Maschek, W.; Gabrielli, F.; Delage, F.; Merle-Lucotte, E.; "Extension of the SIMMER code for the assessment of core thermal expansion feedbacks for transient analysis". International Youth Nucle-

ar Congress (IYNC), Burgos, E, July 6-12, 2014, Proceedings on USB-Stick.

(2) Andriolo, L.; Chen, X.N.; Matzerath Boccacini, C.; Maschek, W.; Rineiski, A.; Delage, F.; Merle-Lucotte, E.; "Preliminary safety analysis of sphere-pac fuels". ITU/INE Research Fellow Day, Karlsruhe, 6. Februar 2014.

(3) Chen, X.N.; Andriolo, L.; Rineiski, A.; Maschek, W.; "SIMMER-III modeling of gas cooled fast reactor". PHYSOR 2014 International Conference, Kyoto, J, September 28 - October 3, 2014, Proceedings on CD-ROM Paper 1106163.

(4) Chen, X.N.; Chen, Z.; Chen, H.; "Water-LBE flow similarity laws and their numerical experiments". Meyer, J.P. [Hrsg.], 10th International Conference on Heat Transfer, Fluid Mechanics and Thermodynamics (HEFAT 2014), Orlando, Fla., July 14-16, 2014, Proceedings on USB-Stick pp.2094-2100, ISBN 978-1-77592-068-7.

(5) Chen, Z.; Chen, X.N.; Rineiski, A.; Zhao, P.; Chen, H.; "Implementation into a CFD code of neutron kinetics and fuel pin models for nuclear reactor transient analyses". 10th International Topical Meeting on Nuclear Thermal-Hydraulics, Operation and Safety (NUTHOS 2014), Okinawa, J, December 14-18, 2014, Proceedings on USB-Stick Paper NUTHOS10-1203.

(6) Gabrielli, F.; Rineiski, A.; Marchetti, M.; Massone, M.; Kriventsev, V.; "Study of the effect of heterogeneity of the control rods in the PHÉNIX reactor". PHYSOR 2014 International Conference, Kyoto, J, September 28 - October 3, 2014, Proceedings on CD-ROM Paper 1106079.

(7) Kriventsev, V.; Rineiski, A.; Maschek, W.; "Application of safety analysis code SIMMER-IV to blockage accidents in FASTEF subcritical core". *Annals of Nuclear Energy* 64(2014) 114-121.

(8) Kriventsev, V.; "Application of minimal energy dissipation principle to turbulence modeling". 10th International Topical Meeting on Nuclear Thermal-Hydraulics, Operation and Safety (NUTHOS 2014), Okinawa, J, December 14-18, 2014, Proceedings on USB-Stick Paper NUTHOS10-1122.

- (9) Kriventsev, V.; Gabrielli, F.; Rineiski, A.; "Coupled thermal-hydraulic and neutronic simulation of Phenix control rod withdrawal tests with SIMMER-IV". 10th International Topical Meeting on Nuclear Thermal-Hydraulics, Operation and Safety (NUTHOS 2014), Okinawa, J, December 14-18, 2014, Proceedings on USB-Stick Paper NUTHOS10-1123.
- (10) Kriventsev, V.; Gabrielli, F.; Rineiski, A.; "Simulation of PHENIX control rod withdrawal experiments with SIMMER-IV". PHYSOR 2014 International Conference, Kyoto, J, September 28 - October 3, 2014, Proceedings on CD-ROM Paper 1104108.
- (11) Li, R.; Chen, X.N.; Boccaccini, C.M.; Rineiski, A.; Maschek, W.; "Fuel dispersion after pin failure of MYRRHA-FASTEF critical core". SEARCH/MAXSIMA International Workshop, Karlsruhe, October 7-10, 2014, Proceedings published online.
- (12) Li, R.; Wang, S.; Rineiski, A.; Zhang, D.; Merle-Lucotte, E.; "Transient analyses for molten salt fast reactor with optimised core geometry". International Youth Nuclear Congress (IYNC), Burgos, E, July 6-12, 2014, Proceedings on USB-Stick.
- (13) Marchetti, M.; Vezzoni, B.; Gabrielli, F.; Rineiski, A.; "Neutron deterministic models of the EBR-II SHRT-45R core configuration". *Transactions of the American Nuclear Society* 111 (2014) 1188-1190.
- (14) Marchetti, M.; Gabrielli, F.; Rineiski, A.; Maschek, W.; "The SIMMER/PARTISN capability for transient analysis". PHYSOR 2014 International Conference, Kyoto, J, September 28 - October 3, 2014, Proceedings on CD-ROM Paper 1104619.
- (15) Massone, M.; Wang, S.; Li, R.; Rineiski, A.; "Safety analysis of liquid fuel fast reactor system". ITU/INE Research Fellow Day, Karlsruhe, 6. Februar 2014.
- (16) Massone, M.; Gabrielli, F.; Rineiski, A.; "SIMMER extension for cross-section collapsing introduction". International Youth Nuclear Congress (IYNC), Burgos, E, July 6-12, 2014, Proceedings on USB-Stick.
- (17) Pascal, V.; Prulhiere, G.; Vanier, M.; Fontaine, B.; Devan, K.; Chellapandi, P.; Kriventsev, V.; Monti, S.; Mikityuk, K.; Chenu, A.; Semenov, M.; Taiwo, T.; Takano, K.; Tiberi, V.; "IAEA benchmark calculations on control rod withdrawal test performed during PHENIX and end-of-life experiments. Benchmark results and comparisons". PHYSOR 2014 International Conference, Kyoto, J, September 28 - October 3, 2014, Proceedings on CD-ROM Paper 1096461
- (18) Vezzoni, B.; Gabrielli, F.; Rineiski, A.; Schwenk-Ferrero, A.; Andriolo, L.; Maschek, W.; "Innovative TRU burners and fuel cycles options for phase-out and regional scenarios". 13th Information Exchange Meeting on Actinide and Fission Product Partitioning and Transmutation, Seoul, Korea, September 23-26, 2014.
- (19) Benchmark Analyses on the Natural Circulation Test Performed during the PHENIX End-of-life Experiments, IAEA TECDOC No. 1703, (<http://cra.iaea.org/cra/stories/2013-10-16-TECDOC-1703-I33012.html>) (2013).



Group: Accident Analysis

## Analysis of Design Basis and Severe Accidents

*Alexei Miassoedov, Giancarlo Albrecht, Thomas Cron, Philipp Dietrich, Beatrix Fluhrer, Jerzy Foit, Stephan Gabriel, Xiaoyang Gaus-Liu, Frank Kretzschmar, Josef Nawrath, Markus Schwall, René Stängle, Thomas Wenz*

### Introduction

The analysis of severe accidents in LWRs at IKET-UNA is focused on the in- and ex-vessel core melt behavior. The overall objective is to investigate the core melt scenarios from the beginning of core degradation to melt formation and relocation in the vessel, possible melt dispersion to the reactor cavity and to the containment, and finally corium concrete interaction and corium coolability in the reactor cavity.

The experimental platform includes three experimental facilities:

- LIVE to investigate the melt pool behavior in the RPV lower head;
- DISCO to study the melt dispersion to the reactor cavity and direct containment heating;
- MOCKA to study molten corium concrete interaction.

The results of the experiments are being used for the development and validation of codes applied for safety assessment and planning of accident mitigation concepts, such as MELCOR and ASTEC. The strong coupling between the experiments and analytical activities contribute to a better understanding of the core melt sequences and thus improve safety of existing reactors by severe accident mitigation measures and by safety installations where required.

The understanding of major processes for the assessment of the plant response and behaviour under design basis or beyond design basis situations still have to be further developed. For this purpose, experimental investigations are carried out in the WENKA and COSMOS facilities addressing the thermal-hydraulics and physico-chemical

phenomena during postulated design and beyond design transients and accidents.

### LIVE experiments

The main objective of the LIVE program is to study the late in-vessel core melt behavior and core debris coolability both experimentally in large scale 2D and 3D geometry and in supporting separate-effects tests, and analytically using CFD codes in order to provide a reasonable estimate of the remaining uncertainty band under the aspect of safety assessment. The LIVE-3D test facility allows the investigation of a melt pool in the lower plenum of a RPV in 3D geometry with simulated internal heat generation. Other test facilities had only a 2D geometry or were performed without heating of the melt. The main part of the LIVE-3D test facility is a 1:5 scaled semi-spherical lower head of the typical pressurized water reactor.

The diameter of the test vessel is 1 meter. The top area of the vessel is covered with an insulation lid. The test vessel is enclosed in a cooling vessel to simulate the external cooling. The melt is prepared in an external heating furnace designed to generate 220 l of the simulant melt. The volumetric decay heat is simulated by 6 spirally formed heating elements providing a maximum power of about 28 kW. To investigate both the transient and the steady state behavior of the simulated corium melt, an extensive instrumentation of the test vessel is realized. The temperatures of the vessel wall inner surface and outer surface are measured at 5 latitudes and 4 locations at each latitude. Heat flux distribution through the vessel wall can be calculated based on these temperatures. Additionally, 80 thermocouples are positioned within the vessel to measure

the temperature distribution in the melt pool and in the crust.

Three LIVE-3D experiments were performed in 2014. In the LIVE-L8C test the melting process of a debris bed with materials having different melting temperature was investigated. In the LIVE-L11 and LIVE-L11TC experiments the heat transfer in a melt pool with boiling water as external cooling medium was studied.

The debris bed in the LIVE-L8C experiment was composed of a homogeneous mixture of a low melting temperature non-eutectic of 20 mol.%  $\text{NaNO}_3$  - 80 mol.%  $\text{KNO}_3$  and granite particles, each amounted 50% of volume fraction (Fig. 1, top). The height of the debris bed was 400 mm. The test vessel was insulated at the top. External cooling with water was performed after the phase of preheating debris. In addition to the temperature measurements, possibility of post-test visual observation inside the debris bed was realized using seven steel tubes as place holders, which were inserted in the debris bed at different radial positions. The test started with preheating of the debris bed to the temperature slightly below the melting temperature of the nitride mixture. Thereafter the power was increased stepwise and progressive melting of the nitride particles inside the debris bed was observed.

During the preheating of debris bed, the low thermal conductivity of debris ( $\sim 0.25 \text{ W/(mK)}$ ) resulted in a low power input rate and large temperature gradient in the debris. The maximum temperatures were located at a height of about 300 mm. In the second phase of the experiment the power was increased to 15 kW. The low melting temperature nitride particles started to melt and the molten material was relocated to the lower part of the debris bed. Some 47 min after the initiation of second phase the upper layer of the debris bed collapsed due to the void generation inside the debris bed. The breakdown of the upper debris layer continued during approximately one hour and the central area of the top two planes of heating elements was uncovered (Fig. 1, bottom). After switching of the uncovered heating elements the residual power in second phase was reduced to 7 kW to achieve the temperature steady state condition. In the third phase of the test the power was increased from 7 kW to 10 kW. During the second and third phases the nitride particles were molten in the upper debris

bed region whereas a thin loose debris layer preserved its form on the lower area near to the vessel wall. Increasing the total power inside the debris bed intensified the heat flux focusing effect in the vessel wall area where the molten pool had direct contact with the vessel wall.

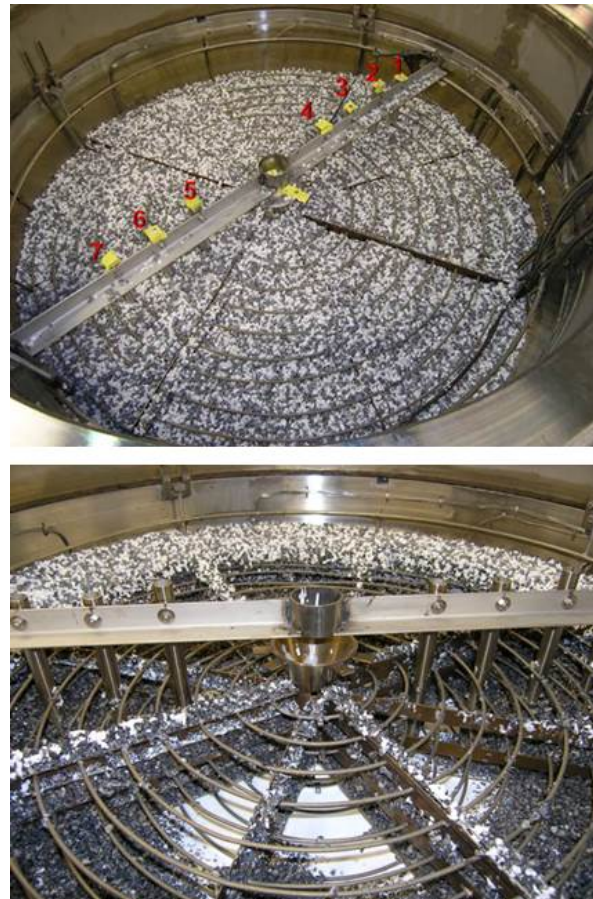


Fig. 1: Debris bed before (top) and after (bottom) the LIVE-L8C test.

The experiments LIVE-L11 and LIVE-L11TC were series of tests in which the molten pool thermohydraulic behaviour was studied under external boiling water conditions. The boundary conditions at the top were different in the two tests: in the LIVE-L11 adiabatic conditions at the melt upper surface were realised, whereas in the LIVE-L11TC the molten pool surface was water cooled. The cooling water level outside the test vessel was slightly above the melt surface and was remained constant during the test by means of compensation of steam evaporation with a small inflow rate at the cooling vessel bottom. The results of the two tests were compared with previous tests with similar heat generation and melt pool conditions except that subcooled water was used for the external cooling. In both LIVE-L11 and LIVE-L11TC tests the heat flux near the

melt surface was higher compared to the previous tests with subcooled water. One of the possible reasons can be the reduced heat conduction inside the vessel wall, since the constant temperature on the wall outer surface led to a lower temperature gradient parallel to the wall orientation.

## DISCO experiments

Ex-vessel Fuel Coolant Interaction (FCI) and debris formation are two high-priority issues. Despite the importance of these issues the database for premixing modelling assessment for application of ex-vessel situation is very limited. There is no possibility to assess the behavior with existing database from e.g. FARO L31 (ISPRA) and TROI-VISU (KAERI, SERENA) experiments. Both are gravity driven melt jets with high density and high temperature and a water subcooling of ~50K. In collaboration with the Institut de Radioprotection et de Sûreté Nucléaire (IRSN) three tests (plus one in the frame of LACOME) in the DISCO-H facility were performed.

The generic representation of the DISCO facility and the arrangement of the reactor pit zone are shown in Fig. 2. The DISCO facility is composed of several parts simulating the containment, the reactor coolant system (RCS), the reactor pressure vessel (RPV), the pit and sub-compartment. The containment geometry characteristic is related to a French P4 reactor with a length scale of approximately 1:10 but it does not reproduce precisely a given reactor. The pit zone was modified in order to obtain a large water pool. The corium melt is simulated by a thermite iron-alumina melt with initial temperature of about 2400 K, obtained from a thermite reaction initiated directly inside the RPV vessel a few seconds before its delivery to the pit through a nozzle. The delivery occurs as a result of the melting of a brass fuse inside the nozzle. Before the delivery, the vessel pressure can be adjusted through a steam accumulator placed outside of the containment vessel and connected to the RCS vessel. To be conservative the tests were performed with a central hole at the lower bottom head. The nozzle diameter was set to 0.060 m (0.030 m in

case of the LACOME experiment) corresponding roughly to 0.60 m (0.30 m) at reactor scale. The gas initial composition in the DISCO containment can be modelled by different mixtures of air, steam and hydrogen. The water level in the reactor pit was set to ~0.54 m, just below the nozzle outlet. The water temperature at the beginning of the test was set to 85 °C to keep the subcooling in the range close to the expected one during the accident.

The major issues addressed in the experiments were the investigation of melt fragmentation processes for high velocity melt jets through a precise analysis of the size of the debris found. The debris bed characteristics are important for its coolability. The pressurization of the pit and the containment and the hydrogen production and combustion provide information for assessing the load on structures. The melt and water dispersion out of the pit during the process are initial conditions for MCCI. To investigate the impact of water on hydrogen production and combustion, the data were compared with those of the dry DCH tests.

The global pressurization of the containment increased up to 0.12 MPa. The pressure in the cavity was characterized by several small peaks. Only in the latest experiment (FCI-6) a steam explosion was observed with a short peak up to 29 MPa (Fig. 3). The water inside the cavity (initially 125 kg) has been totally ejected. Concerning the debris, of the initial melt mass (15.6 kg thermite melt plus 1.0 kg molten steel) up to 16 % remained in the RCS/RPV vessel, 60 % remained in the cavity mainly as compact crusts, 32 % in the case of FCI-6. The fraction of melt transported to subcompartment and containment were about 9 to 15 % and 44 % (FCI-6) respectively. The size distribution supplied by sieve analysis indicated a tendency to small particles. A Sieve Mean Mass Diameter (SMMD) of 0.65 mm and 0.2 mm (FCI-6) were determined in comparison to the dry DCH tests with a SMMD of 0.8 mm to 1.3 mm. The results of the experiment shall be compared with calculations of the MC3D code at IRSN.

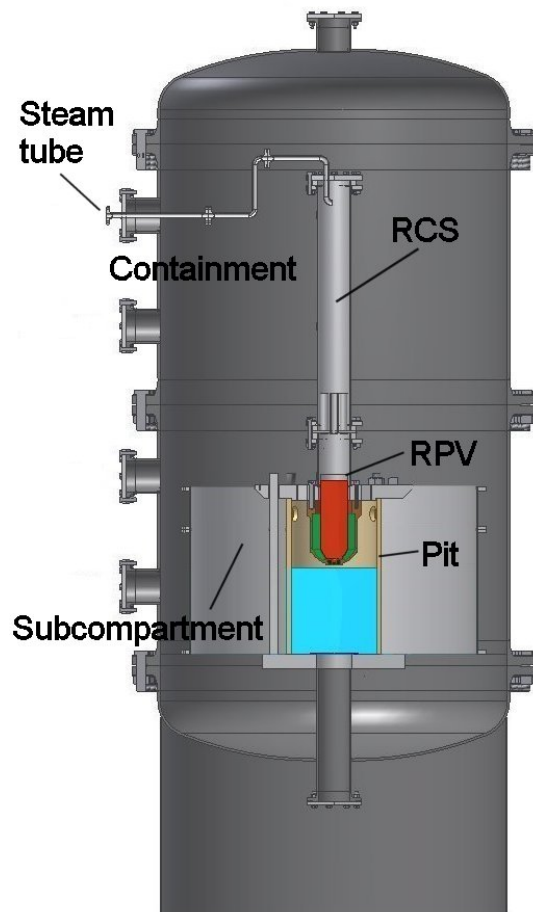


Fig. 2: Scheme of the DISCO facility.

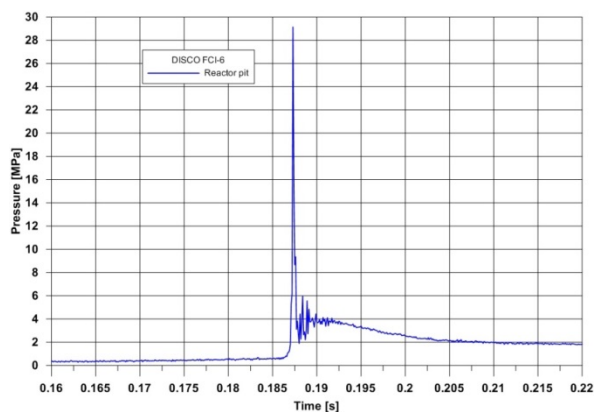


Fig. 3: Pressure peak of 29 MPa in the cavity

## MOCKA experiments

The MOCKA facility is designed to investigate the corium/concrete interaction in an anticipated core melt accident in LWRs, after the metal melt is layered beneath the oxide melt. The experimental focus is on the cavity formation in the basemat and the risk of a long-term basemat penetration by the metallic part of the melt.

In all MOCKA experiments a cylindrical concrete crucibles with an inner diameter of 25 cm are used. Both the sidewall and basemat were instrumented with Type K thermocouple assemblies to determine the concrete erosion as a function of time. The initial melt consists of 42 kg Fe together with 4 kg Zr, overlaid by 68 kg oxide melt (initially 56 wt.%  $\text{Al}_2\text{O}_3$ , 44 wt.%  $\text{CaO}$ ). The initial height of the metal melt was about 13 cm. The melt temperature at start of interaction was approximately 2273 K. The initial temperature was estimated from the reaction enthalpy of the used thermite taking into account the temperature measurements from the former BETA tests. The CaO admixture lowers the solidus temperature and the viscosity of the oxide melt. The resulting solidus temperature of approx. 1633 K is sufficiently low to prevent a formation of an initial crust at the oxide/concrete. The internal heat generation in the oxide phase is simulated by a succession of additions of pure thermite and Zr metal to the melt from the top being the first of a kind heating method realized for high temperature melts worldwide. The heat generated by the exothermal oxidation reactions of the continuously added Zr is deposited in the oxide phase. Due to density-driven phase segregation the metal melt at the bottom of the crucible is fed by the enthalpy of the Fe melt which is generated in the oxide phase by the thermite reaction of the added thermite. Approximately 80 % of the heating power was deposited in the oxide phase and 20 % in the iron melt. In this way a prototypic heating of both melt phases was achieved.

An important finding from the MOCKA tests with limestone/common sand (LCS) concrete is that the cavity erosion behaviour is different in comparison to the CCI-2 test performed at Argonne National Laboratory with the same type of concrete. MOCKA tests in the LCS concrete crucibles exhibited a highly pronounced lateral ablation. The lateral/axial ratios of the ablation depth for the MOCKA tests are approximately 3 in contrast to 1 estimated for the CCI-2 experiment. MOCKA tests on siliceous concrete without rebar have shown more pronounced downward erosion by the metal melt. The post-test section of the MOCKA 6.3 concrete crucible is shown in the Fig. 4. The final maximum downward erosion was 50 mm, the lateral erosion by the metal melt was 120 mm and the final ablation by the overlying oxide exceeded 120 mm. Approximately 75 % of the heating power is deposited in the oxide

phase and 25 % in the metal melt. In this way a rather prototypic heating of both melt phases can be achieved. The power input was estimated to be 454 kW to the oxide melt and 142 kW to the metal melt.



Fig. 4: Section of the MOCKA 6.3 concrete crucible with an indication of the initial size of the crucible. The orange line indicates the initial height (13 cm) of the metal melt and the red line marks the outer surface of the LCS cylindrical crucible.

The efficient heat transfer from the metal melt leads to a fast decrease in temperature (Fig. 5), therefore, the concrete ablation will be influenced by crust formation processes. The progression of the concrete erosion found in MOCKA 6.3 test is depicted in Fig. 6. During the early phase of the interaction, the observed low erosion rate of 0.7 mm/min is a consequence of the formation of a stable crust at the metal/concrete interface. This low concrete erosion rate gave rise to a considerable heat-up of a rather thick layer of concrete behind the slowly moving melt front. Decomposition of concrete during heat-up starts with evapo-

ration of physically bound water around 100 °C. Dehydration of chemically bound water occurs up to 550 °C. Decarbonation of  $\text{CaCO}_3$  from the cement and carbonate aggregates occurs from 700 to 900 °C. Liquid phases start to form between 1100-1250 °C. The subsequent increase of the temperature and of the mass of the metal melt due to the continuous addition of thermite caused a melting of the crust at about 1700 s and, consequently, a start of a somewhat faster progression into the thermally damaged concrete. A maximum lateral progression of approx. 6 mm/min of the metal melt front was estimated. Similar behaviour, i. e. a fast removal of a thermally destructed concrete was also observed in experiments which were performed within the SURC, ACE and CCI programs as well as in other MOCKA tests.

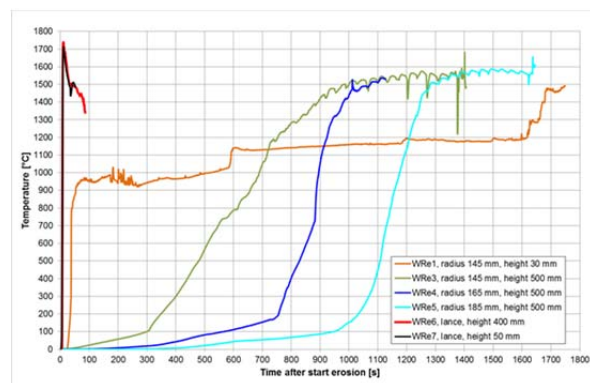


Fig. 5: Melt temperatures at different positions as a function of time in the MOCKA 6.3 test.

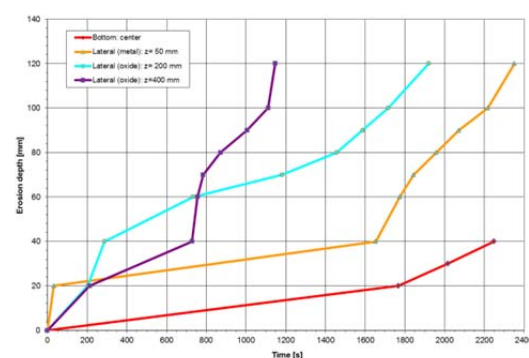


Fig. 6: Erosion depth as a function of time in the MOCKA 6.3 test

## COSMOS experiments

The objective of the COSMOS (Critical-heat-flux On Smooth and Modified Surfaces) experiments is to study the influence of safety-relevant com-

ponents of light water reactors (fuel assemblies, grid spacers etc.) on heat removal, boiling crisis, pressure loss and other important issues. The focus is on how these parameters are influenced by the material properties of the structures. New measurement technologies like fiber optic void sensors will be used to provide qualified data for the development and validation of physical correlations used in the systems codes and for the validation of detailed CFD codes in the long-term. The focus shall be on the use of up to date and innovative measurement techniques (e.g. LDA, PIV, high-speed cameras) of high spatial and temporal resolution and the possibility of their use in applications involving high temperatures and pressures.

The water loop for flow boiling heat transfer experiments at low pressure COSMOS-L was constructed and put into operation. A comprehensive series of two-phase flow experiments was successfully completed. The influence of the rod surface structure on critical heat flux (CHF) for flow boiling of water was investigated for Zircaloy tubes in a vertical annular test section. Though only a small influence of surface structures on critical heat flux was observed for the pressure of 120 kPa in the COSMOS-L test section the increase of CHF value is expected to be more pronounced (up to 30%) at higher pressure for certain clad surface modifications, like oxide layers, formed on the clad surface of operating fuel rods.

To quantify these phenomena for high pressures with an objective of increasing the safety margin to the start of the boiling crisis in prototypic conditions, the COSMOS-H experimental facility is being constructed. The facility consists of a high-pressure water loop and two cooling circuits and is designed for investigations of the CHF under non-scaled thermohydraulic conditions. The test section of the facility is approximately 3.7 m high and includes an outer pressure tube, which encloses the test fuel rod bundle guided by a circular or rectangular separation tube. The test section consists of several segments including those that are specially designed for the visual analysis of the flow. The modular construction of the section allows different vertical positioning of these special segments depending on the experimental conditions and test requirements (Fig. 7). To test and approve the test section design a single cladding tube will be used in the first experi-

ments. In the future tests larger fuel rod bundles of 2x2, 3x3 and hexagonal arrangements will be included in the study.

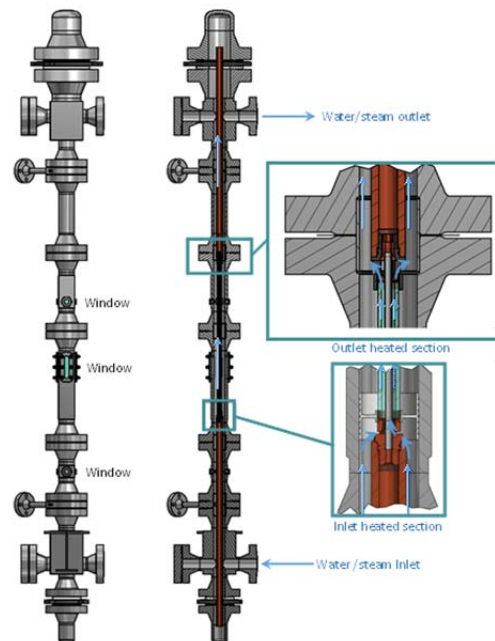


Fig. 7: Scheme of the COSMOS-H test section

The low pressure loop COSMOS-L was used in 2014 mostly for testing the high pressure COSMOS-H concept, material selection and instrumentation for the test section of the COSMOS-H facility.

## WENKA experiments

The WENKA channel (Water Entrainment channel Karlsruhe) serves the investigation of counter-current stratified two-phase flows. These complex flow phenomena are relevant in accident scenarios of pressurized water reactors like the reflux condensation mode after a Loss Of Coolant Accident (LOCA). The objective of the experimental work is the provision of detailed datasets for development and validation of turbulence and phase interaction models for the CFD codes for which local measurements of various flow parameters with high spatial resolution are required. The WENKA channel has a modular construction concept and operates under ambient conditions. Water and air flow rates can be controlled in a wide range. The current configuration allows the observation of different flow regimes, such as supercritical flow, supercritical

flow with droplet entrainment, partially reversed flow and fully reversed flow. These flow regimes include flow phenomena like hydraulic jumps, bubble and droplet entrainment and propagation of capillary and gravity waves.

For the measurements advanced optical methods are used such as intrusive devices. The velocity and velocity-fluctuation profiles are measured by particle image velocimetry (PIV). For measurement in water fluorescent tracer particles are used to suppress reflections at the liquid surface. To provide high-resolved void fraction data a special method was developed. The method uses sequences of high speed images to calculate a 2D distribution of the volumetric void fraction. After the image post-processing the probability of existence of a two-phase region is calculated by averaging over a period of 16 s; the void fraction is then calculated by integration of the intensity values. The validation of the method was performed by comparing its results to the electric needle probe data, demonstrating a measurement uncertainty of 8.6 %. Using these and other instruments an extensive database containing high-speed movies, flow maps, turbulence and velocity data including droplet mass flow has been obtained within the last three years. The measurement data can be directly compared with the results of CFD simulations.

### Application of the MELCOR code

The severe accident code MELCOR is used at IKET-UNA to investigate hypothetical core melt accidents in nuclear power plants.

Since 2010 IKET-UNA works together with EON, RWE and EnBW in the frame of a VGB service contract. The main goal of the collaboration is to clarify the influence of the uncertainties in modelling of several reactor components in MELCOR on the results of the analysis. Several LOCA scenarios were analysed for a KONVOI-type plant using data sets provided by several German institutions. The focus was on the influence of the modelling of the core region on the hydrogen production and the failure mode of the reactor pressure vessel.

The difference in modelling of the lower core plate behavior is given here as an example. Two

cases were considered, the first one where the core plate was thermally connected to the reactor lower plenum and the second one without the thermal exchange. The scheme used for the analysis is shown in Fig. 8. Ten different modelling options were investigated, however, mainly the thermal resistance of the core plate was influenced, since the plate can be cooled by the water present in the lower plenum in the first case (in the CV020 node).

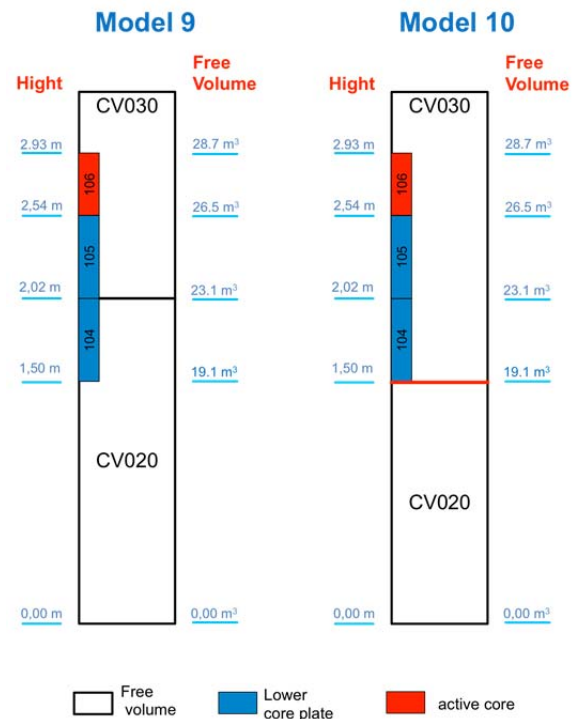


Fig. 8: Modelling of the lower core plate

The analysis of the molten core material relocation to the region of the core plate and the lower plenum are given in Fig. 9. The MELCOR code predicts a significantly lower core melt mass in the lower plenum in the first case. The main reason is that due to the cooling of the core plate the crusts form at the core structures preventing the further molten material relocation. This leads to larger masses remaining in the core region.

In order to improve the MELCOR code predictions IKET-UNA participates in the WASA-BOSS project, which is supported by the Federal Ministry of Education and Research. In this project the new models with a more detailed description of molten core material behaviour in the lower plenum are to be coupled to MELCOR. The coupling of new models to MELCOR is realised by the program DINAMO (Direct Interface for Adding Models). This program was developed at the

IKET-UNA and contains coupling routines based on the Message Passing Interface (MPI) standard to communicate with the coupling interface in MELCOR 1.8.6 as well as an interface for the implementation of new models. Using DINAMO it is possible to use new or additional models in MELCOR without the necessity of the complex modification of the MELCOR source code to implement the models.

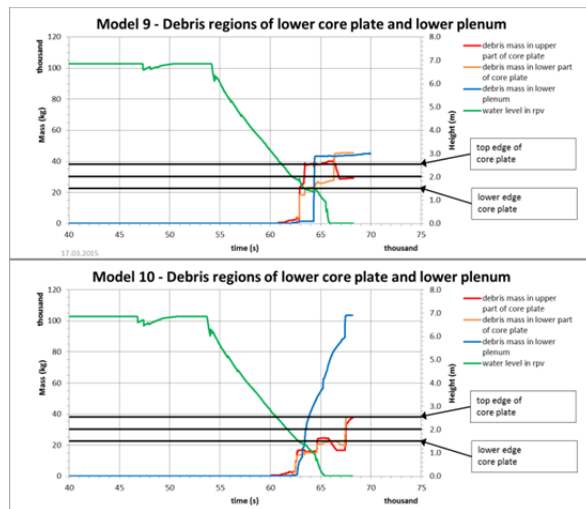


Fig. 9: Relocation of the molten material with (top) and without (bottom) cooling of the core plate by water in the lower plenum

The Phase-Change Effective Convectivity Model (PECM) was developed at the Royal Institute of Technology (KTH) in Sweden. This model can simulate the behavior of molten core material in the lower plenum more accurately than MELCOR. Instead of solving the momentum and mass transport equation for the molten corium, the PECM considers only the energy conservation equation. The convective currents, which occur due to the internal heating by the decay heat and the applied cooling conditions of the molten core material, are approximated in the PECM by characteristic velocities, which are determined by empirical correlations. In cooperation with the KTH the PECM was implanted in the CFD code OpenFOAM. Using the interface for the communication with OpenFOAM in DINAMO it is now possible to use the PECM for the calculation of molten core material in the lower plenum of a RPV in MELCOR. The coupling process between MELCOR, DINAMO and the PECM in OpenFOAM via the communication program MPIEXEC is shown in Fig. 10.

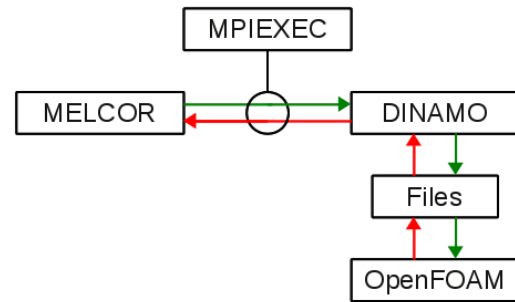


Fig. 10: Scheme of the coupling process used for the implementation of the PECM in MELCOR

Based on the implementation of the PECM in MELCOR the analysis of the IKET-UNA LIVE experiments was performed. In the Fig. 11 the temperature of the molten material in the LIVE-L1 test during the steady state phase at a heating power of 10 kW is presented. The temperature calculated by the stand-alone MELCOR code is higher than the temperature measured in the experiment. In the contrary to MELCOR, which treats the molten material in the lower head as a uniform continuum with uniform properties, with a coupled PECM it is now possible to obtain a local temperature distribution in the molten material.

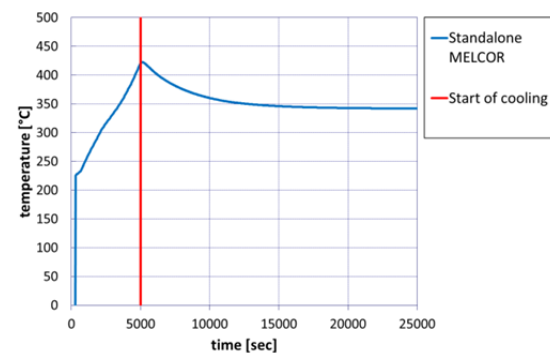


Fig. 11: Temperature evolution in the LIVE-L1 test calculated by MELCOR

The comparison between the temperatures calculated by the PECM and the data obtained in the LIVE-L1 test are shown in Fig. 12.

Using the local temperature distribution allows the estimation of the thickness of the crust formed at the vessel wall at the end of the test. In MELCOR the crust behaviour is not modelled.

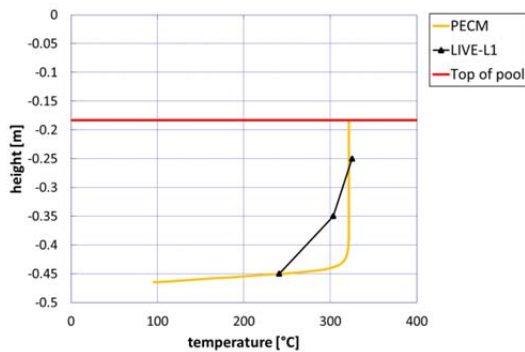


Fig. 12: Temperature profile calculated by the PECM code compared to the experimental findings in LIVE-L1

Using DINAMO to couple the PECM to MELCOR in order to simulate the behaviour of the molten core material in the lower head has significantly improved the details and the accuracy of the simulation results. Coupling new models to MELCOR is a way to improve the prediction of a hypothetical accident progression which will contribute to the development and optimization of safety measures in nuclear power plants.

## References

- (1) Cranga, M.; Spengler, C.; Atkhen, K.; Fargette, A.; Fischer, M.; Foit, J.; Gencheva, R.; Guyez, E.; Haquet, J.F.; Journeau, C.; Michel, B.; Mun, C.; Piluso, P.; Sevon, T.; Spindler, B.; "Towards an European consensus on possible causes of MCCI ablation anisotropy in an oxidic pool". *Annals of Nuclear Energy* 74(2014) 72-88.
- (2) Dietrich, P.; Gabriel, S.; Kretzschmar, F.; Miassoedov, A.; Class, A.; "Expansion of the model-basis in MELCOR". Jahrestagung Kerntechnik, Frankfurt, 6.-8.Mai 2014, Berlin: INFORUM GmbH, 2014 CD-ROM, ISBN 978-3-926956-99-6.
- (3) Fluhrer, B.; Miassoedov, A.; "SAFEST: towards a pan-European laboratory on corium experimental R&D". 20th International QUENCH Workshop, Karlsruhe, November 11-13, 2014, Steinbrück, M. [Hrsg.], Proceedings of the 20th International QUENCH Workshop, Karlsruhe, November 11- 13, 2014, Karlsruhe: Karlsruhe Institute of Technology, Campus North, 2014, ISBN 978-3-923704-88-0.
- (4) Foit, J.J.; Fischer, M.; Journeau, Ch.; Langrock, G.; "Experiments on MCCI with oxide and steel". *Annals of Nuclear Energy* 74 (2014) 100-109.
- (5) Foit, J.J.; "MCCI of a metal and oxide melt with reinforced siliceous concrete in MOCKA experiments". 22nd International Conference on Nuclear Engineering (ICONE22), Praha, CZ, July 7-11, 2014, Proceedings on DVD Paper ICONE 22-30200, New York, N.Y.: ASME, 2014.
- (6) Gabriel, S.; „Experimentelle Untersuchung der Tropfenabscheidung in einer horizontalen, entgegen gerichteten Wasser/Luft-Schichtenströmung“. Helmholtz-Zentrum Dresden-Rossendorf, 27. März 2014.
- (7) Kienzler, B.; Borkel, C.; Finck, N.; Heck, S.; Hilpp, S.; Schlieker, M.; Metz, V.; Plaschke, M.; Soballa, E.; Cron, T.; Miassoedov, A.; "Characterization and radionuclide retention properties of heat-treated concrete". *Physics and Chemistry of the Earth* 70-71(2014) 45-52.
- (8) Klein-Heßling, W.; Sonnenkalb, M.; Jacquemain, D.; Clement, B.; Raimond, E.; Dimmelmeier, H.; Azarian, G.; Ducros, G.; Journeau, C.; Herranz Puebla, L E.; Schumm, A.; Miassoedov, A.; Kljenak, I.; Pascal, G.; Bechta, S.; Güntay, S.; Koch, M.K.; Ivanov, I.; Auvinen, A.; Lindholm, I.; "Conclusions on severe accident research priorities". *Annals of Nuclear Energy* 74 (2014) 4-11.
- (9) Meignen, R.; Raverdy, B.; Buck, M.; Pohlner, G.; Kudinov, P.; Ma, W.; Brayer, C.; Piluso, P.; Hong, S. W.; Leskovar, M.; Ursic, M.; Albrecht, G.; Lindholm, I.; Ivanov, I.; "Status of steam explosion understanding and modelling". *Annals of Nuclear Energy* 74 (2014) 125-153.
- (10) Meyer, L.; Albrecht, G.; Kirstahler, M.; Schwall, M.; Wachter, E.; "Large scale separate effects test on hydrogen combustion during direct containment heating events". KIT Scientific Report, KIT-SR7663 (April 2014).
- (11) Miassoedov, A.; Albrecht, G.; Meyer, L.; Meignen, R.; "Ex-vessel fuel coolant interaction experiment in the DISCO facility in the LACOME-CO project". 10th International Topical Meeting on Nuclear Thermal-Hydraulics, Operation and Safety (NUTHOS 2014), Okinawa, J, December 14-18, 2014, Proceedings on USB-Stick Paper NUTHOS10-1100.

- (12) Miassoedov, A.; Gaus-Liu, X.; Cron, T.; Fluhrer, B.; "LIVE experiments on melt pool heat transfer in the reactor pressure vessel lower head". Meyer, J.P. [Hrsg.], 10th International Conference on Heat Transfer, Fluid Mechanics and Thermodynamics (HEFAT 2014), Orlando, Fla., July 14-16, 2014, Proceedings on USB-Stick pp.2078-2086, ISBN 978-1-77592-068-7.
- (13) Miassoedov, A.; Foit, J.; Cron, T.; "MOCKA experiments on MCCI of metal and oxide melt with siliceous concrete". Transactions of the American Nuclear Society, 111 (2014) 979-981.
- (14) Miassoedov, A.; Stuckert, J.; Tromm, W.; "Overview of severe accident research at the Karlsruhe Institute of Technology". International Workshop on Nuclear Safety and Severe Accident (NUSSA 2014), Chiba, J, September 3-5, 2014.
- (15) Miassoedov, A.; "SAFEST: Towards a pan-European laboratory on corium experimental R&D". PLINIUS 2 International Seminar, Marseille, F, May 16, 2014
- (16) Pitz, P.; Zeismann, F.; Brueckner-Foit, A.; Foit, J.; Mattheis, B.; Vesper, T.; "Analysis of the crack opening displacement of a surface crack using X-ray tomography". *Procedia Materials Science* 3 (214) 1908-1913.
- (17) Seiler, J.M.; Ratel, G.; Combeau, H.; Gaus-Liu, X.; Kretzschmar, F.; Miassoedov, A.; "Transient refractory material dissolution by a volumetrically-heated melt". *Nuclear Engineering and Design* 280 (2014) 420-428.
- (18) Spengler, C.; Foit, J.; Fargette, A.; Agethen, K.; Cranga, M.; "Transposition of 2D molten corium-concrete interactions (MCCI) from experiment to reactor". *Annals of Nuclear Energy* 74 (2014) 89-99.
- (19) Szabo, T.; Kretzschmar, F.; Schulenberg, T.; "Obtaining a more realistic hydrogen distribution in the containment by coupling MELCOR with GASFLOW". *Nuclear Engineering and Design* 269 (2014) 330-339.
- (20) Szabo, T.; „Verbesserte Berechnung der Wasserstoffverteilung im Sicherheitsbehälter bei der Analyse schwerer Störfälle in Kernkraftwerken durch Kopplung von MELCOR und GASFLOW“. Dissertation, Karlsruher Institut für Technologie 2014, Karlsruhe : KIT Scientific Publishing, 2014, ISBN 978-3-7315-0149-7.
- (21) Zeismann, F.; Haase, S.; Zellmer, L.; Bode, B.; Motoyashiki-Besel, Y.; Brückner-Foit, A.; Tomizato, F.; Kobayashi, M.; Toda, H.; Uesugi, K.; Takeuchi, A.; Suzuki, Y.; Erb, R.; Seiler, B.; Dost, M.; Foit, J.; "Untersuchung des Risswachstums in 3D - Verformungsmessung mittels Röntgenmikrotomographie". Bruchmechanische Werkstoff- und Bauteilbewertung : Beanspruchungsanalyse, Prüfmethode und Anwendungen; 46. Tagung des DVM-Arbeitskreises Bruchvorgänge, Kassel, 11.-12. Februar 2014, Berlin: Deutscher Verband für Materialforschung und -prüfung, 2014 S. 1-11 (DVM-Bericht ; 246).

Group: KARlsruhe Liquid metal LABORatory

## Liquid Metal Technologies for Energy Conversion

*Thomas Wetzel, Julio Pacio, Leonid Stoppel, Luca Marocco, Frank Fellmoser, Markus Daubner, Karsten Litfin*

### Introduction

In 2014 the Karlsruhe Liquid Metal Laboratory (KALLA) has focused its research activities on three major fields of liquid-metal (LM) technology:

- Experiments for cooling of core components (rod cooling and spallation target thermal hydraulics) of Accelerator Driven Systems (ADS)
- Experiments and modeling of direct pyrolysis of methane in a liquid metal bubble column reactor

Fundamental simulation studies and concept development of a solar furnace for the investigation of LMs as efficient heat transfer fluids for concentrated solar power (CSP) systems

In the following sections, the main scientific outcomes obtained during 2014 are presented. One great overall success of the laboratory was the 5-year evaluation of the German national research funding of the HELMHOLTZ Association of German research centers, in which the work of KALLA is embedded. Two fields of the laboratory's work, namely ADS thermal hydraulics and liquid metal technology for CSP systems have been under evaluation and reached highest scores in their fields by the international review panels.

The following three chapters give a brief overview on our work. For more details on the results you might want to have a look at the list of publications provided at the end of the article or simply contact us.

### Core thermal-hydraulic experiments with LBE

Heavy-liquid-metals, such as pure lead and the lead-bismuth eutectic alloy (LBE) are prominent candidate coolants for advanced reactor concepts, which can contribute to the reduction of nuclear waste. In particular, HLMS are considered for the transmutation of long-lived fission products and minor actinides, either in critical reactors or ADSs. In this context, HLM technology is being studied at several institutions worldwide. Since 2002, KALLA has been constantly participating in the related European research programs (FP5, FP6, and FP7). During 2014, significant progress has been made in the FP7 projects THINS; SEARCH and MAXSIMA.

#### Study of a liquid-metal windowless spallation target

In order to demonstrate and investigate a free surface target for the MYRRHA ADS ([www.sckben.be/myrrha](http://www.sckben.be/myrrha)), a near full scale prototype with a nozzle diameter of 88 mm has been set up and investigated within the THINS project. The nozzle produces a ring-like liquid metal curtain, converging into a liquid metal jet by surface tension effects, and thus forming an inner and an outer free surface. The inner surface is then subjected to a proton beam, while the curtain maintains the separation between beam line and reactor pool. Particular attention has to be given in the exact detection of the surface shape, as the high intensity proton beam with a power of 2.4MW must not impinge on the recirculation zone of the jet. While the outer free surface is easy to detect, the inner free surface is not directly accessible to optical investigation. Restrictions arise from the target design and as a consequence the inner free surface has to be characterized through the proton beam tube. A

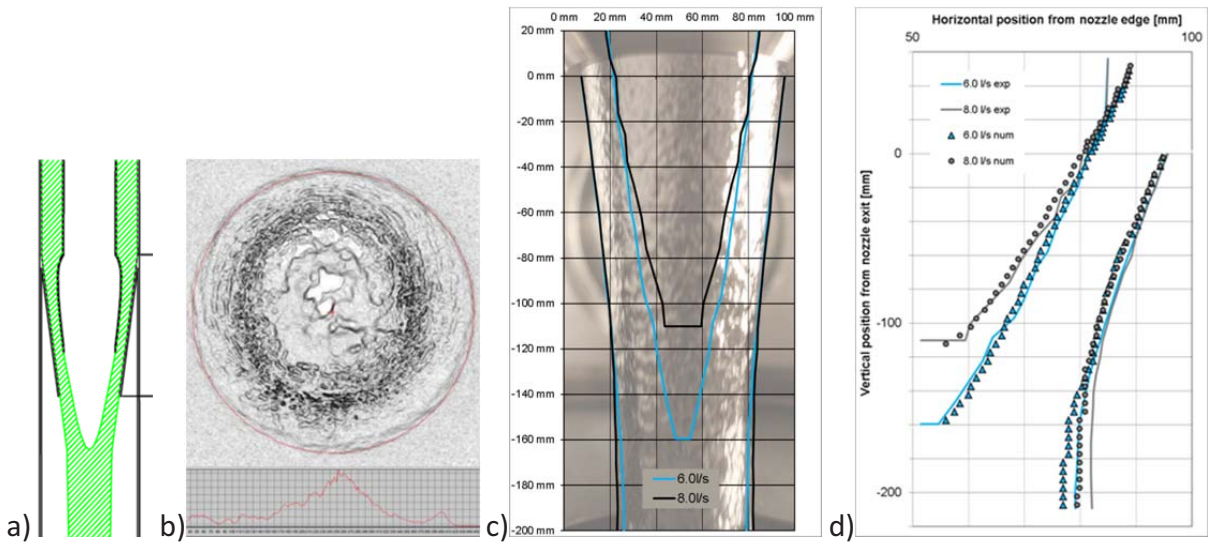


Fig. 1a) Illustration of target (© SCK·CEN), b) processed image for surface detection, c) reconstructed jet surfaces, d) comparison of measured surface shape with CFD predictions

solution was found by detecting the inner free surface using a digital camera and reconstructing the surface shape by using depth of field information of the images. Comparisons with numerical pre-calculations employing the commercial CFD code Star-CD show a very good agreement of experimental and numerical data. The experimental campaign has been completed in 2014 and results are in press at Journal of Nuclear Engineering and Design. Fig. 1 gives some impressions of the setup and the achieved results.

Thermal-hydraulic tests on a wire-wrapped rod bundle cooled by LBE

Hexagonal rod bundles with wire spacers are a typical geometry for fuel assemblies in ADSs and are considered as the reference design for the MYRRHA ADS. The flow and heat transfer of LBE in this geometry under normal and accidental operating conditions is, then, a key thermal-hydraulic issue to be investigated. Such flow scenarios are challenging for modeling and simulations, particularly due to the low Prandtl num-

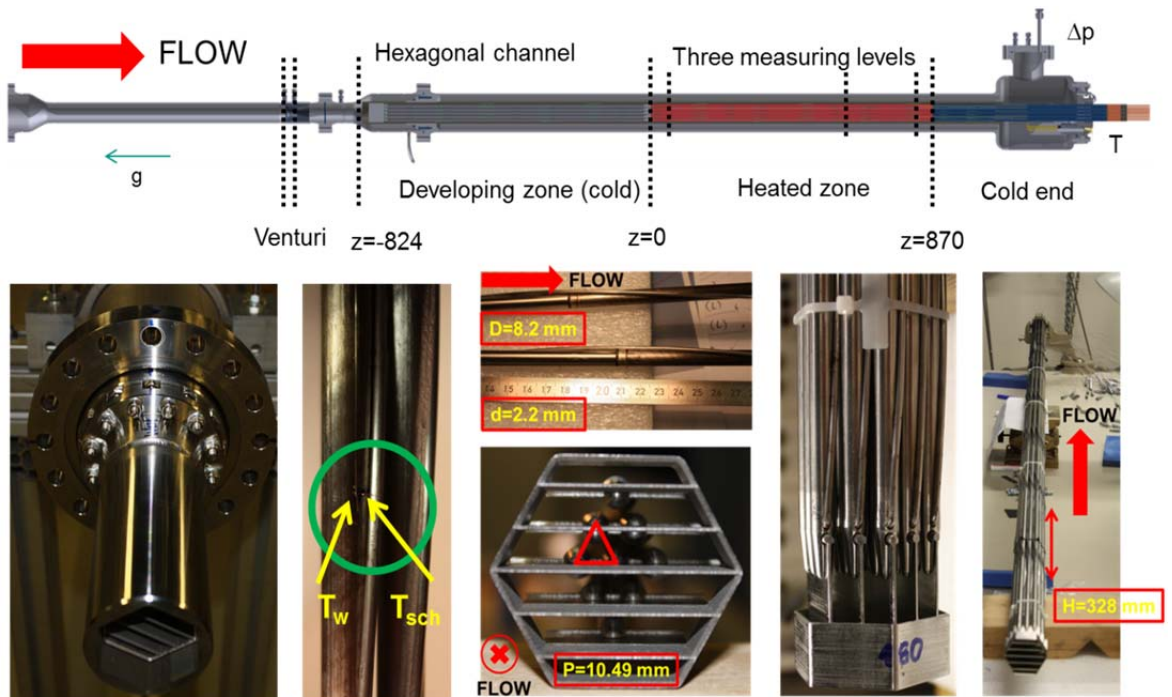


Fig.2. Test section for the thermal-hydraulic tests on a wire-wrapped 19-rod bundle, cooled by LBE

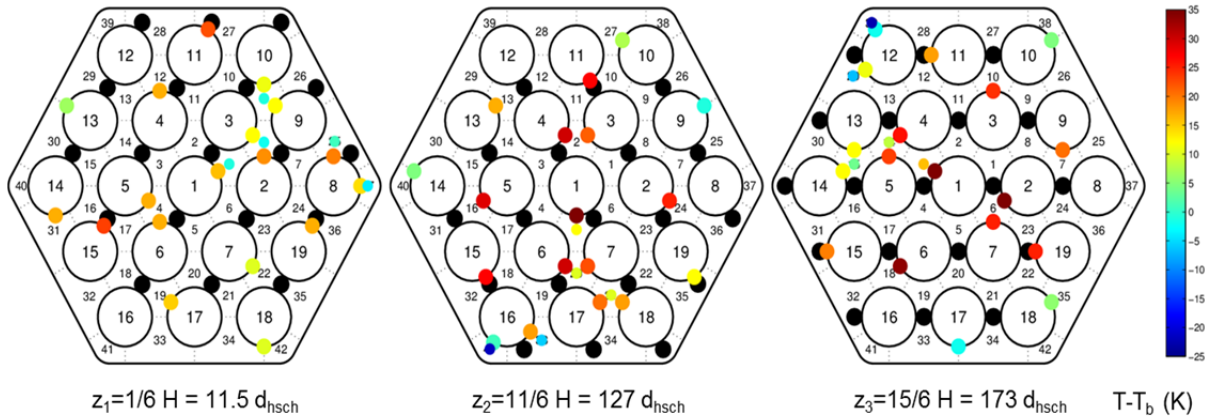


Fig. 3. Measured temperature profiles at reference conditions ( $T_{in}=200^{\circ}\text{C}$ ,  $m=16\text{kg/s}$ ,  $Q=197\text{ kW}$ )

ber of LBE ( $Pr\sim 0.025$ ). In this context, an experimental campaign is performed at KALLA within the FP7 project SEARCH, considering a test section with 19 heated rods and wire spacers, as shown in Fig. 2. Detailed temperature profiles were obtained by means of thermocouples located at three axial positions (18 at the rod wall, and 5 in the sub-channels, at each measuring level).

During 2014, the test section has been fully assembled and mounted on the THEADES loop test facility. After commissioning, first test were completed at the end of 2014: reference temperature profiles are shown in Fig. 3. These tests shall be continued considering an extensive test matrix, at prototypical conditions in terms of operating temperature ( $200^{\circ}\text{C} - 450^{\circ}\text{C}$ ), power density (up to  $1.0\text{ MW m}^{-2}$ ) and velocity (up to  $2\text{ m s}^{-1}$ ) of the LBE.

Within the FP7 MAXSIMA project, flow-blockage elements shall be added to this test section in order to study the temperature profiles in a non-normal scenario. Thus, the results obtained in SEARCH are the basis for comparing those with in MAXSIMA.

As part of the Education and Training activities of both projects, an international workshop was held at KIT from 7<sup>th</sup> to 10<sup>th</sup> October, 2014. The main achievements of both projects, as well as their synergies with other international activities are highlighted. This workshop included 5 keynote lectures and 41 technical presentations, covering topics of core thermal-hydraulic and core components; steam generator and cooling safety; coolant chemistry control and HLM corrosion; fuel and fuel safety; among others. With 85 registered participants, see Fig. 4, the workshop suc-

ceeded in its goal of promoting the technical information exchange within the scientific community working on HLM systems. Conference proceedings were published based on the individual abstracts and presentations ([www.iket.kit.edu/590.php](http://www.iket.kit.edu/590.php)).



Fig.4. Group photo of the participants of the SEARCH/MAXSIMA International Workshop at the KIT-FTU (7<sup>th</sup>-10<sup>th</sup> October, 2014), organized by KIT-IKET and KIT-IHM

### Methane cracking

The project "Hydrogen from Methane without  $\text{CO}_2$  Emissions" starting in December 2012 made substantial further progress during 2014. In this project, KIT, being the member of the Helmholtz Alliance for Liquid Metal Technologies (LIMTECH), cooperates with the Institute for Advanced Sustainability Studies (IASS) in Potsdam. The main idea of this project is to develop  $\text{CO}_2$ -free hydrogen production processes based on direct thermal methane pyrolysis in a liquid metal bubble column. For this purpose, the experimental facility HELiS has been developed

and built. During 2014 several experimental campaigns were conducted to test and optimize different reactor concepts and bubbling devices. Due to the strong chemical activity of liquid tin at high temperatures, quartz glass with steel jacket as a reactor wall material was selected. The quartz glass reactor tube is about 1300mm long and has an inner diameter of 40.6mm. The methane feed gas is injected into the liquid tin through a single orifice ( $\varnothing 0.5$  mm) within the bottom of the reactor. The achieved hydrogen yield, measured at different temperature levels, is shown in Figure 5. The resulting hydrogen yield increases for higher temperature and lower methane volume flow rates, which represent higher gas residence times in the liquid metal reactor. A very important point of the investigation was the location of the produced carbon black. In the experiments it was determined that the carbon powder was not strongly attached to the reactor inside components but mostly accumulated in the gas phase above the liquid metal surface. In order to have a better understanding of the processes happening in the reactor, a thermochemical model has been also developed. The model allows predicting the hydrogen yield at different operating conditions. Further experimental investigations and theoretical modeling are under way.

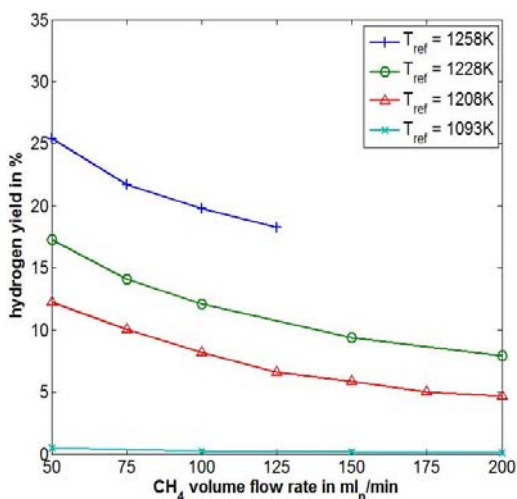


Fig. 5. Hydrogen yield vs. methane volume flow rate at different temperature levels.

## Concentrated Solar Power (CSP)

Liquid metals have been identified as attractive heat transfer fluids (HTF) for next generation CSP plants. Therefore, SOMMER (SOlar furnace arrangement with Molten-METal-cooled Receiver) [1], a 10kW experimental facility operated with lead-bismuth-eutectic (LBE), is under design and construction at the KALLA laboratory. It consists of a solar collecting system (heliostat mirror and a concentrating dish), a heat transfer system (receiver, pump, cooler, electric heater) and perspective a storage system, as schematically shown in Fig.6.

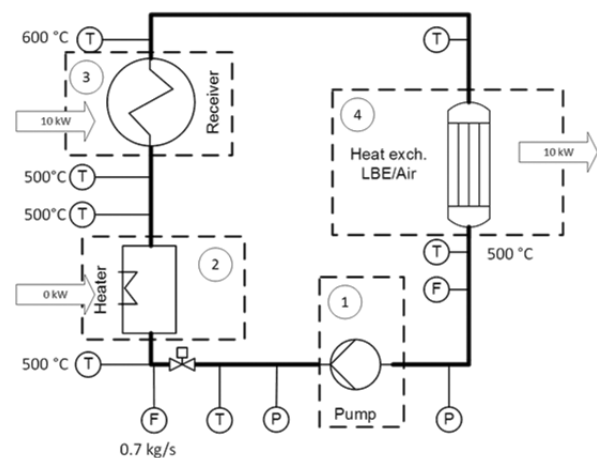


Fig. 6: Schematic representation of the SOMMER loop with an upper temperature of 600°C

Even though liquid metals have the potential to operate at temperatures much higher than molten nitrate salts, which are limited at appr. 600°C because of chemical stability, an upper temperature of 600°C has been initially fixed for SOMMER, in order to demonstrate the feasibility and advantages of liquid metals as HTF at the same upper temperature as state-of-the-art HTFs.

Due to the size of the focal point, the test receiver is limited in its aperture area to approximately 10 cm by 10 cm. On this area the flux of the parabolic mirror shown in Fig.7 is projected. According to an evaluation of possible receiver designs, a spiral wound solution, shown in Fig.8, has been preferred over the others.

The heat flux in solar thermal power plants is typically varying along the tube axis and the tube circumference, causing high thermal stresses in the walls. For example, only one half of the pipe's surface is exposed to the highly concentrated solar radiation, resulting in strongly non-uniform boundary conditions. The magnitude of the resulting stresses depends on the cooling effect of the heat transfer fluid. For a proper thermo-hydraulic, as well as a mechanical design of the receiver, good knowledge of the local wall temperature and convective heat transfer coefficient is required. Even though it has been already shown that for medium-to-high Prandtl number fluids the mean heat transfer coefficient can be evaluated with the Nusselt number correlations valid for uniformly distributed heat flux on the wall, the question is still open for low Prandtl number fluids such as liquid metals. Therefore, an experimental campaign is ongoing for the liquid metal flow in a pipe with constant heat flux applied on only half of the tube's surface but with a constant axial distribution, as shown in the Fig.9.



Fig. 7: Parabolic mirror of SOMMER

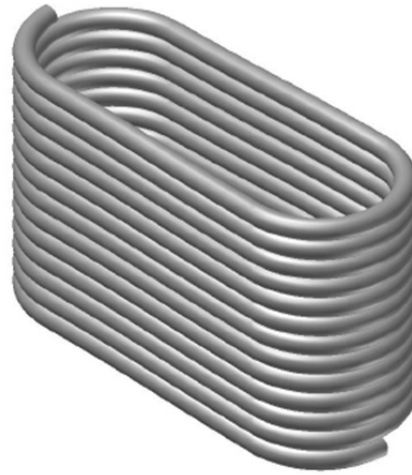


Fig. 8: Spiral wound receiver for SOMMER loop

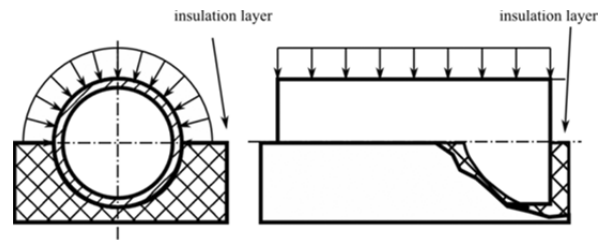


Fig. 9: Boundary conditions for AVANTI experiment

For this purpose, a dedicated test section has been added to KALLA's small thermal hydraulics test loop GALINKA. This project is funded by a LIMTECH Seed Grant, which was awarded to the SOMMER team in a competition earlier in 2014. The test rig, operated with an eutectic composition of Indium-Gallium-Tin, has been named according to its purpose of also validating numerical simulations [2]: AVANTI ("Anlage zur Validierung Numerischer Simulationen"; German for 'Loop for the validation of numerical simulations').

## Conclusions

2014 has again been a busy and successful year for KALLA. Highlights have been the excellent review results during the evaluation of the German national research program on energy research and the International SEARCH/MAXSIMA Workshop in October, which gave us the opportunity to host a great portion of the international

HLM experts community here at IKET and KALLA. More than 20 publications and presentations have shown the productivity and the positive spirit of the 15 KALLA team members, including engineers, technicians, PhD students and scientists.

### List of Acronyms

Acronym	Meaning
ADS	Accelerator-driven system
AVANTI	Anlage zur Validierung Numerischer Simulationen
CSP	Concentrated Solar Power
HLM	Heavy liquid metal
KALLA	Karlsruhe Liquid Metal Laboratory
LBE	Lead-bismuth eutectic
MAXSIMA	Methodology, Analysis and experiments for the safety in Myrrha assessment
MYRRHA	Multi-purpose hybrid research reactor for high-tech applications
SEARCH	Safe Exploitation Related Chemistry for HLM cooled reactors
SOMMER	Solar furnace arrangement with Molten-Metal-cooled Receiver
THINS	Thermal-hydraulic of innovative nuclear systems

### References

- (1) Pacio, J.; Weisenburger, A.; Wetzel, T. (Eds.). Proceedings of the SEARCH/MAXSIMA 2014 International Workshop, Karlsruhe, 07-10 October, 2014. Karlsruhe Institute of Technology
- (2) Pacio, J.; Marocco, L.; Wetzel, T. Review of data and correlations for turbulent forced convective heat transfer of liquid metals in pipes, *Heat and Mass Transfer*, 2014, **50**, 1-12

- (3) Pacio, J.; Fritsch, A.; Singer, C.; Uhlig, R. Liquid metals as efficient coolants for high-intensity point-focus receivers: implications to the design and performance of next-generation CSP systems *Energy Procedia*, 2014, **49**, 647 – 655
- (4) Pacio, J.; Daubner, M.; Fellmoser, F.; Litfin, K.; Wetzel, T. Blockage experiments design and instrumentation report, *Karlsruhe Institute of Technology*, MAXSIMA Deliverable 3.1., 2014
- (5) Pacio, J.; Daubner, M.; Fellmoser, F.; Litfin, K.; Marocco, L.; Wetzel, T. Heat transfer experiments in rod bundles cooled by lead-bismuth eutectic (LBE), In: *Proceedings of the 10th International Topical Meeting on Nuclear Thermal-Hydraulics, Operation and Safety (NUTHOS-10)*, Okinawa, Japan, December 14-18, 2014, Proceedings on USB-Stick, Paper NUTHOS10-1031
- (6) Pacio, J.; Daubner, M.; Fellmoser, F.; Litfin, K.; Marocco, L.; Stieglitz, R.; Taufall, S.; Wetzel, T., Heavy-liquid metal heat transfer experiment in a 19-rod bundle with grid spacers. *Nuclear Engineering and Design*, 2014, **273**, 33 – 46
- (7) Pacio, J.; Litfin, K.; Batta, A.; Viellieber, M.; Class, A.; Doolaard, H.; Roelofs, F.; Manservigi, S.; Menghini, F.; Böttcher, M. Heat transfer to liquid metals in a hexagonal rod bundle with grid spacers: Experimental and simulation results, *Nuclear Engineering and Design*, 2014, (in press, published online. DOI: doi:10.1016/j.nucengdes.2014.11.001)
- (8) Taufall, S.; Daubner, M.; Fellmoser, F., Litfin, K., Marocco, L., Pacio, J.; Stieglitz, R.; Wetzel, T.. Experimental investigation of lead-bismuth-eutectic flow and heat transfer in hexagonal-lattice rod bundles with grid spacers, In: *Proceedings of the THINS 2014 International Workshop, Modena-Italy, January 20-22, 2014*, paper number: 28
- (9) Pacio, J.; Daubner, M.; Fellmoser, F.; Litfin, K.; Wetzel, T. Fuel assembly heat transfer and blockage experiments. In: *Proceedings of the SEARCH/MAXSIMA International Workshop, Karlsruhe, Germany, 7-10 October, 2014*, pp. 699-711
- (10) Pacio, J.; Daubner, M.; Fellmoser, F.; Litfin, K.; Wetzel, T. Fuel assembly heat transfer and blockage experiments. In: *SEARCH/MAXSIMA Technical review meeting, Gent, Belgium, 28-30, April, 2014*

- (11) Litfin, K.; Fetzer, J.; Fellmoser, F.; Batta, A.; Class, A. G.; Wetzel, Th.; Lead bismuth free surface target for high intensity proton beam application. *5th High Power Targetry Workshop, Batavia, USA, May, 2014*
- (12) Litfin, K.; Batta, A.; Class, A. G.; Wetzel, Th.; LBE free surface target experiment. *THINS Technical meeting, Delft, June, 2014*
- (13) Litfin, K.; Fetzer, J. R.; Batta, A.; Class, A. G.; Wetzel, Th.; High power spallation target using a heavy liquid metal free surface flow. *27th International Conference of the International Nuclear Target Development Society (INTDS-2014), Tokyo, Japan, August 31 - September 5, 2014*
- (14) Litfin, K.; Fetzer, J. R.; Batta, A.; Class, A. G.; Wetzel, Th.; High power spallation target using a heavy liquid metal free surface flow. *Journal of Radioanalytical and Nuclear Chemistry, accepted for publication*
- (15) Plevan, M.; Geißler, T.; Stoppel, L.; Wetzel, T.; Heinzl, A.; Weisenburger, A.; Müller, G.; Fazio, C.; Konys, J.; Schroer, C.; Rubbia, C.; Abánades, A.; Falco, C.; Ghannadzadeh, A.; Stückrad, S.; Salmieri, D.; "Thermal cracking of methane in a Liquid Metal Bubble Column" Annual Meeting of the VDI-GVC Processnet Specialist Group Energy Process Technology, March 2014, Karlsruhe, Germany
- (16) Plevan, M.; Geißler, T.; Stoppel, L.; Wetzel, Th.; Abánades, A.; Rathnam, R.; Mehravar, K.; Rubbia, C.: *Thermal cracking of methane in a liquid metal bubble column reactor: Experiments and kinetic analysis*. Submitted to Intl. J. Hydrogen Energy
- (17) Flesch J., Fritsch A., Cammi G., Marocco L., Fellmoser F., Pacio J., Wetzel Th., *Construction of a test facility for demonstration of a liquid lead-bismuth-cooled 10 kW thermal receiver in a solar furnace arrangement – SOMMER*". International Conference on Concentrating Solar Power and Chemical Energy Systems (SolarPACES 2014), Beijing, China, September 16-19, 2014. (accepted for publication)
- (18) Marocco L., Cammi G., Flesch J., Th. Wetzel, *Numerical analysis of a solar tower receiver tube operated with liquid metals*. Intl. J. Heat and Mass Transf. (under review)
- (19) Dietrich, B; Marocco, L; Kind, M; Wetzel, T; *Charakterisierung des Wärmetransports in festen Schwämmen bei Flüssigmetall-Durchströmung. Chemie Ingenieur Technik*, 86 (9), S. 1598, 2014, Wiley Online Library
- (20) Wetzel, T.; Pacio, J.; Marocco, L.; Weisenburger, A.; Heinzl, A.; Hering, W.; Schroer, C.; Müller, G.; Konys, J.; Stieglitz, R.; *Liquid metal technology for concentrated solar power systems: Contributions by the German research program*. AIMS Energy 2 (2014) No. 1, pp. 89-98.
- (21) Wetzel T. and Borchers S.: *Update of energy payback time and greenhouse gas emission data for crystalline silicon photovoltaic modules*. Progress in Photovoltaics, 2014: DOI: 10.1002/pip.2548.



## International Conference on Information Systems for Crisis Response and Management

*Tim Müller, Stella Möhrle, Claudia Landman, Wolfgang Raskob, Dima Trybushnyi*

### Abstract

The PREPARE project that started February 2013 and will end beginning of 2016, aims to close gaps that have been identified in nuclear and radiological preparedness in Europe following the first evaluation of the Fukushima disaster. As the communication and information sharing in Europe showed some deficits, a so called Analytical Platform will be developed exploring the scientific and operational means to improve information collection, information exchange, and the evaluation of such types of disasters. The Platform contains components to support radiation experts in analysing an event, understanding long-term consequences and communicating with the public.

### Introduction

The European project PREPARE (Innovative integrated tools and platforms for radiological emergency preparedness and post-accident response in Europe) aims at closing gaps that have been identified in nuclear and radiological preparedness following the first evaluation of the Fukushima disaster (Raskob 2015). Though significant progress was made in the area of radiological and nuclear emergency management and rehabilitation following the Chernobyl accident and in particular within the European research Projects EURANOS (Raskob, 2010) and NERIS-TP, the Fukushima accident revealed problems in respect of long lasting releases, cross border radiation monitoring, food safety, source term estimation, and dispersion modelling including hydrological pathways for European water bodies. In addition, information collection, information exchange, and the evaluation of such types of disasters were not harmonized as pointed out by several international organisations (e.g.

HERCA, 2013). To close this gap, a so called Analytical Platform is developed exploring the scientific and operational means for information exchange and communication at the European level.



Fig. 1: The project PREPARE has 45 partners.

The general idea of the Analytical Platform is to provide an easy to access platform for information exchange in time of a nuclear or radiological crisis, to allow discussions between experts and to disseminate congruent information to the public community. If an alert is issued, members of different organizations would be attached to the platform and start working. Experts can meet in a particular “virtual” meeting room where they can exchange information and documents. Once information is confirmed, it can be released to other expert groups and the public community.

A knowledge database on historic events is the core of the platform and will serve as a starting point to further discuss possibly suitable countermeasures. The platform will contain, inter alia,

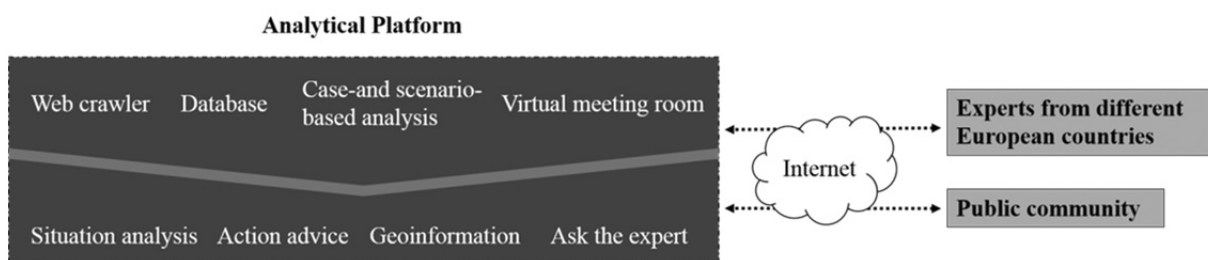


Fig. 2. Analytical Platform with its components and web-based access of experts and public community

crowd sourcing facilities, a virtual meeting room and messaging modules, and a geo-information component to provide visual data on the accident. Furthermore, the application will be realized web-based to be easily accessible. Figure 2 on a high level illustrates the idea of the components of the platform interacting as a web-based application

### Knowledge database

Information on historic events and scenarios should be stored in a way to support the fast assessment of a current event. Therefore, attrib-

utes and attribute ranges need to be pre-defined in order to describe an event in a unique manner. An accident is subdivided into four distinct phases ('pre-release phase', 'release phase', 'transition phase', and 'long-term post-accident phase') and so far more than 60 attributes are taken into account to describe an event. The attributes are determined with the help of experts and will be revised continuously. Table 1 illustrates the data that experts have provided for a particular historic case. As the historic events from Chernobyl and Fukushima will not cover all possible types of accidents, particular generic scenarios will be developed to include as many different events as possible.

Table 1. Example of information that have been provided for an historic case

General event description	Release	Area affected by the release	Area which underwent the long-term post-accident phase
Type of nuclear power plant	Time of day of release	Number of people affected	Exposure pathways
Gross & net output	Season of release	Size of area	Risk assessment
Number of blocks	Cause of release	Exposure pathways	Average 50 year effective adult dose
Burnup	Release height & duration	Risk assessment; experience from other emergencies	Endangered objects & countermeasures; some information on the evaluation afterwards
Inventory	Accident scenario type	Average adult effective dose in first year	Agricultural areas affected by restrictions; number of holdings & animals; duration of restriction
Thermal power	Weather at release	Disruption of infrastructure	Indirect costs approximately per annum
Country	Source term	Endangered objects & countermeasures	
		Fatalities; injured, decontaminated, evacuated, sheltered, relocated people	
		Agricultural areas affected by restrictions; number of holdings & animals; duration of restriction	
		Impairment of protected areas & waterbodies	

The methodology case-based reasoning (CBR) will be used to suggest solutions for events that are not actually included in the database, assuming that similar events require similar solutions. CBR is a methodology to solve new problems by utilizing knowledge of previously experienced problem situations. Aamodt and Plaza (1994) describe CBR as a cycle process starting problem solving with identifying, assessing, and describing the current problem situation (case) – see Figure 3. Afterwards, similar historic cases from a case base should be determined to reuse their solutions and to adapt them to the current problem situation, if necessary. The knowledge in the case base is updated by storing the new case with its possibly corrected or improved and confirmed solution. Besides the previous cases, a CBR system includes knowledge in terms of vocabulary and in particular knowledge representation, similarity measures, and adaptation knowledge (Richter, 1995).

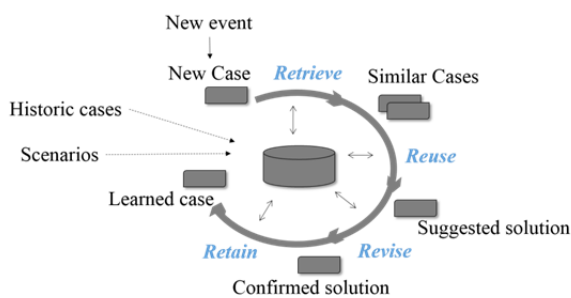


Fig. 3: Case-based reasoning illustrated by a cycle process based on (Aamodt and Plaza, 1994). The case base is extended by scenarios

To identify scenarios close to the current one dedicated similarity functions are under development. Here, affected areas undergoing specific accident phases are regarded. Since the phases restrict possibly suitable countermeasures, query and case need to match with respect to the event phase. An affected area is described by several attributes that are locally (attribute-wise) compared before analyzing the more complex structure. In order to reflect the influence of each attribute to the global similarity, weights can be assigned.

## Crowd sourcing

To support the expert in answering questions from the public, crowd sourcing tools will be integrated within the Analytical Platform. These tools are organized as two services:

- The Web Content Discovery Service that crawls the Web, categorizing content according to its relevance to a theme of interest, and extracting statistics regarding emerging trends in the concerns and issues discussed in public forums, social media, and in general the publicly accessible Web
- The Ask the Expert Service where the public can access publicly available information regarding nuclear and/or radiological events and their consequences via a question-answering interface

## Virtual meeting room

The experts need a platform to exchange their views and opinions based on the assembled data. More specific they need means to exchange time stamped messages and to receive notifications in case of specific events taking place. Messages can be acknowledged to guarantee they have been delivered and read by the receiver. Furthermore documents and data sets like e.g. reports or source term information need to be exchanged bilaterally similar to the attachment management of common email applications. In contrast to common emailing a history is logged to provide retracing later on e.g. for evaluation purposes. As an additional advantage communication in the virtual meeting room is secured and cannot be eavesdropped from unauthorized persons, thus allowing a more open discussion and preventing on purpose spread misinformation. The virtual meeting room is structured in working groups to provide more specific areas for the different tasks the experts will process.

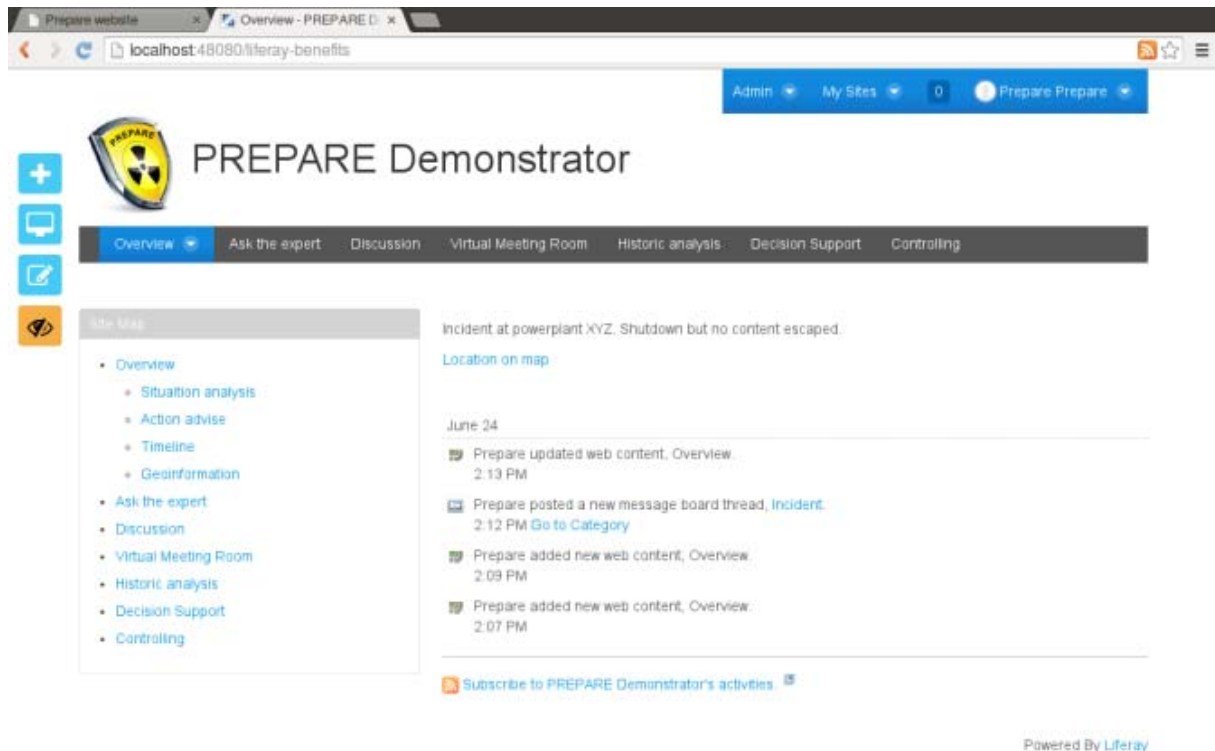


Fig. 4: First Demonstrator of the Analytical Platform

## Web component

The Analytical Platform as such will be realized as a web platform under the LIFERAY umbrella. LIFERAY provides many different services including user management and databases. The LIFERAY community edition is free and provides comprehensive software tools to allow the integration of different functionalities inside one platform. At present, prototypes of all components are integrated in the Analytical Platform.

## Conclusions and outlook

With the Analytical Platform, a European wide information sharing and managing Web Platform will be established. It contains means that allow to analyse the ongoing event and to support decision makers in selecting appropriate management options. Further to this, it provides help in communicating with the public, a topic that is of uppermost importance to keep trustworthiness. A first version for external users is expected for the second half of 2015. At the end of 2015, tests and demonstrations will be carried out as part of the project PREPARE. Following the end of PREPARE and a successful demonstration of its

capabilities, the Analytical Platform can be operated either as part of the NERIS Platform or under the umbrella of an international organisation.

## References

- 1) Aamodt, A. and Plaza, E., 1994. Case-Based Reasoning: Foundational Issues, Methodological Variations, and System Approaches, *AI Communications*, 7, 1, 39-59.
- 2) Richter, M.M., 1995. The Knowledge Contained in Similarity Measures. Invited talk at the First International Conference on CBR (ICCB-95).
- 3) Raskob W, Hugon M (eds) (2010) Enhancing nuclear and radiological emergency management and rehabilitation: Key Results of the EURANOS Project. *Radioprotection* 45(5 Supplément) (© EDP Sciences)
- 4) Raskob, W., Schneider, T., Gering, F., Charon, S., Zhelezniak, M., Andronopoulos, S., Heriard-Dubreuil, G., Camps, J., (2014) PREPARE: Innovative Integrated Tools and Platforms for Radiological Emergency Preparedness and Post-Accident Response in Europe, in *Radiation Protection Dosimetry*, Sep. 2014

- 5) NERIS-TP (2014) <http://www.eu-neris.net/>, approached January 2015
- 6) HERCA (2013) [http://www.herca.org/herca\\_news.asp?newsID=28](http://www.herca.org/herca_news.asp?newsID=28), approached Jan. 2015
- 7) Liferay (2015) <http://www.liferay.com/de/products/liferay-portal/features/portal>, approached January 2015
- Read more:
- 8) Deines, E.; Wandler, S.; "DSM CIP: Modelling and simulation of critical infrastructure using an agent- based approach". Zschau, J. [Hrsg.], CEDIM Annual Research Report 2013 : Focus on Forensic Disaster Analysis in Near Real-Time, Potsdam : Center for Disaster Management and Risk Reduction Technology, 2014 pp.80-81, ISBN 978-3-9816597-9-5.
- 9) Lin, L.; Möhrle, S.; Münzberg, T.; Raskob, W.; "A decision support approach: evaluating the effectiveness of security measures by scenario-based multi-criteria analysis". Thoma, K. [Hrsg.], Future Security: 9th Security Research Conference, Berlin, September 16-18, 2014, Proceedings pp. 266-273, Stuttgart: Fraunhofer Verl., 2014, ISBN 978-3-8396-0778-7.
- 10) Lin, L.; Meng, S.; Möhrle, S.; "DSM CIP: The RIKOV project, risks and costs of terrorist threats against public rail transport systems". Zschau, J. [Hrsg.], CEDIM Annual Research Report 2013: Focus on Forensic Disaster Analysis in Near Real-Time, Potsdam: Center for Disaster Management and Risk Reduction Technology, 2014 pp. 74-75, ISBN 978-3-9816597-9-5.
- 11) Möhrle, S.; Raskob, W.; "Development of a CEDIM database and implementation of case-based reasoning for analytical support". Zschau, J. [Hrsg.], CEDIM Annual Research Report 2013: Focus on Forensic Disaster Analysis in Near Real-Time, Potsdam: Center for Disaster Management and Risk Reduction Technology, 2014 pp. 24-25, ISBN 978-3-9816597-9-5.
- 12) Möhrle, S.; Raskob, W.; "Fallbasierte Analyseunterstützung zur schnellen Bewertung von Naturkatastrophen". 14. Forum Katastrophenvorsorge, Leipzig, 4.-5. November 2014.
- 13) Möhrle, S.; "On the assessment of disaster management strategies". Hiltz, S.R. [Hrsg.], 11th International Conference on Information Systems for Crisis Response and Management, University Park, Pa., May 18-21, 2014, Book of Papers pp. 215-219, University Park, Pa.: Pennsylvania State University, 2014, ISBN 978-0-692-21194-6.
- 14) Motzke, A.; Schätter, F.; "DSM CIP: The SEAK project, decision support for managing disruptions in food supply chains". Zschau, J. [Hrsg.], CEDIM Annual Research Report 2013: Focus on Forensic Disaster Analysis in Near Real-Time, Potsdam: Center for Disaster Management and Risk Reduction Technology, 2014 pp. 76-77, ISBN 978-3-9816597-9-5.
- 15) Motzke, A.; Balster, A.; Hansen, O.; Herrmannsdörfer, M.; Schätter, F.; Friedrich, H.; Raskob, W.; Wiens, M.; Schultmann, F.; "The SEAK project: Decision support for managing disruptions in food supply chains". Thoma, K. [Hrsg.], Future Security: 9th Security Research Conference, Berlin, September 16-18, 2014, Proceedings pp. 581-584, Stuttgart: Fraunhofer Verl., 2014, ISBN 978-3-8396-0778-7.
- 16) Münzberg, T.; Wiens, M.; Schultmann, F.; "A strategy evaluation framework based on dynamic vulnerability assessments". Hiltz, S.R. [Hrsg.], 11th International Conference on Information Systems for Crisis Response and Management, University Park, Pa., May 18-21, 2014, Book of Papers pp. 45-54, University Park, Pa.: Pennsylvania State University, 2014, ISBN 978-0-692-21194-6.
- 17) Münzberg, T.; Wiens, M.; Schultmann, F.; "Assessment of indirect losses and economic impacts". Zschau, J. [Hrsg.], CEDIM Annual Research Report 2013: Focus on Forensic Disaster Analysis in Near Real-Time, Potsdam: Center for Disaster Management and Risk Reduction Tech., 2014 pp. 25-26, ISBN 978-3-9816597-9-5.
- 18) Münzberg, T.; Wiens, M.; Schultmann, F.; "Ausfall kritischer Infrastrukturen: Gefahrenabwehrpläne und Notfallkonzepte auf kommunaler Ebene". 62. Jahresfachtagung der Vereinigung zur Förderung des Deutschen Brandschutzes, Dortmund, 16.-18.Juni 2014, Tagungsband S. 675-686, Altenberge : vfdb, Vereinigung zur Förderung des Deutschen Brandschutzes e.V, 2014.
- 19) Münzberg, T.; Möhrle, S.; Raskob, W.; "Decision support methods in the field of critical infrastructure protection (DSM CIP): overview". Zschau, J. [Hrsg.], CEDIM Annual Research Report 2013: Focus on Forensic Disaster Analysis in Near Real-Time, Potsdam: Center for Disaster Management and Risk Reduction Technology, 2014, pp. 72-75, ISBN 978-3-9816597-9-5.

- 20) Münzberg, T.; Motzke, A.; Wiens, M.; Schultmann, F.; "Disruptions of food supply chains: A spatial vulnerability assessment approach for disaster management". Thoma, K. [Hrsg.] Future Security: 9th Security Research Conference, Berlin, September 16-18, 2014, Proceedings pp. 48-55, Stuttgart: Fraunhofer Verl., 2014, ISBN 978-3-8396-0778-7.
- 21) Münzberg, T.; "DSM CIP: Critical infrastructure disruption, decision support through assessing spatial vulnerabilities". Zschau, J. [Hrsg.], CEDIM Annual Research Report 2013: Focus on Forensic Disaster Analysis in Near Real-Time, Potsdam: Center for Disaster Management and Risk Reduction Technology, 2014 pp. 82-83, ISBN 978-3-9816597-9-5.
- 22) Münzberg, T.; Wandler, S.; Deines, E.; "DSM CIP: THE KritisF&E project, review on critical infrastructure protection related research projects". Zschau, J. [Hrsg.], CEDIM Annual Research Report 2013: Focus on Forensic Disaster Analysis in Near Real-Time, Potsdam: Center for Disaster Management and Risk Reduction Tech., 2014 pp. 78-79, ISBN 978-3-9816597-9-5.
- 23) Münzberg, T.; Wiens, M.; Schultmann, F.; "Dynamic-spatial vulnerability assessments: a methodical review for decision support in emergency planning for power outages". *Procedia Engineering* 78 (2014) 78-87.
- 24) Münzberg, T.; Wiens, M.; Schultmann, F.; "Resilienz verstehen: Eine ganzheitliche und raumzeitliche Analyse der Wirkungen von Stromausfällen". 14. Forum Katastrophenvorsorge, Leipzig, 4.-5. November 2014
- 25) Raskob, W.; "Atmospheric dispersion modelling". Wilhelm and Else Heraeus Physics School on Ionizing Radiation and Protection of Man, Bad Honnef, August 10-22, 2014.
- 26) Raskob, W.; Möhrle, S.; "Knowledge databases as instrument for a fast assessment in nuclear emergency management". 3rd International Conference on Radioecology and Environmental Radioactivity, Barcelona, E, September 7-12, 2014.
- 27) Raskob, W.; Schneider, T.; Liland, A.; Duranova, T.; Andronopoulos, S.; Mustonen, R.; "Main achievements of the European research project NERIS-TP". 4th European Regional IRPA Congress, Geneve, CH, June 23-27, 2014 Book of Abstracts p.154.
- 28) Raskob, W.; Schneider, T.; Gering, F.; Charon, S.; Zhelezniak, M.; Andronopoulos, S.; Heriard-Dubreuil, G.; Camps, J.; "PREPARE: Innovative integrated tools and platforms for radiology emergency preparedness and post-accident response in Europe". 4th European Regional IRPA Congress, Geneve, CH, June 23-27, 2014, Book of Abstracts p. 321.
- 29) Raskob, W.; Landman, C.; Trybushnyi, D.; "The real-time on-line decision support system JRODOS". Regional Cooperation on EP&R in South East Asia, Bruxelles, B, August 4-8, 2014.
- 30) Schneider, T.; Biguenet, S.; Bardelay, J.; Duranova, T.; Gallego, E.; Gering, F.; Hardeman, F.; Heriard Dubreuil, G.; Murith, C.; Oughton, D.; Raskob, W.; "NERIS: The European platform on preparedness for nuclear and radiological emergency response and recovery". 4th European Regional IRPA Congress, Geneve, CH, June 23-27, 2014, Book of Abstracts pp. 320-321.
- 31) Schröter, K.; Khazai, B.; Mühr, B.; Elmer, F.; Bessel, T.; Möhrle, S.; Dittrich, A.; Kunz-Plapp, T.; Trieselmann, W.; Kreibich, H.; Kunz, M.; Zschau, J.; Merz, B.; "June flood 2013 in Central Europe. Focus Germany". Zschau, J. [Hrsg.] CEDIM Annual Research Report 2013: Focus on Forensic Disaster Analysis in Near Real-Time, Potsdam: Center for Disaster Management and Risk Reduction Technology, 2014 pp. 40-48, ISBN 978-3-9816597-9-5.

## Some Highlights of the Hydrogen Group in 2014

Thomas Jordan

### LOCA Containment Analysis of APR1400

Besides the continued research on basic phenomena regarding the transient behavior of flames in premixed gas systems, see (1) to (6), several major third party funded projects have been conducted or finalized in 2014. The most relevant projects and their main results be highlighted in the following.

For the European version of the Korean advanced pressurized water reactor (PWR) APR1400 full 3d hydrogen distribution and combustion simulations for a postulated large break loss of coolant accident (LBLOCA) with a late failure of the reactor pressure vessel have been analyzed with the HYCODES, GASFLOW and COM3D. The applied an unusually dry steam-hydrogen source in relevant phases with significant hydrogen release. The low steam concentrations below 20% in the source have never been seen in similar scenarios - for instance for German Konvoi PWRs - together with these significant injection rates of hydrogen. So the purpose of these quite conservative simulations was more to show, that with the designed mitigation measures –PARs and sprays - the resulting combustion loads are still far below the structural load limits of the reactor containment. This has been effectively shown for cases with ignition of the most sensitive gas mixtures.

Flammability, flame acceleration, and deflagration-detonation-transition hazards have been evaluated for the cases with and without spray. Only mildly accelerating conditions have been identified around the point with the peak release rate of hydrogen and for the maximum hydrogen inventories before RPV failure. Detonable conditions are predicted in the reactor cavity during a short period with almost dry hydrogen re-lease after RPV failure.

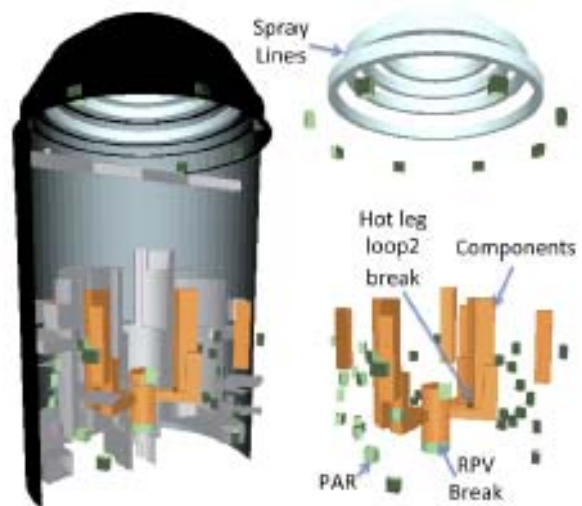


Fig. 1: 3D view of the GASFLOW containment model for APR1400 with PARs

The simulations with and without spray activation confirm the strong mitigation effect of the water spray, that is also known from previous analyses of other containments with spray. Simple combustion simulations with GASFLOW at the point with maximum hydrogen inventory, immediately before RPV failure, give peak volume averaged combustion pressures of 4.6 and 2.4 bar (absolute) for the simulations without and with spray. The lower combustion pressure of the spray case calculated with GASFLOW is attributed to the heat removal by the spray droplets.

For the COM3D geometry model highlighted in the figure below a new preprocessing tool using conventional CAD data has been applied. Thus the so far very tedious and error-prone process of geometry and mesh generation has been automated and accelerated considerably. The detailed COM3D analyses confirm that dynamic effects of the combustion of the most sensitive configurations before RPV failure yield only minor dynamic pressure effects and that these cases are rather dominated by a quasi-static rise of the containment pressure, which is also well predict

ed with the simple GASFLOW combustion model. However, gas ignition in the reactor cavity after RPV failure results in a detonation. The criteria for the hazard potential evaluated in GASFLOW show up the potential for this development, which is confirmed with the COM3D results. COM3D calculates considerable dynamic loads widely above 20 bar. Only a detailed analysis of this domain with an appropriate coupling to the structural dynamics could give an indication, whether additional mitigation measures, like an inertization of the cavity, are required. In the analyzed LBLOCA the combustion evaluations of the identified points with maximum hazard potential provided final quasi-static containment pressures well below the acceptable load limits.

Similar analyses have been done for a Suisse power station and for a German Konvoi type reactor.

Acknowledgements

The work was funded by KEPCO under Contract KCN04-14-08

**GASFLOW Simulations for Containment Venting Systems**

In a hypothetical core melt severe accident in nuclear power plants, a large amount of burnable gas, such as hydrogen and carbon monoxide, with certain amount of oxygen is released into the containment. In case of high containment pressure a filtered venting is designed as a mitigation measure. After aerosols and condensable portions of the gas mixture from the containment are purged, the remaining burnable gases flows into a chamber connected to horizontal venting pipes and further to a vertical stack, which is open to free atmosphere at the top. The main goal of the associated studies is to investigate the chemical sensitivity of the burnable and potentially detonable gas mixture in the venting system by means of computational fluid dynamic computer simulations. These results provide a higher resolution in space, better physical models and therefore higher credibility compared to the investigations done with engineering codes in the past. Although the analyses conducted with these engineering codes are deemed to be conservative in many aspects, in particular the involved distribution and combustion processes require more detailed insights for a solid risk evaluation.

Fig. 2: Steam-hydrogen release into the reactor cavity after RPV failure and averaged and peak data for the cavity room

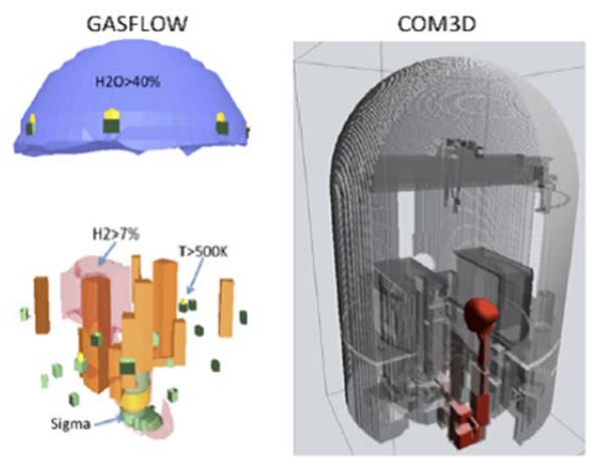
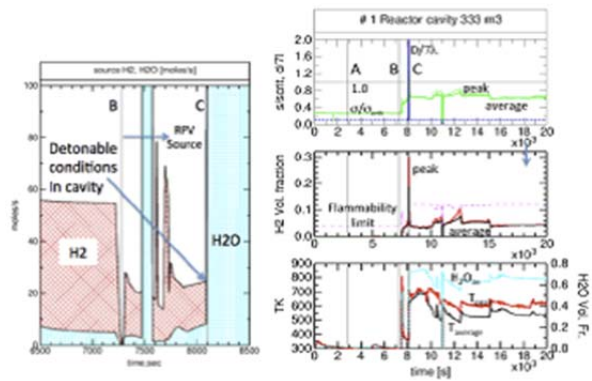


Fig. 3: Snapshot at the late phase of the LBLOCA; left: GASFLOW results without spray, steam cloud in blue, reference recombiner equipment in green and Sigma cloud; right: COM3D results with 800K isotherm from combustion 0.93 s after ignition, geometry imported from CAD data with automatic mesh generation

Based on several GASFLOW calculations for several installations with different scenarios and boundary conditions the potential for flame acceleration and deflagration-to-detonation-transition (DDT) have been evaluated. Some results for a German installation are reflected here. The principal set-up is shown in the corresponding figure. For the considered containment venting system it has been concluded that for the major accident scenarios and the associated source terms there is no risk of flame acceleration and detonation if the power supply of the ventilation fans can be maintained. In case of a station blackout, the whole system has no risk of deto-



Fig.4: Containment filtered venting system as analysed with GASFLOW

nation if the scrubber – purging water pool – can get boiling in 10 minutes, owing to the heating effect resulted from the latent heat of the condensable gases into the water pool. It is because the injected steam from the boiling scrubber inerts the mixture of hydrogen, carbon monoxide plus oxygen, effectively and significantly. In this case, a gas mixture only in a very local region in the stack, as small as about 0.16 cubic meter, is in a risk of flame acceleration. This is in principle negligible because of the relatively small pre-mixed cloud volume, involved inventory respectively.

### Acknowledgements

The work was funded and supported by VGB.

### **Parallelization of GASFLOW**

GASFLOW is - besides COM3D - one of the major components of the software suite HY-CODES of IKET / KIT. It is a CFD software solution used to predict fluid dynamics, heat and mass transfer, chemical kinetics, aerosol transportation and other related phenomena during a postulated severe accident in the containment of nuclear power plant (NPP). The generalized 3-D transient, two-phase, compressible Navier-Stokes equations for multi-species are solved in GASFLOW, using a proven semi-implicit pres-

sure-based algorithm of Implicit Continuous Eulerian – Arbitrary Lagrangian-Eulerian (ICE'd-ALE) methodology. GASFLOW has been intensively validated with international experimental benchmarks, and has been widely used in the hydrogen explosion risk analysis involving NPP containments. The simulation results of the GASFLOW code have been widely accepted by the nuclear authorities in several European and Asian countries. GASFLOW was originally designed as a supercomputer serial code and could be only run on vector machines with a single processor. With the increasing requirement of the users from the nuclear industry, detailed geometrical and physical models were used in the GASFLOW simulations. The users in nuclear industry heavily suffered from the extremely long computational times utilizing a single processor, even up to as much as 3-4 months, which were unacceptable for most of the industrial users. Therefore, a project was initiated in 2013 and almost finished in 2014 in order to parallelize GASFLOW using the paradigms of Message Passing Interface (MPI) and domain decomposition.

The data structure and parallel linear solvers in the Portable Extensible Toolkit for Scientific Computing (PETSc) were employed in the GASFLOW parallel version, which has been named GASFLOW-MPI. The scaling of the GASFLOW-MPI was studied and a highly per-

formant behavior has been identified. GASFLOW-MPI has been validated using the well accepted benchmarks by the CFD community, and it was also applied for the real large scale nuclear containment applications. Very good agreements were obtained compared to the results of the GASFLOW sequential version. The computational time can be dramatically reduced depending on the size of the problem and the high-performance computing (HPC) cluster. GASFLOW parallelization adds tremendous value to large scale containment simulations by enabling high-fidelity models, including more geometric details and more complex physical phenomena that occur during a severe accident, which yield detailed and precise insights. Maintaining the key user interfaces, GASFLOW-MPI provides almost full compatibility with the previous sequential version. In particular the complex input generated by users may be used identically for the new version and thus it saves huge work invested in modelling complex geometries and mitigation measures in the past. GASFLOW-MPI will be further developed as the high performance engineering CFD code for the thermal hydraulics and safety analyses in NPP containments and other large scale industrial applications. The first fully tested release version will be made available in 2015.

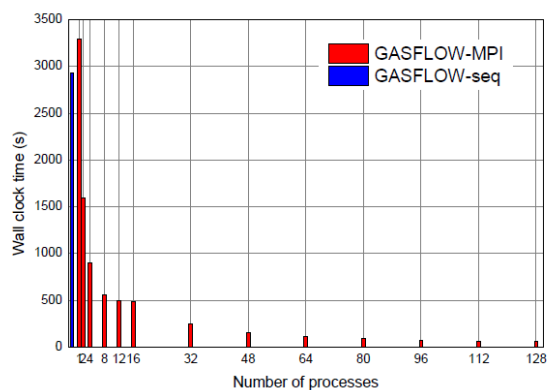


Fig. 5: Wall clock time of the sequential version of GASFLOW and GASFLOW-MPI for a large standard test problem

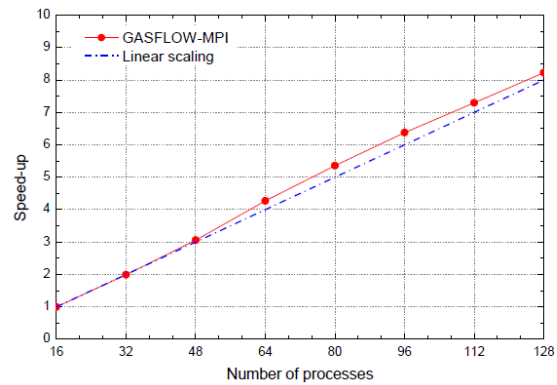


Fig. 6: Speed-up of the GASFLOW-MPI for a large standard test problem

## Setting up the Cyber Laboratory

The Cyber Laboratory is being developed as an instrument to promote and sustain further collaboration between fuel cells and hydrogen technologies with contributions from many partners via several projects, in particular H2FC and SUSANA, both coordinated by KIT. The development of this new tool for service and exchange of knowledge is one of most promising activities to receive common impact to the whole hydrogen and fuel cell community. This activity will bring together first time most promising simulation and modelling in fuel cells and hydrogen technology - which appear currently separated - to strengthen theoretical science in fuel cells, safety and hydrogen technologies. The collaboration and exchange of knowledge shall serve not only the scientific community but also the involved industry by providing the state-of-the-art in an easy accessible and applicable manner.

Most of the partners in H2FC European Infrastructure are active in modeling and simulation, and therefore the exchange of data and results is important. The Cyber Laboratory should be the platform and instrument to transfer and store data on secure basis. Although other databases exist, the status of the information basis is fragmented and barely visible. One important point is to integrate those databases and build a portal to models and data.

## References

- (1) Grune, J.; Sempert, K.; Kusnetsov, M.; Jordan, T.; "Experimental investigation of flame and pressure dynamics after spontaneous ignition in tube geometry". *International Journal of Hydrogen Energy* 39 (2014) 20396-20403.
- (2) Grune, J.; Sempert, K.; Kuznetsov, M.; Jordan, T.; "Experimental study of ignited unsteady hydrogen releases from a high pressure reservoir". *International Journal of Hydrogen Energy* 39 (2014) 6176-6183.
- (3) Grune, J.; Breitung, W.; Kuznetsov, M.; Yanez, J.; Jang, W.; Shim, W.; "Flammability limits and burning characteristics of CO-H<sub>2</sub>O-CO<sub>2</sub>-N<sub>2</sub> mixtures at elevated temperatures". Skjold, T. [Hrsg.], Proceedings of the 10th International Symposium on Hazards, Prevention, and Mitigation of Industrial Explosions (ISHPMIE 2014), Bergen, N, June 10-14, 2014, Bergen: GexCon AS, 2014 pp. 313-325, ISBN 978-82-999683-0-0.
- (4) Kotchourko, N.; Kuznetsov, M.; Kotchourko, A.; Grune, J.; Lelyakin, A.; Jordan, T.; "Concentration measurements in a round hydrogen jet using Background Oriented Schlieren (BOS) technique". *International Journal of Hydrogen Energy* 39 (2014) 6201-6209.
- (5) Kuznetsov, M.; Stern, G.; Kljenak, I.; Matkovic, M.; Mavko, B.; "Upward flame propagation experiments on hydrogen combustion in a 220 cub.m vessel". 22nd International Conference on Nuclear Engineering (ICONE22), Praha, CZ, July 7-11, 2014, Proceedings on DVD Paper ICONE22-30160, New York, N.Y.: ASME, 2014.
- (6) Kuznetsov, M.; Friedrich, A.; Stern, G.; Kotchourko, N.; Jallais, S.; L'Hostis, B.; "Medium-scale experiments on vented hydrogen deflagration". Skjold, T. [Hrsg.], Proceedings of the 10th International Symposium on Hazards, Prevention, and Mitigation of Industrial Explosions (ISHPMIE 2014), Bergen, N, June 10-14, 2014, Bergen : GexCon AS, 2014 pp.521-536, ISBN 978-82-999683-0-0.
- (7) Ren, K.; "Local mesh refinement in COM3D for combustion simulation". Dissertation, Karlsruher Institut für Technologie 2014, KIT Scientific Report, KIT-SR 7670 (August 2014).
- (8) Sander, M.; Brighenti, F.; Gehring, R.; Jordan, T.; Klaeser, M.; Kraft, D.; Mueller, R.; Neumann, H.; Schneider, Th.; Stern, G.; "LIQHYSMES - Liquid H<sub>2</sub> and SMES for renewable energy applications". *International Journal of Hydrogen Energy* 39 (2014) 12007-12017.



## Pressure Drop in Fuel Assemblies

*Abdalla Batta, Andreas Class*

### Introduction

The AREVA Nuclear Professional School (ANPS) represents an organizational unit of the IKET which (i) develops analytical and numerical modelling strategies to support design and analysis of components of nuclear industries, and (ii) provides comprehensive training courses on nuclear topics for our industrial partner AREVA GmbH. As an example taken from a wide variety of applications we present studies on the component “fuel assembly” demonstrating our typical approach to use scientific studies to develop and validate robust engineering tools.

Fuel assemblies are the most essential components in a reactor core and their thermal hydraulic behavior is eminent for safety features of the considered nuclear reactor. In some innovative nuclear reactor concepts, including accelerator driven systems (ADS) and the lead cooled fast reactor (LFR), heavy liquid metal is proposed as coolant. State of the art practice is to develop correlations for the pressure drop in fuel assemblies which discriminate between the lumped pressure drop across obstructions such as the spacers and the distributed friction losses in the bare regions of the bundle. Moreover, common practice is to experimentally develop these correlations. A wide variety of data is reported in the literature where various shapes of spacers have been analyzed. To obtain a deeper understanding of flow features, CFD studies began to play an increasing role during the last decades. Yet these studies were considered qualitative for a long time. The ANPS participated in benchmark studies, e.g. OECD benchmark studies LACANES and MATTIS-H [1-3], which aimed at validation of CFD-studies and assessed precision of different numerical techniques. The experience gained in these studies is that the uncertainty of correlations based on experiments is comparable with the uncertainty of CFD. These

benchmark studies demonstrate that the accuracy of results not only depends on the physical models which are used but to substantial extent on the experience of the CFD-user. We exploit our experience gained in benchmark studies for pre and post-test analysis of HLM 19-pin rod-bundle experiments performed at the Karlsruhe Liquid Metal Laboratory (KALLA) of IKET within the framework of the EUFP7 project THINS (thermal hydraulics of innovative nuclear systems) [4]. The experiment uses lead-bismuth eutectic as working fluid (LBE) and supports the design of bundles for European ADS Gen-IV reactors. Comprehensive pre and post-test CFD analysis was also performed on corresponding experiments using the fluid water within the EU FP6 EUROTRANS project, see [5, 6]. In the pre-test analysis a best practice approach to achieve reliable numerical results was developed which was adopted in the post test analysis where the nominal flow rate was considered. In general correlations just relate pressure drop across spacers with blockage ratio and Reynolds number. In a few cases they also distinguish whether the leading edge of the spacer is sharp or round. Yet there are many other effects, which may influence pressure drop. In our post-test analysis we specifically investigate the effect of surface roughness, which usually is not considered in correlations. Moreover, we consider two cases with identical characteristic blocking ratios but exhibit distinct blockage at the leading edge. This can be accomplished with the tested spacer grid which has different blockage ratio at the leading and trailing side. This provides insight to the effect of blockage ratio at the inlet compared to the characteristic blockage of the spacer. All the three selected flow cases are formally identical when applying correlations based on pressure loss coefficient and local blockage. Yet these cases differ in roughness and leading-edge blockage ratio.

## Pressure drop correlations

The measured pressure drop at each spacer has two contributions, namely the lumped pressure drop of the spacers and the distributed friction losses in the bare regions of the bundle. For our spacer shown in Fig 1a the pressure drop in the spacer is calculated by subtracting the frictional pressure drop corresponding to the bare region between measurement probes from the measured pressure drop. These are represented in terms of two non-dimensional parameters:  $K_{sp}$  and  $f$ , defined in Eqs.1-2, respectively.

$$K_{sp} = \frac{\Delta P_{sp}}{1/2 \rho u_b^2}, \quad (1)$$

$$f = \frac{\Delta P_f}{1/2 \rho u_b^2} \frac{d_{h,bdl}}{L}. \quad (2)$$

In our study we consider the frequently recommended correlation, which is based on the data of Rehme [7], i.e. correlations of Cigarini [8]; Epiney, et. al. [9] and compare these to experimental data obtained in KALLA [10]. Details about these correlations are given in [11]. Fig 1b shows a comparison of measured data to the correlations. The lowest curve corresponds to [8] based on data of Rehme [7] which is recommended to predict spacer losses for rounded edges. The middle curve corresponds to the correlation [9] valid for sharpe edged spacers. The tested spacer shown in Fig. 1a has several walls with variable thickness. As a result, the tested spacer exhibits a blockage ratio of 0.16 at the leading edge (spacer inlet), 0.29 at the spacer mid-plane, and 0.27 at the spacer exit. Here the blockage ratio or solidity ( $e$ ) is defined as the ratio of the projected spacer grid cross section at a given position to the undisturbed flow cross section in bundle. Commonly spacers are characterized by their maximum blockage ratio, i.e. in our case  $e = 0.29$ . As shown by Fig. 1a the spacer used in the experiments exhibits sharp edges and in addition a complex design due to the presence of dimples. Thus higher pressure drop is observed, i.e. the upper curve in Fig 1b.

The objectives of our numerical studies are to get some insight into the wide variety of pressure drop predictions.

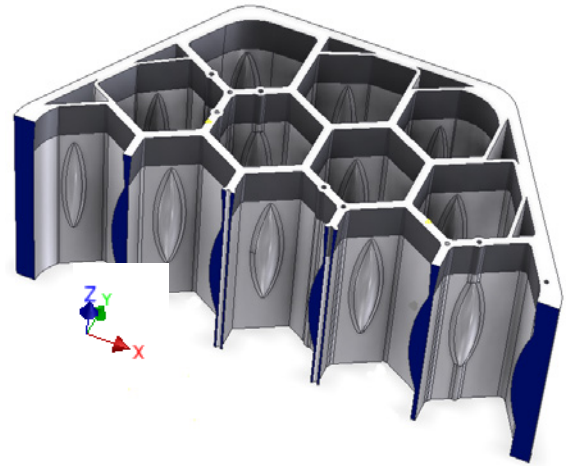


Fig. 1: (a) Spacer employed in the KALLA rod-bundle experiment

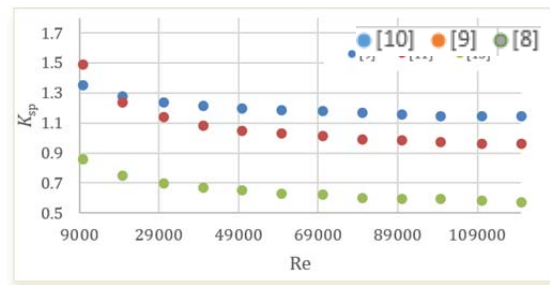


Fig. 1: (b) comparison between experimental data of KALLA [10] and correlations of, [8, 9]

## Numerical study

Our pre-test studies within EU-FP7 THINS project employed the exact spacer geometry and predicted a lower pressure drop compared to measured values. Accordingly other factors were discussed, including roughness [11]. It was shown that roughness is an important factor which generally increases pressure drop and consequently decreases the difference between experimental and numerical results. The roughness of the tested spacer is 35-40  $\mu\text{m}$  whereas the heated rods are considered smooth. For the post-test study it is decided to consider the roughness in the spacer as well as the exact geometry in the experiment. This enables quantitative comparison between numerical and experimental results.

Correlations relate pressure drop to blockage ratio but ignore detailed geometrical features the blockage. In particular, the tested spacer in figure

1a is characterized by a maximum blockage located in the center plane. Obviously, inlet and outlet blockage can differ for various spacer designs exhibiting identical characteristic blockage ratio. By simply reversing the flow direction for our spacer (see Fig. 1a) we may explore the uncertainties related to “the how the blockage is formed” without the need to study a spacer with a new geometry. In the experiment the flow enters the spacer subject to a sudden blockage ratio of 0.16, i.e. corresponding to a sharp edge. Downstream the flow accelerates until the blockage ratio of 0.29 is reached in the center plane decelerates following the dimples and slightly accelerates towards the exit where the blockage ratio becomes 0.27. In the reversed case the flow passes a strong sudden blockage of 0.27 blockage at the leading edge and then slightly decelerates as it approaches the dimples where it has to accelerate again. Downstream of the dimples the flow decelerates substantially until it exits at the location of minimal blockage ration. In particular both cases differ by the fact that at the leading edge substantially different blockage is observed. Since the correlations for sharp and round edged leading edges indicate sensitivity of pressure drop on the leading edge we expect the case of reverse flow with the more pronounced blockage to exhibit larger pressure drop.

The present study is carried out for the nominal mass flow rate of 26 kg/s. The experimentally measured average pressure drop for this nominal case is 27.5 kPa  $\pm$ 7%.

The uncertainty is deduced from the variations between the measurements of the three successive spacers and also some variations of temperature during the experimental campaigns. The measured pressure drop represents the pressure drop between pressure measuring probes located 100 mm apart. Considering that the spacer length is 25 mm, the measured pressure drop accounts for the spacer and additional 75 mm part of the bare bundle. The experimental correlation [10] results in 23.8 kPa for the spacer pressure drop at  $Re=88 \cdot 10^3$  (nominal flow rate). For the bare rod region of 75 mm length, a frictional loss of approximately 3.7 kPa is predicted by the Blasius equation and other correlations.

The post-test analysis of the experiment considers a sector of the bundle which includes one spacer. In the pretest study the smallest possible sector of  $60^\circ$  proved sufficient [12]. Due to the  $120^\circ$  symmetry of the new spacer we also use the smallest sector possible corresponding to a  $120^\circ$  sector of the bundle. A mesh of 1.65 million computational cells is generated. The simulations employs the Star-CCM+ code, high-Reynolds-number  $k-\varepsilon$ -turbulence model with automatic wall treatment. The heated rods are considered smooth while the spacer exhibits a surface roughness of 35-40  $\mu\text{m}$ . Accordingly, the mesh is generated such that the first wall distance is kept in the range of the spacer roughness. In case of the rough wall boundary condition, the code picks the minimum of the specified roughness wall or the wall distance. Fig. 2 shows the wall distance of the first cell centroid in our post-test simulation.

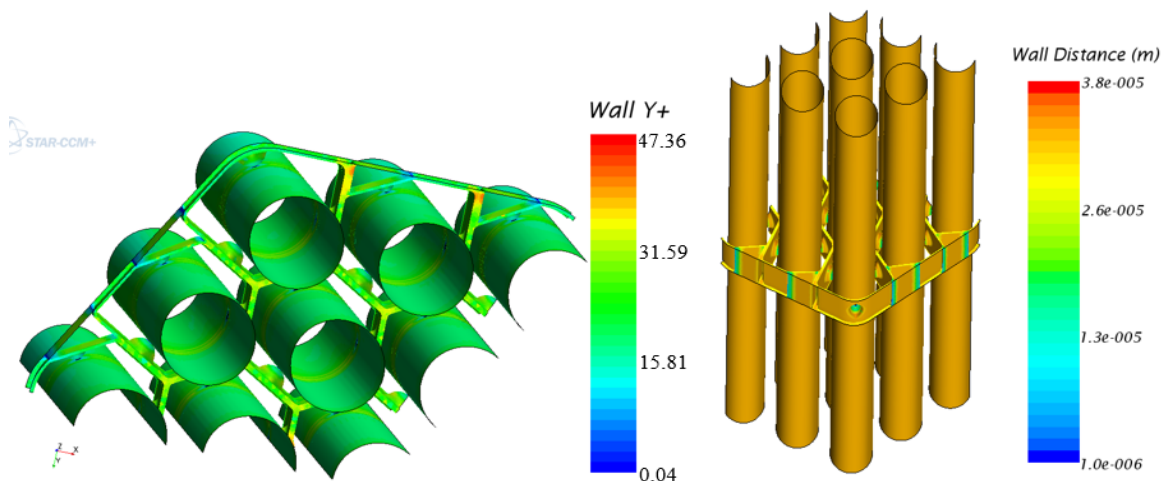


Fig. 2: Contours of the  $y^+$  and wall distance

The study is carried out for the nominal mass flow rate of 26 kg/s with uniform inlet velocity and constant fluid temperature,  $T=300\text{C}^\circ$ . This corresponds to volumetric flow rate of  $9.1\text{ m}^3/\text{h}$ . Experimental results are available for a range of flow rate,  $1\text{-}11.5\text{ m}^3/\text{h}$ . A nearly constant pressure loss coefficient is obtained for a wide range around the nominal case. The experimentally measured pressure drop for our nominal case is  $27.5\text{ kPa} \pm 7\%$ . Three cases are presented in the post-test study. In the first case (i) the condition of the experiment with rough spacer and smooth rods is considered. In the second case (ii) identical conditions ignoring roughness are considered in order to evaluate the effect of roughness. In these cases (i and ii) the orientation of the spacer (shown in Fig. 1a) with flow in the +z direction is considered, which also corresponds to the flow direction of the experiments. In a third case (iii) the conditions of case (ii) are considered but the flow direction is now reversed. This enables to check the validity of relating the pressure drop coefficient to the spacers' characteristic blockage ratio but ignoring the local blockage at the leading edge. In case (iii) the spacer has blockage ratio of 0.27 at the spacer leading edge, 0.29 at spacer middle plain and 0.16 at the trailing edge.

Fig. 3 shows the pressure drop along selected lines across the spacer for all cases (i-iii). In the experiment probes were installed 50 mm upstream and downstream of the spacer middle plane, i.e. at a distance of 100 mm. The planes in the figure are positioned at the measurement positions. The pressure drop is calculated based

on the difference between the area average pressures up and down stream of the spacers as shown in Fig 3b by pressure contours. Accordingly, the pressure losses in the spacer including 100 mm is about 25.0 kPa. The calculated pressure profile in Fig 3a also shows the axial pressure gradient of 55 kPa/m which corresponds to frictional losses of 4.1 kPa in the bare rod region of 75 mm length. The calculated pressure gradient is determined sufficiently far from the spacer where the pressure profile behaves linear. This value can be compared to predictions based on the Blasius equation for pressure drop and [13], which both result in approximately 3.7 kPa.

Fig. 3c,d shows a comparison of the cases (ii) and (iii). In both cases a smooth spacer with negligible roughness is considered. The flow direction is reversed for case (iii). We observe for the smooth spacer in forward direction, i.e. case (ii) approximately 23.0 kPa between the measurement probes. Note, that this value is area averaged computed pressure 50 mm upstream and downstream of the spacer middle plane. The additional effect of roughness can be deduced from the difference of cases (i) and (ii) and accumulates to just 2 kPa. Reversing the flow direction we compute at the same probe positions a higher pressure drop of 26.3 kPa. The additional pressure is attributed to the higher leading edge blockage  $e=0.27$  of the spacer in reverse direction, i.e. case (iii) compared to the leading edge blockage  $e=0.16$  in forward direction, i.e. case (ii). Since cases (i-iii) all have the same spacer geometry, i.e. blockage ratio and the same

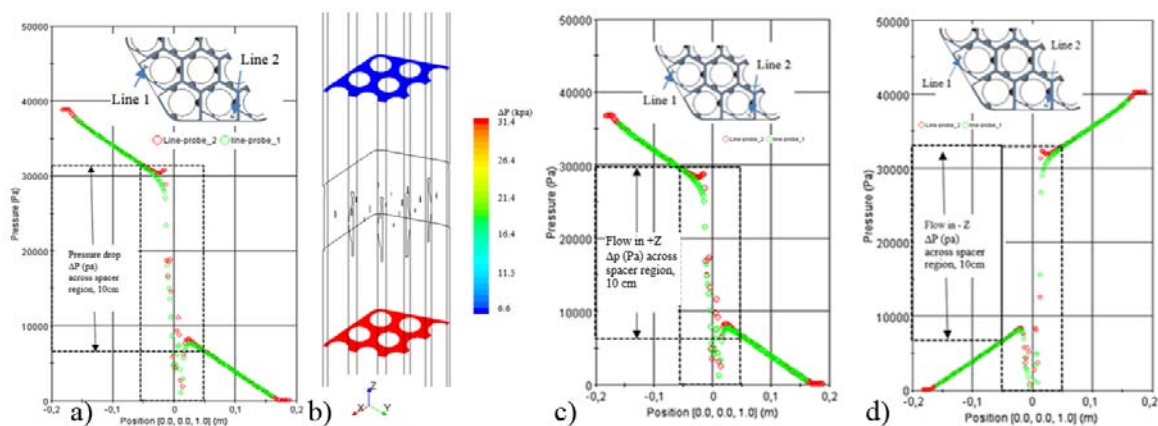


Fig. 3: Pressure drop along selected lines across the spacer and pressure contours 50 mm upstream and downstream of spacer middle plane, a) case (i): forward flow direction similar to experiment, rough; b) pressure contours at measurements plane; c) case (ii): forward flow direction similar to experiment, smooth; d) case (iii) : reversed flow, smooth

Reynolds number they should have the same pressure loss according to recommended correlations. Yet there is a substantial difference, which highlights the importance of leading edge blockage and roughness.

Table I summarizes and compares the resulting pressure drop across the spacers for the considered cases. The comparison between numerical and experimental results shows that the numerically predicted pressure is 10% less than measured. Better accuracy was observed in the pre-test studies where spacers with blockage ratio of 0.27 (water experiments) were considered [14, 15]. According to previous experience we speculate that the remaining small difference, within the accuracy bounds of the measurements, between numerical and experimental values might indicate some additional blockage in the spacer due to crude deposition. This speculation is further supported by the fact, that the experimentally measured pressure drop across a spacer is always lower compared to its successive spacer, even though the opposite effect is expected due to the developing flow conditions. The comparison of cases (ii) and (iii) shows the pronounced effect of leading edge blockage on the pressure drop in the spacer. Note that both cases correspond to the classification of a sharp edge according to [9]. Thus in addition to the shape of the leading edge, correlations should also consider leading edge blockage and possibly further parameters like the length of the spacer as well as the profile of blockage along the length.

Since CFD is capable to distinguish all these factors and many more within the uncertainty range of the experimental data it can be recommended for the prediction of spacer pressure losses. Moreover, CFD is very well suited to explore general trends when making variations in design. It should be noted that the available correlations are based on limited data points and specific spacer geometry. Therefore the actual uncertainty when applying correlations for a

brand new spacer geometry is quite large. We recommend to develop a new spacer design by first applying correlations for a rough estimation, then applying CFD for the detailed design work, and verification of the final design based on experiments.

## Conclusions

Our investigation of pressure loss in rod-bundle geometries with spacer grids explored an experiment which was performed at KALLA and used liquid metal as fluid. CFD has shown to reproduce the measured data within the range of uncertainty of the experiment. The state of the art procedure when designing new spacers is to apply correlations. We found numerous correlations applicable to the same design, which mainly depend on Reynolds number and blockage ratio. One correlation accounted for the shape of the leading edge, by distinguishing round and sharp. CFD can be performed using the actual geometry of the spacer including all its geometrical features and thus can be used to study these effects in much detail. Specifically we studied three cases which are all equivalent according to the correlations and yet show substantial difference in their pressure losses, e.g. roughness accounted for 6 % and leading edge effect for 14%.

In pretest studies we applied a systematic scheme which leads to accurate predictions. This begins by selecting a suitable domain, mesh and turbulence model. For parametric studies we use the smallest representative geometry with a well resolved numerical mesh concentrated in the spacer region. The obtained difference between post-test numerical and experimental values shows that CFD can be recommended for the prediction of pressure loss in spacer with equivalent accuracy as found in the experiment.

Table I: Comparison of pressure losses for considered cases

	<b>experimental</b>	<b>rough spacer, case (i)</b>	<b>smooth spacer, case (ii)</b>	<b>smooth spacer reversed, case (iii)</b>
<b><math>\Delta p</math> (kPa)</b>	27.5±7%	25.0	23.0	26.3
<b>roughness error in %</b>	reference (27,5 kPa)	-10%	-16.4	-
<b>flow direction effect, error in %</b>	-	-	reference (23 kPa)	+14.3%

## References

- (1) Cho, J., et. al., Benchmarking of thermal hydraulic loop models for Lead-Alloy Cooled Advanced Nuclear Energy System (LACANES), phase-I: Isothermal steady state forced convection, *Journal of Nuclear Materials* 08/2011; 415(3):404-414
  - (2) Batta, A., et. al., CFD analysis of heavy liquid metal flow in the core of the HELIOS loop, *Nuclear Engineering and Technology* 12/2010; 42(6).
  - (3) Batta, A.; Class, A.G.; "CFD study of isothermal water flow in rod bundle with split-type spacer grid". International Conference on Supercomputing in Nuclear Applications and Monte Carlo (SNA & MC 2013), Paris, F, October 27-31, 2013.
  - (4) Annex I – "Description of Work for THINS project", Seventh framework programme of EURATOM for nuclear research and training activities (2007-2011), theme: nuclear fission and radiation protection, grant agreement for: Collaborative project "large-scale integrating project, no.: 249337
  - (5) Annex I, EUROpean Research Programme for the TRANsmutation of High Level Nuclear Waste in an Accelerator Driven System, Project acronym: EUROTRANS, Contract no.: FI6W-CT-2004-516520, Feb. 2005
  - (6) Litfin, K., "EUROpean Research Programme for the TRANsmutation of High Level Nuclear Waste in an Accelerator Driven System", FI6W-CT2004-516520, Workpackage N°: W 4.5, Identification N°: D 4.68.
  - (7) Rehme, K., Pressure drop correlations for fuel element spacers, *Nuclear Tech.*, 17, pp. 15-23, 1973
  - (8) Cigarini, M., Dalle Donne, M., "Thermohydraulic optimization of homogeneous and heterogeneous advanced pressurized reactors", *Nuclear Technology*, Vol.80, pp.107-132 (1988).
  - (9) Epiney, A., Mikityuk, K., Chawla, R., 2010. TRACE qualification via analysis of the EIRgas-loop experiments with smooth rods. *Ann. Nucl. Energy* 37 (6), 875–887.
  - (10) Pacio, J., et. al., Heavy-liquid metal heat transfer experiment in a 19-rod bundle with grid spacers. *Nucl. Eng. Des.* 2014, 273, 33–46
  - (11) Batta, A., Class, A., Analysis of pressure drop in rod bundles in heavy liquid metal, The 16th International Topical Meeting on Nuclear Reactor Thermal Hydraulics, will be published in NURETH-16, August 30-September 4, 2015
  - (12) Batta, A., Class, A. G., Study of enhanced entrance pressure losses in a rod bundle experiment employing heavy liquid metal coolant, NURETH-14 Toronto, Ontario, Canada, 2011
  - (13) Cheng, S.-K., Todreas, N.E., 1986. Hydrodynamic models and correlations for bare and wire-wrapped hexagonal rod bundles – bundle friction factors, subchannel friction factors and mixing parameters. *Nucl. Eng. Des.* 92 (2), 227–251.
  - (14) Batta, A., Class, A., Litfin, K., Wetzel, T., "Numerical Study on Flow Distribution and Turbulent Flow in XT-ADS Rod Bundle Water Experiment", NUTHOS-8, paper N8P0232, Shanghai, China, Oct 10-14, 2010
  - (15) Batta, A., Class, A., et.al., Rehme Correlation for Spacer Pressure Drop Compared to XT-ADS Rod Bundle Simulations and Water Experiment, JTK 2011
- Read more:
- (16) Class, A.G.; Fazio, C.; Fetzer, J.R.; Gordeev, S.; "Conceptual design studies for the liquid metal target META:LIC". *Journal of Nuclear Materials* 450 (2014) 204-211.
  - (17) Fetzer, J.R.; Class, A.G.; Wolters, J.; "Design measures to counteract pressure wave effects in the liquid metal target META:LIC". *Journal of Nuclear Materials* 450 (2014) 212-218.
  - (18) Fetzer, J.R.; Class, A.G.; Wolters, J.; "Studies on physics and design of beam trip induced pressure waves in spallation targets". Jahrestagung Kerntechnik, Frankfurt, 6.-8. Mai 2014, Berlin : INFORUM GmbH, 2014, CD-ROM, ISBN 978-3-926956-99-6.
  - (19) Heinze, D.; Schulenberg, T.; Behnke, L.; "Simulation of direct contact condensation of steam jets submerged in subcooled water by means of a one-dimensional two-fluid model". Meyer, J.P. [Hrsg.], 10th International Conference on Heat Transfer, Fluid Mechanics and Thermodynamics (HEFAT 2014), Orlando, Fla., July 14-16, 2014, Proceedings on USB-Stick pp. 1571-1578, ISBN 978-1-77592-068-7.
  - (20) Litfin, K.; Fetzer, J.R.; Batta, A.; Class, A.G.; Wetzel, Th.; "High power spallation target using a heavy liquid metal free surface flow". 27th International Conference of the International Nuclear Target Development Society (INTDS-2014), Tokyo, J, August 31 - September 5, 2014.
  - (21) Noack, R.; Class, A. G.; "Two-fluid modelling with coarse-Grid-CFD". Jahrestagung Kerntechnik, Frankfurt, 6.-8.Mai 2014, Berlin : INFORUM GmbH, 2014, CD-ROM, ISBN 978-3-926956-99-6.

- (22) Pang, B.; "Numerical study of void drift in rod bundle with subchannel and CFD codes". KIT Scientific Report, KIT-SR 7669 (Juli 2014).
- (23) Pang, B.; Cheng, X.; "Proposal of a new type of two-phase interchannel mixing model for application to subchannel analysis of PWR conditions". *Annals of Nuclear Energy* 73 (2014) 108-121.
- (24) Prill, D. P.; Stockmaier, M.J.; Class, A. G.; "On grid-free pool models using proper orthogonal decomposition based reduced order models". International Workshop on Thermal Hydraulics of Innovative Nuclear Systems (THINS 2014), Modena, I, January 20-22, 2014.
- (25) Prill, D. P.; Class, A. G.; "Semi-automated proper orthogonal decomposition reduced order model non-linear analysis for future BWR stability". *Annals of Nuclear Energy* 67 (2014) 70-90.
- (26) Ranft, M.; Class, A.G.; "Stochastic-field cavitation model". Jahrestagung Kerntechnik, Frankfurt, 6.-8. Mai 2014, Berlin : INFORUM GmbH, 2014, CD-ROM, ISBN 978-3-926956-99-6.
- (27) Raquet, M.; "Safety analysis for a fuel qualification test with supercritical water". Dissertation, Karlsruher Institut für Technologie 2014, KIT Scientific Report, KIT-SR 7682 (Januar 2015).
- (28) Roelofs, F.; Batta, A.; Bandini, G.; van Tichelen, K.; Gerschenfeld, A.; Cheng, X.; "European liquid metal thermal-hydraulics R&D: present and future". Proceedings of the European Nuclear Conference (ENC 2014), Marseille, F, May 11-14, 2014, Bruxelles: European Nuclear Society, 2014 pp.191-200, ISBN 978-92-95064-21-8.
- (29) Roelofs, F.; Shams, A.; van Tichelen, K.; Gerschenfeld, A.; Batta, A.; DiPiazza, I.; "Thermal hydraulic challenges for liquid metal fast reactors in Europe". IAEA Technical Meeting on Priorities in Modelling and Simulation for Fast Neutron Systems, Wien, A, April 14-16, 2014, Folien online veröffentlicht.
- (30) Ruzickova, M.; Schulenberg, T.; Visser, D.C.; Novotny, R.; Kiss, A.; Maraczy, C. ; Toivonen, A.; "Overview and progress in the European project: 'Supercritical Water Reactor - Fuel Qualification Test'". *Progress in Nuclear Energy* 77 (2014) 381-389.
- (31) Ruzickova, M.; Schulenberg, T.; Visser, D.; Maraczy, C.; Toivonen, A.; Kiss, A.; Novotny, R.; "Overview and progress in the European project: 'supercritical water reactor - fuel qualification test'". 19th Pacific Basin Nuclear Conference (PBNC-2014), Vancouver, CDN, August 24-28, 2014, Proceedings on USB-Stick Paper PBNC2014-107, ISBN 978-1-926775-16-2.
- (32) Schulenberg, T.; "Research expectations for advanced nuclear systems". FISA 2013 : 8th European Conference on Euratom Research and Training in Reactor Systems, Vilnius, LT, October 14-17, 2013, Conference Proceedings pp.396-406, Luxembourg: Publications Office of the European Union, 2014, EUR 26845 EN (2014), ISBN 978-92-79-41107-6.
- (33) Schulenberg, T.; Leung, L.K.H.; Oka, Y.; "Review of R&D for supercritical water cooled reactors". *Progress in Nuclear Energy* 77 (2014) 282-299.
- (34) Schulenberg, T.; Raque, M.; "Safety analysis for an in-pile SCWR fuel qualification test loop". 19th Pacific Basin Nuclear Conference (PBNC-2014), Vancouver, CDN, August 24-28, 2014, Proceedings on USB-Stick Paper PBNC2014-106, ISBN 978-1-926775-16-2.
- (35) Schulenberg, T.; Raque, M.; "Transient heat transfer during depressurization from supercritical pressure". *International Journal of Heat and Mass Transfer* 79 (2014) 233-240.
- (36) Weinhorst, B.; Fischer, U.; Class, A.G.; Fetzer, J.R.; "Radiation damage analysis for the liquid metal target META:LIC". *Journal of Nuclear Materials* 450 (2014) 219-224.
- (37) Zeiger, T.; Schulenberg, T.; Flad, M.; Raque, M.; "Indirect consequences of pressure tube rupture during SCWR fuel qualification test". 19th Pacific Basin Nuclear Conference (PBNC-2014), Vancouver, CDN, August 24-28, 2014, Proceedings on USB-Stick Paper PBNC2014-115, ISBN 978-1-926775-16-2.
- (38) Zeiger, T.; Schulenberg, T.; "Validation of fragment penetration analysis with ANSYS". Jahrestagung Kerntechnik, Frankfurt, 6.-8.Mai 2014 Berlin : INFORUM GmbH, 2014, CD-ROM, ISBN 978-3-926956-99-6.



## Experimental Validation of a Numerical Model – Application of an Open Source Code towards Geothermal Conditions

Pia Orywall

### Introduction

The usage of the geothermal energy has a long tradition with regard to the appliance of the thermal water in spas. The electricity generation from geothermal energy can be dated back to over one hundred years. The first trials took place already in 1904 in Lardarello / Italy (Sanner, 1992). Therefore the geothermal fluid has to be produced and the heat will be deprived. The fluid itself is in the reservoir formation in equilibrium with the enclosing rock formation. When this fluid will be mined it undergoes a pressure release and a heat extraction. Therefore the thermodynamic properties and the chemical composition are changed. Re-injecting of this fluid into the reservoir can lead to significant changes in permeability. At worst the reservoir formation may be affected by dissolution and / or precipitation (Chang and Civan, 1997).

The modified water hits the reservoir rock and consequently chemical interactions occur (Ochi and Vernoux, 1998). In the close vicinity of the borehole (Fig. 1) mineralogical modifications are expected, because there is the spot of the media fluid and minerals. Regarding further distances the reaction front should thin down.

The relevant geochemical processes for this research are the dissolution and the precipitation of minerals. But also ion exchange, sorption and complexation are phenomena which should be mentioned (Yeh and Tripathi, 1989). These interactions, however, are very site-specific and require the use of numerical modeling and adapted laboratory experiments in order to understand the occurring processes in detail. This work shows how to establish a geochemical transport model and further to validate it with suitable experimental tests.

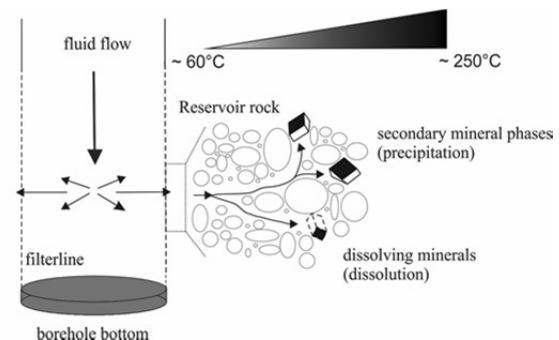


Fig.1: Scheme of the processes in the nearfield of the injection well

### Methodology

For a development of the multidimensional numerical model the idea is to couple open source codes by using an operator splitting. The result is a modular approach (Fig. 2) with already available codes, which compounds result in a new application (Dimier, 2011). This splitting can be combined with a sequential iterative approach (SIA) between hydrological and chemical equilibrium computations (Yeh and Tripathi, 1989).

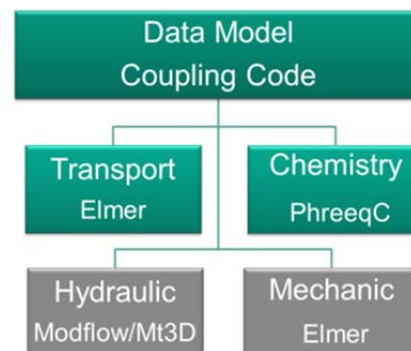


Fig. 2: Modular structure of the Open Source Model

## Elementary Tools

The programs are normally utilized for specific applications like the chemistry, the transport or the temperature distribution. Through the coupling it is possible to get a kind of multi-physic application (Montarnal et al., 2005).

The common chemical modelling programs are based on equilibrium formulation, there exist e.g. WATEQ4F (Ball and Nordstrom, 1991), MINTQA2 (Allison et al., 1991), EQ 3/6 (Wolery, 1979), Chess (MINES, Paris), TOUGHREACT (Xu et al., 2006), CrunchFlow (Steeffel, 2009) and PhreeqC (U.S. Geological Survey). At this, PhreeqC is chosen and the reasons are: It is an open source code, the reaction equations are written in the syntax of chemical formulas and it has a GUI (Merkel and Planer-Friedrich, 2009). Additionally, it is the most widely used geochemical model, it gives a wide variety of geochemical aqueous calculations, it is based on an equilibrium chemistry of the aqueous solutions interacting with e.g. mineral phases and includes the modelling of kinetically controlled reactions. The program has a couple of databases which are case-specific selectable for low and high ionic strength (Parkhurst and Appelo, 1999). The addenda of them are very helpful. For geothermal related experiments with a high-saline fluid (high ionic strength) the database pitzer.dat can be selected. But hereby limitations are gaps in the database of some considered minerals of reservoir rocks, like e.g. the kinetic of hematite.

For the Pre-processing, associated to the finite element code, the mesh generation is implemented by the open source code named Gmsh developed by Geuzaine and Remacle (2009). Therefore a Python-module has to be defined to manipulate e.g. the mesh elements and bodies, which are retrieved from the mesh file. Via this Python interface the mesh bodies become objects which can be associated to material properties or aqueous states characterizing the problem to be modelled.

The flow, the transport and the temperature can be described by Elmer. This code is written by the IT Center of Science and it uses a finite element formulation. The code involves the diffusion, convection and reactions which are needed

for the research topic. Elmer being interfaced with major commercial mesh generators, depending on user's needs, meshes from different sources can be used (Raback et al., 2014).

The Post-processing, thus the visualization application is made with Paraview. It is also open-source, originally created by Kitware together with Jim Ahrens of the Los Alamos National Laboratory (Henderson et al., 2004).

The used programming language for the data model and for the coupling of all the previously mentioned codes is Python (Beazley, 2008).

## Coupling process

For example, to match with PhreeqC requirements, a generic species class has to be created (Yeh and Tripathi, 1989). After that a master species and a secondary species class will inherit from that ancestor to enable part of the chemical problem definition. Thereby a feature of Python allows the definition of a case study through class instantiation and module parameterization. This script contains all data being read through the interpreter. In that way two specific data files, called shared objects, of Elmer and PhreeqC were generated: WElmer.so and WPhreeqc.so (Dimier, 2011).

Over a wrapping process Elmer and PhreeqC functionalities become part of Python modules. The type of wrapping for which Python is suitable, is based on a memory exchange. Thereby codes are integrated in the platform as dynamic libraries and this optimized CPU costs (Montarnal et al., 2005). For a possible communication between the software and Python, the first step is to create C wrapping functions. These functions allow data manipulation between the tool itself and the Python interpreter and based on the specific structures of each program. Thereby the initialization is the first method, where specific data files are created by Python. This allows launching the software, reading the file and generating suitable structures. E.g. the time step is chemistry driven and will be managed by Python. Similar to that, we created a Python module to manipulate the mesh, which satisfies the Gmsh-format.

## Equations

### Geochemical module

The used Software PhreeqC assumes that the dissolved species are in thermodynamic equilibrium. But minerals often do not react to equilibrium during the predefined time frame. When a reaction is kinetically controlled it generates concentration changes according to the rate equation:

$$\frac{dm_i}{dt} = c_{i,k} R_k \quad (1)$$

Where  $c_{i,k}$  is the stoichiometric coefficient of species  $i$  in the kinetic reaction, and  $R_k$  is the overall reaction rate for substance  $k$  [mol/kgw/s] (Parkhurst and Appelo, 1999). This rate has to be numerically integrated over a time period; therefore PhreeqC enables the use of a Runge-Kutta or the CVODE Algorithm (Cohen and Hindmarsh, 1994).

The rate for a kinetic reaction of solid or minerals is:

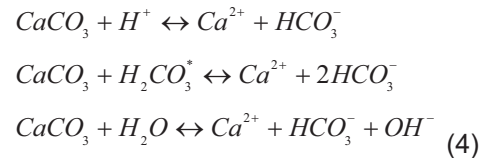
$$R_k = r_k \frac{A_0}{V} \left( \frac{m_k}{m_{0,k}} \right)^n \quad (2)$$

$A_0$  is the initial surface area of the solid,  $r_k$  is the specific rate,  $V$  is the amount of solution,  $m_{0,k}$  is the initial moles of solid,  $m_k$  is the moles of solid at a given time,  $(m_k/m_{0,k})^n$  is a factor to account for changes in  $A_0/V$  during e.g. dissolution.

The dissolution and precipitation of calcite ( $\text{CaCO}_3$ ), which is for this research of interest, is given by the equation (3) of Plummer et al. (1978):

$$r = k_1 a_{\text{H}^+} + k_2 a_{\text{H}_2\text{CO}_3^*} + k_3 a_{\text{H}_2\text{O}} - k_4 a_{\text{Ca}^{2+}} a_{\text{HCO}_3^-} \quad (3)$$

Where  $a$  represents the activity,  $k_1$ ,  $k_2$ ,  $k_3$  are the forward rate constants and  $k_4$  the backward rate, as a function on temperature. Therefore, for the forward rates of calcite three main reactions are occurring. These steps are depending of the pH-value (Plummer et al., 1978):



As mentioned before the activity is a relevant variable for the kinetic of calcite. The activity defines the influence of the salt content to the equilibrium constant.

$$a_i = f_i * c_i \quad (5)$$

Where  $f_i$  is an ion-specific correction factor and  $c_i$  the concentration of the Ion  $i$ .

Activity coefficients of aqueous species are defined by approximation equations like the Davies-Equation or here the extended Debye-Hückel equation:

$$\log f_i = - \frac{Az_i^2 \sqrt{I}}{1 + Ba_i \sqrt{I}} \quad (6)$$

Where  $z_i$  is the ionic valency of aqueous species  $i$ ,  $A$  and  $B$  are parameter dependent on temperature and  $a_i$  is an ion-specific parameter (Merkel and Planer-Friedrich, 2008; Parkhurst and Appelo, 1999).

The validation of (6) for calculating the activity coefficient depends on the ionic strength  $I$  of the fluid (Debye und Hückel, 1923):

$$I = \frac{1}{2} \sum_i c_i (z_i)^2 \quad (7)$$

For these solutions some assumptions have to be made. Hereby the ionic interactions caused by the Coulomb forces, the ionic size do not change with the ionic strength and ions with the same sign have no interaction. These assumptions are valid for ionic strength smaller than 0.5 mol/kg, therefore the Debye-Hückel equation is valid ( $I < 0.005$  mol/kg). With increasing ionic strength the solver can be the extended Debye-Hückel, the Güntelberg and the Davies-Equation. Above 0.5 mol/kg, which are values of a geothermal fluid e.g. in the Upper Rhine Valley, the assumptions are invalid. Additional an increasing part of hydrate covers were build and resulting the amount of free water-molecules are getting smaller and the concentration of the activity coef-

ficient rises. With this character of the fluid the Pitzer-equation is valid (Merkel and Planer-Friedrich, 2008).

### Hydrologic transport

The main mechanisms for the transport are advection, diffusion and dispersion. Beside that the chemical substance be defeated by processes like the adsorption / desorption, decay and the dissolution / precipitation. Thereby the sorption and the decay are not mentioned, because these processes are not relevant for this research. The transport equation which should be solved:

$$\frac{d_c}{d_t} = -\nabla(uc) + \nabla(D\nabla c) + S \quad (8)$$

Where  $u$  is the pore space velocity,  $c$  the concentration,  $D$  the diffusion/dispersion coefficient,  $t$  the time,  $\nabla$  the nabla-operator in three dimensions ( $(d/d_x)/(d/d_y)/(d/d_z)$ ) and  $S$  the source/sink term (Rausch et al., 2005).

The diffusive motion is caused by the Brown'sche molecular movement and can be described by the Ficks Law. The first Ficks law is valid for steady state processes and whereby the second Ficks law considers the concentration over time. In the porous media the ions have to flow through the channels of the rock. The effective diffusion coefficient contemplates these effects with the impedance factor/tortuosity:

$$D^* = D_m \frac{\theta}{\tau^2} \quad (9)$$

Where  $D^*$  is the effective diffusion coefficient,  $D_m$  the molecular diffusion,  $\theta$  the porosity and  $\tau$  the tortuosity (Lege et al., 1996).

The advective transport of a substance is working by the flow of the groundwater, even though the dispersion acts as distributer and concentration reducer. This process can affects in the longitudinal (flow direction) and the transversal direction (orthogonal to the flow direction). The simulation with the software Elmer is based on the governing equation after Zheng and Wang (1999) with the assumption, that the transported quantity is carried by an incompressible fluid:

$$\frac{\partial(\theta C^k)}{\partial t} = \frac{\partial}{\partial x_i} \left( \theta D_{ij} \frac{\partial(C^k)}{\partial x_j} \right) - \frac{\partial}{\partial x_i} (\theta v_i C^k) + q_s C_s^k + \Sigma R_n \quad (10)$$

Where  $C_k$  is the dissolved concentration of species  $k$ ,  $\theta$  is the porosity of the medium,  $t$  is time,  $x_{ij}$  is the distance along the coordinate axis,  $D_{ij}$  is the hydrodynamic dispersion coefficient tensor;  $v_i$  is the pore water velocity;  $q_s$  is the volumetric flow rate representing sources (+) or sinks (-),  $C_s^k$  is the concentration of the source/sink flux for species  $k$  and  $\Sigma R_n$  is the chemical reaction term. Assumption thereby is the Darcy regime of the fluid velocity.

### Experimental setup

A flow through experiment is needed for the validation of the model, therefore a reliably experimental design. The requirements are (1) reproducible results and (2) relatively fast implementation of the experiments. Therewith the modeling results can be fixed to the experimental ones.

The setup itself consists out of a synthetically sample with known parameters like the permeability with  $\sim 152$  mDarcy and the hydraulic conductivity of  $\sim 1.5 \cdot 10^{-6} \text{ ms}^{-1}$ . This body is split into two parts; one upper and one lower one, and in-between one artificial layer is built with a defined mineral phase (Fig. 3).

The material of the synthetically sample is a Borosilicate developed by the company ROBU (Tab. 1).

Table 1: Chemical composition of the Borosilicate (ROBU, 2014).

Element	Weight percentage [%]
SiO <sub>2</sub>	80,60
B <sub>2</sub> O <sub>3</sub>	12,60
Na <sub>2</sub> O <sub>3</sub>	4,20
Al <sub>2</sub> O <sub>3</sub>	2,20
CaO	0,10
Cl	0,10
MgO	0,05
Fe <sub>2</sub> O <sub>3</sub>	0,04

The layer, which is built-in between the two Borosilicate parts, is out of calcite grains (sh minerals GmbH). The thickness of this layer depends on the possibility of the fitment with the practical experience, but should be around 10 mm. Pressure and temperature conditions are: Room conditions in the laboratory (20°C and 1bar). The chemistry of the water consists out of a nitric acid solution. Thereby the background is a fast solution of the calcite layer.



After the flow through of the solution and the associated dissolution of the layer the  $\text{Ca}^{2+}$  will be detected at the outlet of the cell. The chemical components will be measured by ICP-OES ( $\text{Ca}^{2+}$ ). An internal standard will be used for a higher accurateness of the results. This serves as a relative reference to exclude systematic errors. Within the measured chemical concentration the modelled breakthrough curve can be checked and if it is necessary the model can be adjusted.

## Preliminary Results

### Mesh Generation

A first step was to build up a mesh for the cylindrical body. Therefore the program code is generated with the software Gmsh. The mesh itself was generated as a structural one, for the best fitting to the present problem (Fig. 3a). Figure 3b shows the cylindrical body with the horizontal calcite layer.

For the first runs the chemistry is chosen like mentioned before. The kinetic of the calcite dissolution is given in the database e.g Phreeqc.dat, Wateq4.dat after Plummer et al., (1978).

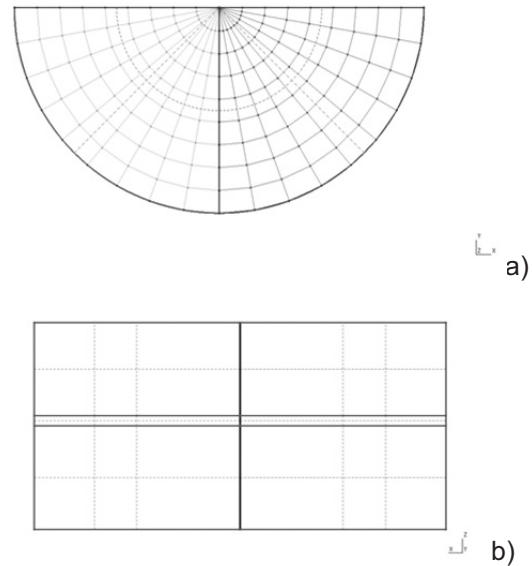


Fig. 3a: (top), view within the z-axis of the mesh, 3b: view within the x,y plane; horizontal layer.

## Simulation

There is build up a simulation to see how the experimental setup will behave. Concerning the simulation duration, key parameters are the pH-value of the inlet solution, the permeability and the porosity of the various materials. Hereafter, for a calcite layer, perpendicular to the flow, we plot the calcite amount after five days of simulation (Fig. 4). The pH has been fixed to 3 and the velocity is of  $1 \cdot 10^{-6} \text{ ms}^{-1}$ .

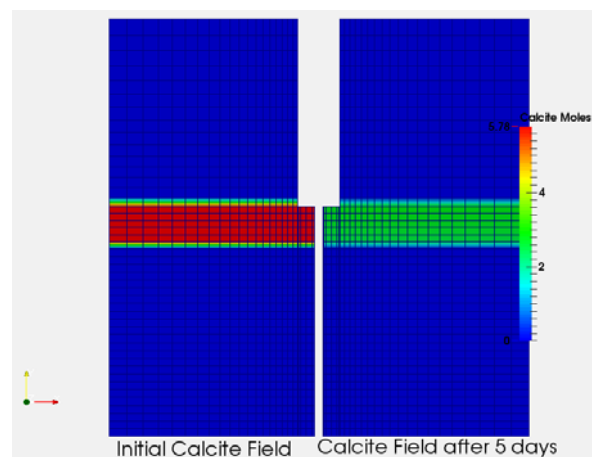


Fig. 4: Simulation of the calcite dissolution. Left: Initial concentration, right: after 5 days

Considering those numerical results, which doesn't take the fault porosity evolution, and making an extrapolation of them, we would reach the complete calcite dissolution after two weeks duration of the experiment. Once the different materials will be characterized, we will use the simulation to make a coarse estimation of the necessary experiment duration.

## Discussion and Outlook

The presented numerical research comes originally of the CO<sub>2</sub> Storage modeling, but is transferrable to geothermal question formulations regarding the near surface geothermal energy; the borehole heat exchangers and the deep geothermal energy use. A closer look to the deep geothermal energy, mentioned before, the model is a base for an injection or production well and therefore the environment of the reservoir rock in the near field of the wells.

Here the built-up of the model is shown and the first values of the geochemical flow in these different arranged bodies are computed. For a better adaption to the real conditions a feasible up-scaling to geothermal conditions is necessary. So the experimental setup and conditions will be adjusted to a high temperature and a high pressure environment and the model will be validated additional to these ones.

## Acknowledgements

The present research will be performed with the European Institute for Energy Research (EIFER) from Karlsruhe. Special thanks go to sh minerals GmbH (Lengefeld) for the prompt material provision (calcite grains) and to EnBW AG (Energie Baden-Württemberg AG) for the kind assistance and support.

## References

(1) Allison, J.D., Brown, D.S., and Novo-Gradac, K. J.: MINTEQA2/PRODEFA2 - A geochemical assessment model for environmental systems - Version 3.0 user's manual, *Environmental Research Laboratory*, U.S. Environmental Protection Agency, Athens, Georgia (1991).

(2) Ball, J. W., Nordstrom, D. K.: WATEQ4F—User's manual with revised thermodynamic data base and test cases for calculating speciation of major, trace and redox elements in natural waters, *U.S. Geological Survey Open-File Report*, (1991), 91-183.

(3) Beazley, D. M.: Python Essential Reference, 3<sup>rd</sup> edition, *Paperback*, Indianapolis (2008).

(4) Chang, F. F., Civan, F.: Practical model for chemically induced formation damage, *Journal of Petroleum and Engineering*, **17**, (1997), 123-137.

(5) Cohen, S. D., Hindmarsh, A. C.: CVODE, A stiff/nonstiff ODE solver, *C. Computer Physics*, (1996), 138-143.

(6) Debye, P., Hückel, E.: The theory of the electrolytes, I. Lowering of freezing point and related phenomena, *Physikalische Zeitschrift*, **24**, (1923), 185-206.

(7) Dimier, A.: An Open Source Coupling Algorithm with applications towards CO<sub>2</sub> Storage modelling, *Proceedings, 25th European conference on modelling and simulation*, Krakow, Poland (2011).

(8) Geuzaine, C., Remacle, J.-F.: Gmsh: a three-dimensional finite element mesh generator with built-in pre- and post-processing facilities, *International Journal for Numerical Methods in Engineering*, **79 (11)**, (2009), 1309-1331.

(9) Henderson, A., Ahrens, J., Law, C.: The ParaView Guide, *Kitware Inc.*, Clifton Park, NY (2004).

(10) Lege, T., Kolditz, O., Zielke, W.: Strömungs- und Transportmodellierung, Handbuch zur Erkundung des Untergrundes von Deponien und Altlasten Band 2, BGR, *Springer Verlag*, (1996).

(11) Montarnal, P., Dimier, A., Deville, E., Adam, E., Gaombalet, J., Bengaouer, A., Loth, L., Chavant, C.: Coupling methodology within the software platform alliances, *Proceedings, International Conference on computational Methods for coupled problems in Science and engineering*, Barcelona (2005).

(12) Merkel, J.B., Planer-Friedrich, B.: Groundwater Geochemistry, A Practical Guide for Modeling of Natural and Contaminated Aquatic Systems, *Springer-Verlag*, (2008).

(13) Ochi, J., Vernoux, J.-F.: Permeability decrease in sandstone reservoirs by fluid injection Hydrodynamic and chemical effects, *Journal of Hydrogeology*, **208**, (1998), 237-248.

(14) Parkhurst, D. L., Appelo, C. A. J.: Users Guide to PhreeqC (version2) - A computer program for speciation, batch-reaction, 1D transport and inverse geochemical calculations, *Water-*

*Resources Investigations Report 99-4259*, USGS, (1999).

(15) Plummer, L. N., Wigley, T. M. L., Parkhurst, D. L.: The kinetics of calcite dissolution in CO<sub>2</sub>-water systems at 5°C to 60°C and 0.0 to 1.0 atm CO<sub>2</sub>, *American Journal of Science*, **278**, (1978), 179-216.

(16) Raback, P., Malinen, M., Ruokolainen, J., Pursula, A., Zwinger, T.: *Elmers Models Manual*, CSC-IT Center of Science, Finland (2014).

(17) Rausch, R., Schäfer, W., Therrien, R., Wagner, C.: *Solute Transport Modelling – An Introduction to Models and Solution Strategies*, Gebrüder Borntraeger Verlagsbuchhandlung Science Publishers, Berlin Stuttgart (2005).

(18) Sanner, B.: *Erdgekoppelte Wärmepumpen: Geschichte, Systeme, Auslegung, Installation.*-IZW Berichte 92-2, 328 S. (1992).

(19) Steefel, C.: *CrunchFlow: Software for Modeling Multicomponent Reactive Flow and Transport*, User's Manual, Lawrence Berkeley National Laboratory, Berkeley (2009).

(20) Wolery, T. J.: Calculation of chemical equilibrium between aqueous solution and minerals - The EQ3/6 software package, *Lawrence Livermore National Laboratory Report*, UCRL-52658, Livermore, CA (1979).

(21) Xu, T., Sonnenthal, E., Spycher, N., Pruess, K.: TOUGHREACT - A simulation program for non-isothermal multiphase reactive geochemical transport in variably saturated geologic media: Applications to geothermal injectivity and CO<sub>2</sub> geological sequestration, *Computers & Sciences*, **32**, (2006), 145-165.

(22) Yeh, G. T., Tripathi, V., S.: A critical evaluation of recent developments in hydrogeochemical transport models of reactive multichemical components, *Water Resources Research*, **25(1)**, (1989), 93-108.

(23) Zheng, C., Wang, P.P.: A modular three-dimensional multispecies transport model for simulation of advection, dispersion and chemical reactions of contaminants in groundwater systems, *MT3DMS, Documentation and Users Guide*, University of Alabama, (1999).

Read more:

(24) Herfurth, S.: "MoNiKa - pilot plant for geothermal engineering". 5th European Geothermal PhD Day (EGPD 2014), Darmstadt, March 31 - April 2, 2014.

(25) Krau, C.I.: „Laseroptische Untersuchungen turbulenter Strömungsstrukturen beim Wärmeübergang in überkritisches Kohlendioxid nahe des pseudo-kritischen Punktes“. Dissertation,

Karlsruher Institut für Technologie 2014, KIT Scientific Reports, KIT-SR 7679 (Oktober 2014).

(26) Kuhn, D.: "Geothermal energy from low enthalpy sources". Institute for Water Structure and renewable Energy (IWSrE), International Conference and Workshop, Surakarta, RI, March 27-28, 2014.

(27) Kuhn, D.; Schröder, E.; Canic, T.; Orywall, P.; "Topic 4: Surface technology for underground - Storage and reservoir exploitation". International Workshop 'Problem and Perspective of CO<sub>2</sub> Capture and Storage in Caucasus', Tbilisi, GE, October 17-18, 2014.

(28) Nusiaputra, Y.Y.; Wiemer, H.J.; Kuhn, D.; "Thermal-Economic modularization of small, organic rankine cycle power plants for mid-enthalpy geothermal fields". *Energies* 7 (2014) 4221-4240.

(29) Schröder, E.; Kuhn, D.; Herfurth, S.; "Online Messung der Wärmeleitfähigkeit realer Geothermiewässer". Geothermiekongress 2014, Essen, 11.-13.November 2014, Proceedings auf CD-ROM, Berlin : GtV-Bundesverband Geothermie, 2014, ISBN 978-3-932570-69-8.

(30) Schröder, E.; Neumaier, K.; Nagel, F.; Vetter, C.; "Study on heat transfer in heat exchangers for a new supercritical organic rankine cycle. *Heat Transfer Engineering* 35 (2014) 1505-1519.

(31) Vetter, C.; "Thermodynamische Auslegung und transiente Simulation eines überkritischen Organic Ranking Cycles für einen leistungsoptimierten Betrieb". Dissertation, Karlsruher Institut für Technologie 2014, KIT Scientific Reports, KIT-SR 7674 (August 2014).



The annual report of the Institute for Nuclear and Energy Technologies of KIT summarizes its research activities in 2014 and provides some highlights of each working group of the institute. Among them are thermal-hydraulic analyses for nuclear fusion reactors, accident analyses for light water reactors, and research on innovative energy technologies like liquid metal technologies for energy conversion, hydrogen technologies and geothermal power plants. Moreover, the institute has been engaged in education and training in energy technologies, which is illustrated by an example of training in nuclear engineering.

ISSN 1869-9669  
ISBN 978-3-7315-0407-8

